



CREaTE

Canterbury Research and Theses Environment

Canterbury Christ Church University's repository of research outputs

<http://create.canterbury.ac.uk>

Please cite this publication as follows:

Hounslow, M., McIntosh, G., Edwards, R., Laming, D. and Karloukovski, V. (2017) End of the Kiaman Superchron in the Permian of SW England: Magnetostratigraphy of the Aylesbeare Mudstone and Exeter groups. *Journal of the Geological Society*, 174 (1). pp. 56-74. ISSN 0016-7649.

Link to official URL (if available):

<http://dx.doi.org/doi:10.1144/jgs2015-141>

This version is made available in accordance with publishers' policies. All material made available by CReaTE is protected by intellectual property law, including copyright law. Any use made of the contents should comply with the relevant law.

Contact: create.library@canterbury.ac.uk



1 **End of the Kiaman Superchron in the Permian of SW England:**
2 **Magnetostratigraphy of the Aylesbeare Mudstone and Exeter**
3 **groups.**

4 Mark W. Hounslow*¹, Gregg McIntosh², Richard A. Edwards³, Deryck J. C. Laming⁴,
5 Vassil Karloukovski¹

6 ¹*Lancaster Environment Centre, Lancaster University, Lancaster, LA1 4YW, U.K.*

7 ²*School of Human and Life Science, Canterbury Christchurch University, Canterbury, UK.*

8 ³*Hawkrigde, Thorverton, Devon, EX5 5JL, U.K (formerly British Geological Survey, Exeter, UK)*

9 ⁴*Herrington Geoscience and David Roche GeoConsulting, Renslade House, Bonhay Road,*
10 *Exeter EX4 3AY, Devon, UK.*

11
12 *Corresponding author (e-mail: m.hounslow@lancaster.ac.uk :Tel:+ 44 (0) 1524 510238

13 Number of: words of text (=8223), words in captions (=1140), references (=103), Tables (=1)
14 and figures (=11)

15 Abbreviated title (< 40 characters) : **Kiaman Superchron, SW England**

16 Keywords: **Magnetostratigraphy, Permian, Triassic, Kiaman Superchron, Rotliegend**

17
18 **Abstract:** The chronology of Permian strata in SW England is fragmentary and largely based on
19 radiometric dating of associated volcanic units. Magnetostratigraphy from the ~2 km of
20 sediments in the Exeter and Aylesbeare Mudstone groups was undertaken to define a detailed
21 chronology, using the end of the Kiaman superchron, and the overlying reverse and normal
22 polarity in the Middle and Upper Permian as age constraints. The palaeomagnetic directions are
23 consistent with other European Permian palaeopoles, with data passing fold and reversal tests.
24 The end of the Kiaman superchron (in the Wordian) occurs in the uppermost part of the Exeter
25 Group. The overlying Aylesbeare Mudstone Group is early Capitanian to latest Wuchiapingian in
26 age. The Changhsingian and most of the Lower Triassic is absent. Magnetostratigraphic
27 comparison with the Southern Permian Basin shows that the Exeter and Aylesbeare Mudstone
28 groups are closely comparable in age to the Havel and Elbe Subgroups of the Rotliegend II
29 succession. The Altmark unconformities in these successions appear similar in age as the
30 sequence boundaries in SW England, indicating both may be climate controlled. Clasts in the
31 Exeter Group, from unroofing of the Dartmoor granite, first occurred at a minimum of ~8 Ma
32 after formation of the granite.

33

34 **Supplementary material:** Additional magnetic fabric and palaeomagnetic data is available at:
35 <http://www.geolsoc.org.uk/SUP000>
36

37 Permian and Triassic successions in southern and SW England were produced following the
38 Variscan orogeny and occur in a number of interconnected, sag and fault-bounded basins, the
39 largest being the Wessex Basin, and various sub-basins that form the Channel Approaches Basin.
40 Some basins contain up to 8 km of post-Variscan red-bed fill (Harvey *et al.* 1994; Hamblin *et al.*
41 1992; Butler 1998; McKie & Williams 2009; Fig. 1). The Wessex Basin formed on Rheno-
42 Hercynian basement (Variscan), between the Northern Variscan Front and the Lizard-Rhenish
43 Suture. The sub-basins of the Western Approaches Basin formed on Saxo-Thuringian (Variscan)
44 and Rheno-Hercynian basement (McCann *et al.* 2006; Strachan *et al.* 2014). As such, these
45 basins may share similar tectonic and stratigraphic histories with similarly situated basins in
46 France and Germany such the Saar-Nahe and Saale basins in Germany (Roscher & Schneider
47 2006; McCann *et al.* 2006.). However, our tectono-stratigraphic understanding of the UK basins
48 is poorly integrated into the framework of European Permian basin evolution. These
49 intramontane basins often lack the distinctive late Permian carbonate-evaporite, Zechstein
50 successions, common in basins (e.g. Southern Permian Basin) north of the Variscan front, and
51 lack the early Permian faunas of the southern Variscan basins (Roscher & Schneider 2006;
52 McCann *et al.* 2006).

53

54 The onshore Permian-Triassic successions in the western parts of the Wessex Basin and the
55 Credition Trough, outcrop as the Exeter, Aylesbeare Mudstone and Sherwood Sandstone groups
56 (Figs. 1 & 2). The coastal outcrops form part of the Jurassic Coast World Heritage Site (Barton *et al.*
57 2011). The work of the British Geological Survey, related to the re-mapping of the Exeter
58 area (Edwards *et al.* 1997), generated a better regional understanding of the Permian Exeter
59 Group (Gp). The oldest successions outcropping in the Credition Trough (and Torbay area) may
60 extend into the latest Carboniferous (Edwards *et al.* 1997; Leveridge *et al.* 2003). The units
61 below the base of the Whipton Formation (Fm) in the Exeter and Credition Trough area contain a
62 variety of basaltic and lamprophyric lavas and intrusions, whose Ar-Ar and K-Ar ages (291-282
63 Ma) are older than the more tightly constrained Rb-Sr, U-Pb and Ar-Ar ages (at 280 Ma) for the
64 formation of the Dartmoor Granite (Scrivener 2006). These volcanic and igneous units are coeval
65 with widespread volcanic activity throughout Europe during the latest Carboniferous to early
66 Permian (Timmerman 2004). The isostatic uplift and regional denudation coeval with, and
67 following, Dartmoor Granite emplacement, was probably responsible for a major unconformity
68 (Edwards *et al.* 1997) separating the Whipton Fm from the older units (Fig. 2).

69

70 Miospores from the Whipton Fm around Exeter, and younger units equivalent to the Alphington
71 and Heavitree Breccia formations, demonstrate similarities to assemblages from the Russian
72 Kazanian and Tatarian regional stages (Warrington & Scrivener 1990; Edwards *et al.* 1999).
73 Consequently, the barren overlying Aylesbeare Mudstone Gp has been assigned to the Lower
74 Triassic in some subsequent studies (Newell 2001; Benton *et al.* 2002). Since the Aylesbeare
75 Mudstone Gp is widespread in the Wessex Basin and the western approaches (Hamblin *et al.*
76 1992; Butler 1998; Evans 1990; Barton *et al.* 2011), a Lower Triassic mudstone-dominated
77 lacustrine unit creates a major palaeogeographic problem. That is, southerly-derived clasts in the
78 Lower Triassic units, in central and Northern Britain, could not have been sourced through the
79 Wessex Basin, from the Armorican supply areas to the south, as has been widely concluded for
80 over 100 years (Ussher 1876; Thomas 1909; Wills 1970; McKie & Williams 2009; Morton *et al.*
81 2013).

82

83 To resolve this problem, and constrain in detail the age of the Permian successions, we use
84 magnetostratigraphy as a dating tool. The Kiaman (reverse polarity) superchron (KRPS) extends
85 from the mid Carboniferous to the mid Permian, but had ended by the early Wordian (mid
86 Guadalupian), after which reverse and normal polarity intervals (here called the Illawarra
87 Superchron) occur during the remainder of the mid and late Permian, extending into the Triassic
88 (Steiner 2006; Hounslow submitted). We demonstrate for the first time in the UK, the
89 stratigraphic position of the end of the KRPS, and also the polarity pattern through the upper part
90 of these successions (below the Budleigh Salterton Pebble Beds Fm). Our data allows a new
91 understanding of the precise age of these units, which suggests a new relationship to the better-
92 studied successions in the Southern Permian Basin.

93 **Geology and Lithostratigraphy**

94 Excellent exposures of the Exeter and Aylesbeare Mudstone groups occur in a series of cliff and
95 foreshore exposures between Torbay and Budleigh Salterton (Fig. 1). These sediments have
96 maximum burial temperatures of ca. $80\pm 5^\circ\text{C}$ attained during the early Cretaceous, with estimated
97 maximum burial depths of 2 to 2.5 km (Carter *et al.* 1995). Faulting and folding structures in the
98 Wessex Basin are a response to basin inversion, produced by N-S compression, along mostly E-
99 W trending faults, many of which were former extensional structures. The basin inversion took
100 place during the late Cretaceous and early Tertiary (Underhill & Stoneley 1998).

101

102 *Exeter Group*

103 The Exeter Group is predominantly the deposits of a number of alluvial fans, with aeolian dune
104 sandstones dominating in the Dawlish Sandstone Fm, and in some units in the Torbay Breccia
105 Fm (Fig. 2). The coastal successions in Torbay are separated from those north of Oddicombe
106 (Fig. 1) by the Torquay-Babbacombe promontory which was a palaeogeographic feature in the
107 Permian (Laming 1966). Mapping work indicates the Torbay Breccia Fm (Leveridge *et al.* 2003),
108 can be divided into a number of separate breccias units with differing clast contents (unpublished
109 work of DJCL). The Watcombe Fm which is an on-lapping mudstone-rich breccia unit, which
110 north of the Torquay-Babbacombe promontory is unconformably overlain by the Oddicombe
111 Breccia Fm (and the equivalent Paignton breccias south of this). On the coastal outcrops the
112 Watcombe Fm has a 9-20° dip-discordance with the overlying Oddicombe Breccia (9° at
113 Whitsand Bay and 20° at Oddicombe Cove; Figs. 1, 3d; Laming 1982). The lower parts of the
114 Torbay Breccia Fm (Roundham Head breccias, with clasts derived from SW) are generally poor
115 in volcanic clasts (Laming 1982) like the oldest unit (the Cadbury Breccia Fm; Edwards &
116 Scrivener 1999) in the Crediton Trough, and by inference may have similar ages, prior to the
117 early Permian basaltic volcanism.

118

119 The various breccia units below the Dawlish Sandstone Fm are largely distinguished by their
120 clast contents. These contain a variety of lithologies (limestone, sandstone, vein quartz, quartzite
121 and slate) from various Variscan basement units, together with a variety of volcanic rock
122 fragments associated with the granite and its former or earlier extrusives (Laming 1982; Selwood
123 *et al.* 1984; Edwards & Scrivener 1999). The Watcombe and Whipton formations consist of fine-
124 grained sandy or muddy breccia with clasts of slate and sandstone with occasional porphyry.
125 They contain irregularly interbedded sandstone and mudstone units (Ussher 1913), which
126 dominate the Whipton Fm around Exeter (Edwards & Scrivener 1999). The Oddicombe Breccia
127 Fm (Fig. 2) is rich in locally derived limestone fragments, which typically displays fining-up
128 sequences (into poorly sorted sandstones or fine-breccias; Benton *et al.* 2002) several metres
129 thick, well displayed at Maidencombe Cove and Bundle Head (Figs. 1, 4). The Alphington
130 Breccia Fm is likewise rich in locally derived shale and sandstone fragments, and hornfelsed
131 shale from the underlying Variscan basement (Edwards *et al.* 1997). The Teignmouth and
132 Heavitree formations are distinctive in containing common clasts of pink and white perthitic
133 feldspar (murchisonite), which Dangerfield & Hawkes (1969) interpreted as feldspar megacrysts
134 from the roof zone of the Dartmoor granite; the supply of which probably indicates synchronous

135 unroofing into adjacent alluvial fan successions. The older Alphington and Oddicombe Breccia
136 formations lack the murchisonite clasts (Selwood *et al.* 1984; Edwards & Scrivener 1999).

137

138 All the breccia units tend to be poorly sorted, and may locally contain a high proportion of mud
139 or sand. The fining-up successions in the Teignmouth Breccia Fm tend to be smaller scale (< 1 m
140 thickness) and typically display poor lateral organisation. Breccias in the upper-part of this
141 formation have interbedded aeolian sandstone units, well displayed in the Coryton Cove area (8
142 on Fig. 1; Fig. 4); which is a transitional part of this formation into the overlying Dawlish
143 Sandstone Fm. The estimated thicknesses of the Oddicombe and Teignmouth Breccia formations
144 vary widely between different authors, because of faulting, variable bedding dips and probably
145 significant palaeotopography on the Variscan basement. The thicknesses of Selwood *et al.* (1984)
146 are minimum thickness estimates, whereas Laming (1969; 1982) and this work suggest greater
147 thicknesses at the upper limits indicated in Fig. 2.

148

149 The aeolian dune systems that dominate deposition in the Dawlish Sandstone Fm (Newell 2001),
150 also display interbedded fluvial sandstone and breccia units. Around Exeter and further north in
151 the Crediton Trough, the Dawlish Sandstone Fm onlaps onto older units, to rest on Variscan
152 basement. The overlying Exe Breccia Fm is divisible into a lower porphyry-bearing unit (the
153 Kenton Mbr), typical of most of the outcrop on the west of the Exe Estuary, and an overlying
154 quartzite- and mudstone-bearing breccia (the Langstone Mbr). This upper member is well
155 exposed at Langstone Rock (6 on Fig. 1) which in the upper part is dominated by poorly sorted
156 sandstones and sandy siltstones (Gallois 2014; Fig. 4). The thickness of the Exe Breccia is
157 uncertain, due to faulting along the Exe Estuary; 85 m was suggested by Selwood *et al.* (1984),
158 but up to ~50 m is more likely (Laming & Roche 2013). The uppermost part of the Langstone
159 Mbr at Lymphstone and Sowden Lane (3 on Fig. 1) displays both well-developed shallow fluvial
160 channels and aeolian sandstone units, and is gradational into the mudstones and siltstones
161 forming the base of the Aylesbeare Mudstone Gp (Gallois 2014; Fig. 4). Around Exeter and in
162 the Crediton Trough the Aylesbeare Mudstone Gp is unconformable on the Dawlish Sandstone
163 Fm, also onlapping onto older units (Edwards *et al.* 1997; Edwards & Scrivener 1999).

164 *Aylesbeare Mudstone Group*

165 The Exmouth Mudstone and Sandstone Fm is a lacustrine, red-brown mudstone-dominated unit,
166 with interbedded fine to medium-grained fluvial and lacustrine sandstone units (thicker beds

167 labelled as Beds A to J by Selwood *et al.* 1984). These are most prominent towards the upper
168 part of the formation, where the term Straight Point Sandstone Mbr is introduced for these
169 persistent sandstone beds (i.e. beds I and J of Selwood *et al.* 1984). This member is mapped
170 between the coast and Aylesbeare, north of which the Aylesbeare Mudstone Gp is not sub-
171 divided (Edwards & Scrivener 1999). The upper few metres of the Straight Point Sandstone Mbr
172 at outcrop has patchily developed, immature, nodular and sheet-like groundwater calcretes,
173 locally with rhizoconcretions (Fig. 3B). The base of the overlying Littleham Mudstone Fm is
174 taken at the base of the porphyry and murchisonite bearing breccia unit (Ormerod-Wareing
175 1875), which locally erosively overlies this calcrete-bearing sandstone (Fig. 3C), and grades into
176 overlying interbedded sandstone, siltstone and mudstone beds in the basal parts of the Littleham
177 Mudstone Fm, west of the Littleham Cove fault (Fig. 5).

178

179 The Littleham Mudstone Fm is well-exposed in the cliffs between Littleham Cove and Budleigh
180 Salterton, but is locally disrupted by faulting in the lower part and landslips in the cliff. The
181 complete succession in the cliffs was determined by using a montage of photographs taken from
182 offshore, which shows the full succession is divided by a number of prominent green mudstone,
183 thin sandstone and siltstone beds (Fig. 5). The succession in the cliffs can be divided into three
184 units, a lower unit (Division A) east of the Littleham Cove fault with a few green mudstone beds,
185 a middle unit (Division B) with relatively common sandstone and siltstone beds, and an upper
186 unit (Division C) with more frequent green mudstone beds and some impersistent sandstones.
187 The true thickness of the Littleham Mudstone Fm, in these outcrops, cannot be determined
188 because of the uncertain displacement on the Littleham Cove fault. However, the measured
189 cumulative thickness east and west of the fault (216 m), is similar to the ~205 m and 230 m
190 measured in the Blackhill and Withycombe Rayleigh boreholes respectively (Bateson & Johnson
191 1992; Fig. 1), so the cliff outcrops probably represent most of the Littleham Mudstone Fm. In the
192 Venn Ottery borehole (Fig. 1) the Littleham Mudstone Fm contains pods and veins of gypsum,
193 and thin interbedded aeolian sandstones (Bateson & Johnson 1992; Edwards & Scrivener 1999;
194 N.S Jones pers comm to RAE). A substantial unconformity separates the Littleham Mudstone Fm
195 from the overlying Budleigh Salterton Pebble Beds Fm, shown by the dramatic lithology change,
196 and the sharp and irregular boundary (Fig. 3A) with some authors suggesting a small bedding dip
197 difference (Irving, 1888). Gallois (2014) has suggested this contact is conformable.

198 *Regional relationships*

199 Broadly the Permian units in the study area can be divided into 5 genetic sequences (Pm1 to
 200 Pm5), bounded by a hiatus or unconformity (Fig. 2). The upper three of these are all
 201 characterised by basal breccias units (low stand deposits), with conformable transitions into
 202 overlying finer-grained upper parts. The relationships of the successions in Torbay to those in the
 203 Crediton Trough area is less certain. It is probable that the earliest parts of the Torbay Breccia
 204 Fm is timing-related to the Cadbury Breccia Fm in the Crediton Trough (sequence Pm1), since
 205 both units are very poor in igneous clasts (Edwards *et al.* 1997). These five sequences may relate
 206 to the four sequences (A to D) seen in the Plymouth Bay Basin (Harvey *et al.* 1994). Their oldest
 207 megasequence A likely relates to Pm1 and megasequence B to Pm2, since it is capped by an
 208 inferred volcanic unit. Megasequence C likely relates to Pm3, and is marked by a change in
 209 orientation of the Plymouth Bay Basin depocentres. Divergent bedding dips between units under
 210 and overlying the Watcombe Fm (Pm2), suggest that the most important extensional event
 211 (Leveridge *et al.* 2003; Laming 1982) is at the Pm2-Pm3 boundary, consistent with depocentre
 212 orientation change in the Plymouth bay basin. Megasequence D is probably equivalent to Pm4
 213 and Pm5, since the Pm4-Pm5 boundary is subtle to detect in the field.

214
 215 The continuity of these units to the east in the central parts of the Wessex Basin is uncertain.
 216 Henson (1972) suggested, based on geophysics, that the breccia units thin to the east, so
 217 eastwards the breccias may pass into the mudstone dominated units, equated with the Aylesbeare
 218 Mudstone Gp in the central parts of the Wessex Basin, which are up to ~1.5 km thick (Butler
 219 1998; Hamblin *et al.* 1992). However, Henson's data failed to detect the faults, along the Exe
 220 Estuary, so the interpretation may be flawed. In the Western Approaches basins 1 km or more of
 221 anhydritic mudstones and sandstones underlie the equivalent of the Sherwood Sandstone Gp
 222 (Evans 1990). These locally rest on a Permian volcanic sequence, presumably of a similar age to
 223 the early Permian Exeter Volcanic Rocks (Chapman 1989; Fig. 2).

224 **Palaeomagnetic sampling**

225 Almost the entire succession of the Aylesbeare Mudstone Gp is exposed in the sea-cliffs between
 226 Budleigh Salterton and Exmouth. Only the mid and upper parts of the Exe Breccia could be
 227 sampled at Lypstone (location 3 on Fig.1) and Langstone Rock (6 on Fig. 1; see Supplementary
 228 data for details). Outcrops in the lower parts of the Exe Breccia Fm (Kenton Mbr), were all too
 229 coarse-grained for palaeomagnetic sampling. Most of the Dawlish Sandstone and Teignmouth

230 Breccia are well exposed between Langstone Rock and Teignmouth, adjacent to the main
231 London-Penzance railway-line (Ussher 1913; Selwood *et al.* 1984), but large parts are
232 inaccessible due to rail-safety restrictions. The Dawlish Sandstone Fm was sampled in quarries
233 near Exeter (4 and 5 on Fig. 1; Fig. 4). The uppermost part of the Teignmouth Breccia was
234 available for sampling in the Coryton Cove and Dawlish Station sections (7 and 8 on Figs. 1, 4).
235 Reconnaissance sampling of the Oddicombe and Watcombe Breccias was undertaken. For the
236 most part, these units are fully exposed in sea-cliffs and foreshore exposes between Teignmouth
237 and Oddicombe (Fig. 4). The Knowle Sandstone Fm was sampled at west Sandford (Edwards *et*
238 *al.* 1997).

239

240 Samples from these units were collected using mostly hand samples, oriented with a compass. In
241 total some 153 samples were collected from 13 sites (see Supplementary data), largely focussed
242 on reddened lithologies. Cubic specimens were cut from the hand samples using a circular saw.
243 Some samples from sandstone units in the Dawlish Sandstone and Exe and Teignmouth Breccias
244 were poorly consolidated, and impregnated in the laboratory with a 2:1 mix of sodium silicate
245 and water (Kostadinova *et al.* 2004) to consolidate them prior specimen preparation.

246 **Laboratory Methodology**

247 Measurements of Natural Remanent Magnetisation (NRM) were made using a CCL 3-axis
248 cryogenic magnetometer (noise level ~ 0.002 mA/m), using multiple specimen positions, from
249 which the magnetisation variance was determined. The magnetometer is not housed in a
250 controlled space which cancels the earth's magnetic field. Instead specimens were housed in Mu-
251 metal boxes with an ambient magnetic field < 10 nT at all times, other than when being measured
252 or demagnetised. Generally, 1 to 3 specimens from each sample were treated to stepwise thermal
253 demagnetisation, using a Magnetic Measurements Ltd thermal demagnetiser, in 50-40°C steps up
254 to 700°C. Low frequency magnetic susceptibility (K_{lf}) was monitored after heating stages,
255 measured using a Bartington MS2B sensor. Specimens from the Bishops Court Quarry gave poor
256 quality results and sister specimens were partly treated with a combination of thermal and
257 alternating field (AF) demagnetisation, the latter conducted using a Molspin tumbling AF
258 demagnetiser. In total 166 and 78 paleomagnetic specimens were demagnetised from the
259 Aylesbeare Mudstone and Exeter groups respectively. The bedding dips in the Aylesbeare
260 Mudstone Gp are 5-10° in an easterly direction, so a fold test was not possible. However, in the
261 Exeter Gp dips are more variable and up to 40°, so a fold-test was possible.

262
263 Characteristic remanent magnetisation (ChRM) directions were isolated using principal
264 component-based statistical procedures as implemented in LINEFIND, which uses the
265 measurement variance along with rigorous statistical procedures for identifying linear and planar
266 structure in the demagnetisation data (Kent *et al.* 1983). Both linear trajectory fits and great
267 circle (remagnetisation circle) data were used in defining the paleomagnetic behaviour, guided by
268 objective and qualitative selection of the excess standard deviation parameter (ρ), which governs
269 how closely the model variance, used for analysis, matches the data measurement variance (Kent
270 *et al.* 1983). The PMAGTOOL software (available at
271 <https://www.lancs.ac.uk/staff/hounslow/default.htm>) was used for the analysis of mean directions
272 and virtual geomagnetic poles.

273
274 Progressive isothermal remanent magnetisation (IRM) up to 1T is most and 4 T is some was
275 applied to a representative sub-set of specimens, to investigate the magnetic mineralogy. Back
276 field demagnetisation was also used on some specimens. This used an ASC Scientific IM-30
277 impulse magnetiser and a Molspin pulse magnetiser. The IRM was measured using a Molspin
278 spinner magnetometer. Thermal demagnetisation of a three component IRM was used to
279 investigate the unblocking temperatures (Lowrie 1990). A small set of specimens were measured
280 for magnetic hysteresis (maximum field 0.9 T) and thermomagnetic curves (maximum field 300
281 mT, in air using a Magnetic measurements variable field translation balance, MMVFTB).
282 Selected thin sections were investigated to assess the petrography of the Fe-oxides. The
283 anisotropy of magnetic susceptibility (AMS), of selected specimens, was measured using an
284 Agico KLY3S Kappameter, to assess the preservation of the detrital sedimentary fabric (Løvlie
285 & Torsvik 1984; Tarling & Hrouda 1993), and to assess if fabrics had been modified by the weak
286 tectonism.

287 **Magnetic Mineralogy**

288 Changes in the NRM intensity and K_{if} of specimens are broadly related to:

- 289 a) The amount of silt and clay, with those samples having larger amounts of silt and clay
290 generally having larger NRM intensity and K_{if} . For example, aeolian sandstones such as
291 those in the Dawlish Sandstone Fm, have significantly lower NRM intensity and K_{if} (Fig. 5,
292 see Supplementary data). In the Aylesbeare Mudstone Gp red mudstones possess average

293 NRM intensity and K_{if} of 5.0 mA/m and 20.0×10^{-6} SI respectively, compared to means of 1.8
 294 mA/m and 7.2×10^{-6} SI in the red sandstone beds.

295 b) Reddened and non-reddened samples of the same lithology often possesses dramatically
 296 different NRM intensity and K_{if} ; with the non-reddened samples typically having lower
 297 values. For example grey, green and white sandstones in the Aylesbeare Mudstone Gp have
 298 mean NRM intensity and K_{if} of 0.9 mA/m and 4.4×10^{-6} SI respectively.

299 c) The average NRM intensity and K_{if} shows progressively larger values into the Oddicombe
 300 Breccia and Watcombe formations (see supplementary data). This may relate to a progressive
 301 increase in volcanic-derived detritus (and iron oxide content) in the older units, which is
 302 shown by the Cs content (Merefield *et al.* 1981).

303

304 Specimens analysed do not saturate in IRM fields up to 4 T (Fig. 6A, C), indicating that canted
 305 antiferrimagnetic minerals (haematite or goethite) are important magnetic minerals in these
 306 specimens. Durrance *et al.* (1978) also detected haematite as the main Fe-oxide in the Littleham
 307 Mudstone Fm, with the addition of significant amounts of superparamagnetic haematite.
 308 Thermomagnetic curves were nearly reversible and exhibited Curie temperatures of 657-669°C,
 309 and thermal demagnetisation of the IRM, shows that specimens display blocking temperatures up
 310 to 650-700°C (Fig. 6). Coercivity of remanence (B_{cr}) ranged between 320 and 710 mT, all
 311 suggesting predominant haematite (Frank & Nowaczyk 2008). Although the IRM does not
 312 approach saturation by 4 T (Fig. 6B), there is no clear evidence for goethite, since we have high
 313 SIRM/ K_{if} values, and no well-defined Neel temperature for goethite. Percent IRM acquisition
 314 below 100 mT ($\%IRM_{100mT}$) is mostly 5%-10% of the 1T IRM, for reddened lithologies. Only in
 315 aeolian sandstone units in the Dawlish Sandstone Fm, and grey or red mottled green/grey
 316 lithologies does the $\%IRM_{100mT}$ rise above 10% to ca. 50% at maximum (Fig. 6A,C,E). Data
 317 from synthetic mixtures (Frank & Nowaczyk 2008) suggest such $\%IRM_{100mT}$ values indicate a
 318 magnetite contribution to the iron oxide load of ca. 0.05% (for red lithologies) to a maximum of
 319 ca. 1% for aeolian samples DS16 and DS100 (Fig. 6E). In specimens DS16, (from Dawlish
 320 Sandstone Fm aeolian sandstones; Fig. 6F) and L3 (grey sandstone, Littleham Mudstones Fm;
 321 Fig. 6B) the 100 mT IRM demagnetises by 450°C- 550°C, which could suggest an oxidized, or
 322 Ti-poor magnetite (Fig. 6F). The >300 mT coercivity component in specimen DS16 has a
 323 blocking temperature of ~550°C, probably due to a pigment-dominated haematite remanence
 324 (Turner 1979) in this sample.

325

326 Petrography indicates, like other red-beds, that the haematite is present as two phases, firstly sub-
 327 micron haematite (pigmentary haematite), which coats pore perimeters and is often internal to
 328 some rock clasts; secondly as larger specular haematite particles, most obvious as detrital opaque
 329 grains (Turner 1979; Fig. 3E, F). The pore-lining pigmentary haematite is multiphase in origin,
 330 since it both coats feldspar overgrowths, and to a lesser extent, coats the grains prior to the
 331 overgrowths (observed in Dawlish Sandstone Fm only). Compaction related pressure solution at
 332 some grain contacts, shows greater amounts of pigment coating the pores, and lesser amounts
 333 between the grain contacts, demonstrating both pre and post-compaction pigmentary haematite
 334 formation, with probably the bulk of the pigment produced post compaction. Some of the
 335 pigmentary haematite may have formed pre-deposition, since it is widely dispersed within a
 336 variety of siltstone and phyllite clasts.

337

338 The specular haematite is dominated by detrital opaques, which are either present as haematite
 339 dominated particles, or compound particles in-part composed of other silicate minerals. The
 340 compound particles are occasional haematised clastic rock fragments (intraformational?) but
 341 most are of uncertain origin (Fig. 3E). These two types of specularite grains vary in abundance
 342 from about 1% to trace amounts. Larger amounts of detrital opaques tend to occur in samples that
 343 are finer-grained or less well sorted, and lesser amounts in the well-sorted aeolian sandstones.

344 **Magnetic Fabric**

345 The anisotropy of magnetic susceptibility (AMS) overall shows a primary depositional magnetic
 346 fabric, characterised by vertical-to-bedding K_{\min} directions (Figs. 7 a-d) and largely oblate ($T > 0$)
 347 fabrics (Figs. 7 e - h). The mudstones have the stronger AMS (greater P values) and are always
 348 oblate. The sandstones within the Aylesbeare Mudstone Gp and the various breccia units show
 349 more variable AMS fabrics ranging into the prolate fields ($T < 0$), especially so for some
 350 sandstones from the breccia units (Fig. 7e, h). This may relate to the more poorly sorted,
 351 probably more chaotically deposited grains in the breccia units (possibly related to mudflow
 352 deposition, *cf.* Park *et al.* 2013). K_{\max} axis trends (Figs. 7i) for specimens from the breccia units
 353 (Fig. 7i) show both N-S trends and ENE-WSW trends similar to the clast imbrication directions
 354 (typically between easterly and northerly directions) of Laming (1982) and Selwood *et al.*
 355 (1984). This demonstrates the K_{\max} directions parallel the fluvial transport directions. The N-S
 356 directed K_{\max} axes trends are common near the Babbacombe-Torquay promontory and in the
 357 Teignmouth Breccia Fm. Similar easterly and northeasterly K_{\max} axes trends are present in the

358 Exmouth Sandstones and Mudstones, whereas those in the Littleham Mudstone Fm are more
359 variable.

360

361 Specimens from aeolian sandstones (from the Dawlish Sandstone Fm and upper part of the
362 Teignmouth Breccia Fm) show a larger proportion of prolate fabrics ($T < 0$) with many more K_{\min}
363 axes deviating from vertical (Figs. 7c, g). This may be partly caused by the AMS in these
364 specimens being closer to the sensitivity limits of the KLY3S. However, it is also a reflection of
365 the rolling grain transport on the leeward slip-faces of the aeolian dunes (Ellwood & Howard
366 1981), producing a grain long-axis orientation transverse to the average wind direction
367 (Schwarzacher 1951), which was to the NW to NNW (Laming 1982; Newell 2001). This is
368 clearly shown in the specimens from the Bishops Court Quarry in which the K_{\max} axes are
369 transverse to the aeolian foresets (Edwards & Scrivener 1999).

370 **Mineralogical origin of magnetic properties**

371 In summary, the magnetisation in these units is carried dominantly by haematite, with a likely
372 large range of grain size from superparamagnetic (pigmentary) haematite to larger (specularite)
373 particles of remanence carrying haematite. Magnetite may make a trace contribution. A strong
374 control on the concentration of haematite is related to the clay and silt content, and perhaps also
375 the concentration of volcanic rock detritus. The pigmentary haematite appears to have a
376 multiphase origin, ranging from possible pre-deposition to late diagenetic, a typical feature of
377 European Permian red beds (Turner *et al.* 1995; 1999). Largely detrital, specular haematite,
378 varies in amounts relating to the degree of sediment sorting and the sediment supply. In the
379 breccia units the maximum susceptibility axes reflect palaeocurrent-parallel trends, shown by
380 clast imbrication directions. In aeolian transported sediments, the transverse trends in K_{\max} axes
381 reflect lee-face transport on dune slip faces. In the lacustrine mudstones the K_{\max} directions may
382 represent wave-produced (or perhaps wind-related?) grain orientations in the lake playa systems
383 hence, the AMS shows a primary depositional fabric (unaffected by tectonism), probably carried
384 mostly by haematite.

385 **Palaeomagnetic Results**

386 The majority of the 250 specimens demagnetised show little change in K_{If} during
387 demagnetisation, although the mudstones (particularly from the Littleham Mudstone Fm) tend to
388 show alteration at $>600^{\circ}\text{C}$, with lower temperature alteration in some specimens (Fig. 6). In some

389 specimens, this alteration obscures the recovery of the remanence at higher demagnetisation
390 temperatures.

391

392 Demagnetisation isolates two remanence components. Firstly, a positive, often northerly, steeply
393 inclined component (Component A), between room temperature and often up to 350°C, but
394 sometimes up to 500-600°C (Fig. 8). This component is more northerly in specimens from the
395 Aylesbeare Mudstone Gp (Fisher mean, 005°, +59°, $k=7.7$, $N_s=135$), but more southerly in
396 specimens from the Exeter Gp (Fisher mean, 010°, +82°, $k=6.7$, $N_s=44$; see supplementary data).
397 This component is more prevalent in the Aylesbeare Mudstone Gp (79% of specimens) compared
398 to the Exeter Gp (56% of specimens), in which it is most prevalent in specimens from the
399 Dawlish Sandstone Fm. It does not correspond in direction particularly well to the expected
400 modern dipole field (i.e. inclination of 68°) and probably represents a composite component
401 comprising mostly a Brunhes (viscous?) magnetisation plus the characteristic remanence. In 10%
402 of samples from the Aylesbeare Mudstone Gp, this was the only component present. In the
403 Exeter Gp 15% of specimens are dominated by this component, the bulk of these being from the
404 Dawlish Sandstone Fm.

405

406 A second component is recognised between about 400 and 650-700 °C that is a northerly,
407 positively inclined or southerly, negatively inclined direction (Fig. 8), interpreted as the
408 characteristic remanence (ChRM). In the Littleham Mudstone Fm the unblocking temperature
409 range of this component is mostly above 500°C- 600°C, whereas in specimens from the Exeter
410 Gp, the unblocking of the ChRM often starts at temperatures of ~400°C. Some 52% of specimens
411 (49% in Aylesbeare Mudstone Gp and 57% in Exeter Gp) had suitable linear trajectory ChRM
412 line fits (here termed 'S-type' data; Fig. 8). This S-type demagnetisation behaviour was visually
413 classified into three quality classes, S1, S2 and S3 (Figs. 8, 9). The mean α_{95} linear fits and ρ for
414 these classes indicate the generally larger model variance required to accommodate the less
415 quality line-fits (see supplementary data). Average confidence cone angles for these line-fit
416 classes vary from 3.2 to 13.9°. The mean directions for the ChRM line-fits pass the reversal test
417 (McFadden & McElhinney 1990), for all except those from the Littleham Mudstone Fm (Table 1;
418 Fig. 9a).

419

420 Some 28% of specimens displayed great circle trends, of varying arc length, towards interpreted
421 Permian reverse and normal polarity directions (here referred to as T-type demagnetization

422 behaviour; Fig. 8). This T-type behaviour was visually classified into three quality classes, T1,
423 T2 and T3, based on the visual length and scatter of the demagnetisation points about the great
424 circle, with T1 being the best quality. The mean α_{95} for the poles to the fitted planes, for these
425 three data classes range from 9 to 20° (see supplementary data). These great circle fits included
426 the origin in 67% of these cases.

427

428 Data from the Dawlish Sandstone Fm yield the least well-defined results, particularly those from
429 Bishops Court Quarry, which are dominated by component A. These samples also display mainly
430 low blocking temperatures (i.e. the NRM is largely demagnetised by ~500°C). Some specimens
431 from this locality could be AF demagnetised, indicating that either these sandstones originally
432 had no haematite, or more likely a substantial proportion of haematite had been removed,
433 possibly by Quaternary ground water flow (e.g. Johnson *et al.* 1997). Notably, those samples that
434 did not retain a ChRM generally lacked specular haematite particles in thin section, whereas
435 samples of aeolian sandstone which possessed a ChRM often possessed specularite in small
436 amounts. Hence, the poor palaeomagnetic behaviour in the Bishops Court Quarry samples is due
437 to a paucity of specularite, and the dominance of pigment-dominated magnetisations, like
438 Permian aeolian sandstones such as the Penrith Sandstone (Turner *et al.* 1995).

439 **Mean directions and paleopoles**

440 As well as the conventional means using the ChRM directions (Fig. 9), mean directions were also
441 determined using ‘specimen-based’ means, by combining the great circle paths with the specimen
442 line-fit ChRM (Table 1), to produce combined means using the method of McFadden &
443 McElhinney (1988). This method determines a mean direction, by including the ‘fixed-point’
444 ChRM directions, and those points on the projected great circles, which maximise the resultant
445 length (i.e. points on the great circle which are closest to the combined mean direction). These
446 means are broadly similar to the line-fit ChRM means, except that for the Dawlish Sandstone and
447 Exe Breccia, which have steeper inclination and greater dispersion (Table 1). The great-circle
448 combined means pass the reversal test for the Littleham Mudstone Fm, Exmouth Mudstone and
449 Sandstone Fm, and Dawlish Sandstone plus Exe Breccia formations (Table 1). Using the line-fit
450 ChRM directions alone, the combined mean directions for the Aylesbeare Mudstone and Exeter
451 groups pass the reversal test (Table 1).

452

453 The S-class ChRM directions for the Exeter Gp, pass the fold test, indicating the pre-folding
 454 nature of the magnetisations (Fig. 9b). The fold test of McFadden (1990) produced an f-statistic
 455 ($F [6,82]$) of 1.90. Likewise, these data pass the DC fold test of Enkin (2003), with best
 456 unfolding at 93.5%, with a 95% confidence interval of $\pm 25.2\%$. A progressive unfolding test
 457 (Watson & Enkin 1993) indicated best unfolding at 78%, with 95% confidence intervals on the
 458 percent unfolding of 34% to 114% (Fig. 9b).

459

460 The virtual geomagnetic pole (VGP) data is consistent with other Permian data from stable-
 461 Europe, confirming the Permian age of these magnetisations. The mean direction for the Exeter
 462 Gp produces a virtual geomagnetic pole (VGP) similar to stable-Europe sediments from the
 463 youngest part of the KRPS (see Supplementary Data), although the mean is slightly to the east of
 464 the European apparent polar wander path of Torsvik & Cocks (2005). The Exeter Volcanic
 465 Rocks VGP of Zijdeveld (1967) is similar to that from the Aylesbeare Mudstone Gp (Table 1),
 466 whereas the VGP pole for the Exeter Gp sediments from this study, is displaced slightly more to
 467 the east (see Supplementary Data).

468 **Magnetostratigraphic Interpretation**

469 The line-fit ChRM directions from the Aylesbeare Mudstone Gp (and Exe Breccia Fm) were
 470 converted to virtual geomagnetic pole (VGP) latitude using the line-fit ChRM mean in Table 1
 471 (Figs. 10a,b (iii)). For those specimens that had no line-fit, the point on their great circle nearest
 472 this mean, were used for calculating the VGP latitude (Fig. 10). All specimens were also
 473 assigned a polarity quality (Fig. 10a,b (ii)) based on the quality of demagnetisation behaviour
 474 and, if from T-class specimens, the length and end point position of the great circle trend (similar
 475 to the procedures used by Ogg & Steiner 1991; Hounslow & McIntosh 2003). One specimen of
 476 good-quality polarity (i.e. S-Type) was sufficient to define the horizon polarity, whereas with
 477 specimens of poorer quality at least two are required (Figs. 4, 10). Some 12% of specimens failed
 478 to yield data which could be used to determine horizon polarity (10% in Aylesbeare Mudstone
 479 Gp, 15% in Exeter Gp) and eight horizons failed to yield any specimens which could reliably be
 480 used to determine magnetic polarity (Figs. 4, 5). Most of these are from sandstones, with most of
 481 these in the Dawlish Sandstone Fm at Bishops Court Quarry (Fig. 4).

482

483 All the samples collected from below the Exe Breccia Fm are of reverse polarity, with those
 484 sections situated stratigraphically above the Langstone Rock outcrop having both reverse and

485 normal polarity (Figs. 4, 5). The single sample from the Knowle Sandstone Fm (Fig. 2; Table 1)
486 likewise confirms the reverse polarity results from the age-equivalent Exeter Volcanic Rocks
487 found by Creer (1957), Zijderveld (1967) and Cornwall (1967). Significantly, two sites in the
488 Torbay Breccia Fm sampled in the reconnaissance study of Cornwall (1967) produced reverse
489 polarity, suggesting that reverse polarity probably dominates to the base of the Exeter Gp.

490

491 Major magnetozone reverse and normal couplets have been numbered (Fig. 10) from the base of
492 the first normal polarity samples in the Exe Breccia Fm, using the prefix EA (for Exeter-
493 Aylesbeare). The magnetic polarities of six magnetozones are defined with multiple specimens
494 from a single sampling horizon (EA3n.1r, EA3n.2r, EA5n.1r), and EA3r.1n is defined with a
495 single specimen of S-class behaviour (Fig. 10b).

496 **Discussion**

497 The major geomagnetic polarity marker in the Permian is the end of the Kiaman reverse polarity
498 Superchron, which has been comprehensively studied since the 1950's in Russian successions
499 (Molostovsky 1983; Burov *et al.* 1998). Studies on marine fossil-bearing rocks which
500 demonstrate the end of the Kiaman superchron are discontinuous studies in the SW USA (Steiner
501 2006), and Japan (Kirschvink *et al.* 2015), along with studies on successions in China (Steiner *et*
502 *al.* 1989; Embleton *et al.* 1996). The overlying reverse and normal polarity Illawarra Superchron,
503 has been investigated in marine successions in the Salt Range in Pakistan, China and Iran (Haag
504 & Heller 1991; Gallet *et al.* 2000; Jin *et al.* 2000; Steiner 2006), along with flood-basalts in
505 China (Ali *et al.* 2002; Zheng *et al.* 2010). Studies on non-marine rocks from the Illawarra
506 Superchron have been extensive in Russia, on outcrop and borehole material (Molostovsky 1983;
507 Burov *et al.* 1998) and core material from the Southern Permian Basin (Menning *et al.* 1988;
508 Nawrocki 1997; Turner *et al.* 1999; Lawton & Roberson 2003; Szurlies 2013). These studies
509 together allow the magnetic polarity stratigraphy (Fig. 11) to be defined through the Roadian to
510 Changhsingian (Steiner 2006; Hounslow submitted). The base of the Illawarra superchron is in
511 the lower to mid Wordian, based on magnetostratigraphic data from the Grayburg Fm in Texas
512 and New-Mexico (Steiner 2006) and limestones from Japan (Kirschvink *et al.* 2015).

513

514 Magnetostratigraphic studies in the southern Permian Basin well Mirow 1/1a/74 (Menning *et al.*
515 1988; Langereis *et al.* 2010), and wells in Poland (Nawrocki 1997) show a long-duration reverse
516 polarity interval (equivalent to MP3r –UP1r interval), with under and overlying mixed polarity-

517 intervals (Fig. 11). The normal magnetozones in the Lower Drawa Fm and Havel Subgroup are
 518 probably equivalent with the MP1n to MP3n interval in the GPTS of Hounslow (submitted).
 519 Equivalent normal magnetozones in the Notec and Hannover formations, are more fully
 520 expressed by studies of the Lower Lemn Sandstone, from the Johnston and Jupiter field in the
 521 southern North Sea (Turner *et al.* 1999; Lawton & Roberson 2003; Fig. 11). These correlations
 522 are constrained by the overlying Zechstein, and indicate that the Zechstein successions are
 523 entirely Changhsingian in age, rather than as old as early Wuchiapingian, as suggested by the
 524 conodonts *Merrillina divergens* and *Mesogondolella britannica* (Korte *et al.* 2005; Legler *et al.*
 525 2005; Słowakiewicz *et al.* 2009), and the synthesis of Szurlies (2013). Like the
 526 magnetostratigraphic interpretation here (Fig. 11), Sr-isotope data indicates a short duration for
 527 the Zechstein of ~ 2 Ma, with a likely age range of 255-251.5 Ma, placing it firmly in the
 528 Changhsingian (Denison & Peryt 2009). Attempts at dating the Kupferschiefer at the base of the
 529 Zechstein (Z1 cycle) have failed to yield consistent results, with Re-Os ages giving wide 95%
 530 confidence intervals (Pašava *et al.* 2010).

531

532 Four pieces of information have allowed the Exeter Gp succession to be assigned to the Permian.

- 533 1) Volcanic units interbedded with the Knowle Sandstone of the Exeter area, and similar units
 534 equivalent to the Thorverton Sandstone and Bow Breccia in the Crediton Trough, have Ar-Ar
 535 ages of 291- 282 Ma (Edwards & Scrivener 1999). Volcanic clasts in the breccia units give
 536 Ar-Ar dates of 280 Ma. This suggests the volcanism and associated interbedded sediments
 537 are late Sakmarian through to late Artinskian in age, using the timescale of Henderson *et al.*
 538 (2012).
- 539 2) The Dartmoor Granite has Rb-Sr, U-Pb and Ar-Ar ages of 280 ±1 Ma (Scrivener 2006),
 540 placing its formation in the latest Artinskian (timescale of Henderson *et al.* 2012). Clasts of
 541 the granite begin to occur in the unroofing succession of the Teignmouth and Heavitree
 542 Breccias (Dangerfield & Hawkes 1969; Edwards *et al.* 1997), indicating that these breccias
 543 were deposited several millions years after the granite formation, in order to allow time for
 544 granite unroofing.
- 545 3) Miospore assemblages containing *Lueckisporites virkkiae*, occur from the Whipton Fm,
 546 around Exeter, but also in younger units in the Crediton Trough, equivalent to the Alphington
 547 and Heavitree Breccias (Edwards *et al.* 1997). Assemblages containing this miospore are
 548 widespread in European Zechstein deposits and similar 'Thuringian' and Russian Tatarian-
 549 age assemblages (Visscher 1973; Utting 1996). In the northern hemisphere, *Lueckisporites*

550 *virkkiae* has its first appearance in the latest Kungurian (Shu 1999; Mangerud 1994) to early
 551 Roadian (lower Kazanian in Russia; Utting 1996), but occurrences range into the latest
 552 Changhsingian.

553 4) The foot-print trace-fossil *Cheilichnus bucklandi*, found in the Dawlish Sandstone near
 554 Exeter (Edwards *et al.* 1997) suggests equivalence to the Germanic 'Rotliegend' (McKeever
 555 & Haubold 1996). However, this genus is restricted to aeolian dune units and is probably
 556 only vaguely indicative of the Permian (Lucas & Hunt 2006).

557

558 Constraints on the youngest possible age of the Aylesbeare Mudstone Gp are
 559 magnetostratigraphy and vertebrate fossils from the overlying Otter Sandstone Formation
 560 (Hounslow & McIntosh 2003; Benton 1997), which indicate the Sherwood Sandstone Gp is as
 561 old as early Anisian (Middle Triassic), and probably ranges down into the Olenekian of the
 562 Lower Triassic (Hounslow & McIntosh 2003; Hounslow & Muttoni 2010). Based on regional
 563 climate comparisons between the Budleigh Salterton Pebble Beds and the 'Conglomerate
 564 principal' of the Vosges region in NE France, Durand (2006) suggested a probable early
 565 Olenekian age for the Budleigh Salterton Pebble Beds Fm, generally consistent with the
 566 magnetostratigraphy.

567

568 This work detects the oldest normal magnetozone in the mid-parts of the Exe Breccia (i.e. EA1n),
 569 with a substantial thickness (perhaps up to ~1 to 1.5 km) of reverse polarity in the underlying
 570 parts of the Exeter Gp. Although we cannot locate the base of EA1n precisely due to lack of
 571 suitable outcrop, this normal magnetozone is the earliest evidence of the Illawarra Superchron
 572 (Fig. 11). EA1n is probably equivalent to early MP2n, or the normal polarity part of MP1.
 573 However, ~55 m of unsampled strata occur in the interval between our outcrops at the Exe
 574 Breccia- Dawlish Sandstone boundary (Figs. 4, 11). Therefore, it is possible the equivalent of the
 575 MP1n chron is within this unsampled interval. The end of the KRPS provides an important
 576 dating-point (267.1±0.8 Ma; Hounslow submitted) to the early-mid Wordian in the Middle
 577 Permian (Guadalupian). The oldest occurrence of the *Lueckisporites virkkiae* assemblage is
 578 found in the Whipton Fm, which suggests that this formation could be as old as latest Kungurian
 579 to early Roadian (~272 Ma; Henderson *et al.* 2012). This would give a minimum of ~8 Ma of
 580 exhumation time, between formation of the Dartmoor Granite, and the first granite detritus
 581 appearing in the Teignmouth- Heavitree breccias.

582

583 The overlying normal polarity magnetozone EA3n, is therefore likely to be equivalent to the
 584 MP3n normal magnetozone in the upper and mid parts of the Capitanian (Fig. 11). The EA3r
 585 magnetozone is equivalent to the MP3r to UP1r interval (in the lower part of the Wuchiapingian),
 586 with the overlying normal magnetozones (i.e. EA4n to EA5n) equivalent to those in the upper
 587 parts of the Wuchiapingian to basal Changhsingian (Fig. 11). Reverse magnetozone EA2r, in the
 588 top of the Exe Breccia is probably the equivalent of MP2r in the basal Capitanian. Sub
 589 magnetozone EA3r.1n in the Littleham Mudstone Fm is probably equivalent to UP1n in the
 590 Wuchiapingian.

591 *Alternative Lower Triassic age models?*

592 The alternative Lower Triassic age of the Aylesbeare Mudstone Gp suggested by Warrington &
 593 Scrivener (1990) and Edwards *et al.* (1997), is untenable using the magnetostratigraphy. To
 594 evaluate their hypothesis using this data suggests the most likely early Triassic correlation model
 595 would indicate EA3n is the age equivalent of the first Triassic magnetozone, LT1n (Fig. 11).
 596 Therefore, the overlying EA3r to EA5n interval would extend into the earliest Olenekian, an
 597 interval of some 1.4 Ma (Hounslow & Muttoni 2010). However, this seems unlikely for the
 598 following reasons:

599

- 600 1) The local clast lithologies (e.g. *murchisonite*) seen in the breccia at the base of the Littleham
 601 Mudstone Fm, are similar to those in the Exeter Gp, and very different to those found in the
 602 Budleigh Salterton Pebble Beds (and other Lower Triassic units further north in the UK),
 603 which contain Armorican-derived clasts and zircons from Cadomian basement (Cocks 1993;
 604 Morton *et al.* 2013).
- 605 2) It would require a minimum hiatus of ~ 13-15 Ma between the Exe Breccia and the
 606 Aylesbeare Mudstone Gp, which seems unlikely considering the apparently conformable
 607 nature of the boundary between these formations in the Exe Estuary area.
- 608 3) If the hypothesis of Warrington & Scrivener (1990) was correct, it would predict numerous
 609 normal polarity intervals (from the Illawarra superchron) below the Aylesbeare Mudstone Gp
 610 but we have only found these in the Exe Breccia Fm with no evidence of normal polarity in
 611 the underlying *c.*1 km of the Exeter Gp.
- 612 4) This Lower Triassic model would suggest a ~1.4 Ma duration for the EA3n to EA5n interval
 613 requiring very large accumulation rates, comparable to the deepest grabens in the Southern

614 Permian Basin, north of the Variscan front, which there contain substantial thicknesses of
615 Zechstein.

616 *Wider regional implications*

617 A consequence of these data is that it is now possible to assess the relationship of the SW
618 England successions to the much better studied Rotleigend-II group in the Southern Permian
619 Basin (Fig. 11). The magnetostratigraphy suggests a similarity in age of the Altmark
620 unconformities with the Devon Permian sequence boundaries. The magnetic polarity stratigraphy
621 from the Mirow, Czaplonek and Piła wells suggests that the Altmark III unconformity is roughly
622 equivalent to the base of the Littleham Mudstone Fm (base of Pm5 sequence; Fig. 2), Altmark II,
623 with the base of sequence Pm4 (Figs. 2, 11). Less certain is the correlation of the base of unit B
624 in the Littleham Mudstone Fm, with Altmark IV. The base of sequence Pm3 probably relates to
625 the Altmark I unconformity, which separates the Muritz Subgroup from the Havel Subgroup,
626 across the Saalian unconformity, since underlying successions both contain volcanic units.

627

628 The calcrete and rhizoconcretion bearing sandstone, in the uppermost part of the Straight Point
629 Sandstone Mbr, is unusual in that no other well developed palaeosols are seen in the remainder
630 of these Permian successions. It is not until the mid Triassic (Anisian) Otter Sandstone Fm, that
631 calcretes began to be widely developed in SW England. The Capitanian-Wuchiapingian
632 boundary was an interval with dramatic, but poorly understood shifts in the global carbon cycle
633 (Nishikane *et al.* 2014). A tentative reason for this palaeosol development is the rapid warming
634 associated with increased CO₂ in the atmosphere (and associated increased evaporation rates to
635 create calcretes; Alonso-Zarza 2003), that developed after the extinction at the Capitanian-
636 Wuchiapingian boundary. The peak is associated with a negative $\delta^{13}\text{C}$ excursion (Chen *et al.*
637 2011; Nishikane *et al.* 2014) in the early Wuchiapingian, which corresponds closely to the early
638 parts of MP3r (Zheng *et al.* 2010; Fig. 11).

639

640 The dramatic switch between breccia-dominated facies of the Exeter Gp to the mudstone-
641 dominated facies of the Aylesbeare Mudstone Gp, occurs within the early Capitanian (Fig. 11).
642 We tentatively relate this switch in facies to the Kamura cooling event (seen as a large positive
643 $\delta^{13}\text{C}$ excursion during the Capitanian), which began in the early Capitanian (Isozaki *et al.* 2011).
644 This has been associated with lows in atmospheric CO₂, and cooler oceanic surface waters in
645 both the Panthalassa and Paleo-Tethys Oceans (Isozaki *et al.* 2011; Nishikane *et al.* 2014). This

646 cooling event may have allowed more moisture-bearing weather systems to penetrate further
647 northwards into the heart of Pangaea, from the Paleo-Tethys, so allowing delivery of larger
648 amounts of mud into the playa systems of the Aylesbeare Mudstone Gp.

649

650 The Southern Permian Basin, Parchim and Mirow formations shows a number of similarities to
651 the Devon successions. The Parchim Fm dominantly comprises thick conglomeratic braidplain-
652 type deposits, extending to sandflat and locally playa mudstone deposits in the basin centre
653 (McCann 1998; Rieke *et al.* 2003). Tectonic control of facies was important during the Parchim
654 Fm. Like the Exeter Group in sequence Pm3 (Fig. 2) the Parchim Fm has an earlier wetter phase
655 and a later dryer phase (Rieke *et al.* 2003). This is overlain by the Mirow Fm which is
656 characterized by the progradation of sand-prone fluvial facies with frequent claystones, over a
657 much wider extent in the Southern Permian Basin than the Parchim Fm. The rarity of
658 conglomerates (except at basin margins), with instead claystones (containing fossils indicative of
659 freshwater conditions) and the dominance of sand-prone facies, is very different to the
660 underlying Parchim Fm (McCann 1998). Hence, the start of the Mirow Fm sees a switch to
661 climatically wetter conditions (Rieke *et al.* 2003), like those seen in the Aylesbeare Mudstone
662 Gp. The coincidence in timing and the switch to wetter environmental conditions, seen in the
663 Devon successions and German basins, suggests these major facies changes are climatically
664 controlled.

665 **Conclusions**

666 The palaeomagnetic signal in the Exeter and Aylesbeare Mudstone groups is dominantly carried
667 by haematite, whose mean directions pass the reversal test. The remanence in the Exeter Gp
668 passes a fold test. The AMS indicates the fabric carried by haematite is detrital in origin. Reverse
669 polarity dominates in the lower part of the Exeter Gp, with the start of the Illawarra superchron,
670 in the Exe Breccia Fm dated to the early Wordian. Five normal-reverse couplets are found in the
671 overlying sediments starting in the upper part of the Exe Breccia Fm (Langstone Mbr) and into
672 the Aylesbeare Mudstone Gp. This magnetostratigraphic data allows the Exmouth Mudstone and
673 Sandstone Fm to be assigned to the Capitanian to the earliest Wuchiapingian, and the overlying
674 Littleham Mudstone Fm is earliest Wuchiapingian, to as young as the Wuchiapingian-
675 Changhsingian boundary. With these data, the Permian successions in SW England are now the
676 most precisely dated Permian succession in the UK, and if similar methods were used elsewhere,
677 should provide the foundation for a much better understanding of other UK Permian basins. The

678 similarity in the timing between facies changes and sequence boundaries, here and those of the
 679 Rotliegend-II Group in the Southern Permian Basin, indicates that palaeoclimatic change is a
 680 fundamental metric in their subdivision. The question of the position of the Permo-Triassic
 681 boundary in SW England has now been effectively resolved, and ironically corresponds to the
 682 position taken by Victorian geologists such as Irving (1888).

683 **Acknowledgements**

684 This work was part-funded by a British Geological Survey- University collaboration grant.
 685 Richard Scrivener led fieldwork to the Crediton Trough, and Paulette Posen assisted during
 686 fieldwork to the Exeter Gp. Robert Hawkins and Laurence Thistlewood measured some of the
 687 samples. Sylvie Bourquin and Antoine Bercovici assisted in the fieldwork in 2007. Simon Chew
 688 drafted some of the figures. The MOD kindly allowed access to the Straight Point firing range. A
 689 reviewer Tim Raub provided constructive suggestions for improvement.

690 **References**

- 691 Ali, J. R., Thompson, G. M., Song, X. & Wang, Y. 2002. Emeishan Basalts (SW China) and the
 692 'end-Guadalupian' crisis: magnetobiostratigraphic constraints. *Journal of the Geological*
 693 *Society*, **159**, 21-29.
- 694 Alonso-Zarza, A. M. 2003. Palaeoenvironmental significance of palustrine carbonates and
 695 calcretes in the geological record. *Earth-Science Reviews*, **60**, 261-298.
- 696 Barton, C. M., Woods, M. A., Bristow, C. R., Newell, A. J., Westhead, R. K., Evans, D. J.,
 697 Kirby, G. A., & Warrington, G. 2011. *The geology of south Dorset and south-east Devon*
 698 *and its World Heritage Coast*. Special Memoir of the British Geological Survey, Sheets 328,
 699 341/342, 342/343 and parts of 326/340, 327, 329 and 339. HMSO, London
- 700 Bateson, J. H. & Johnson, C. C. 1992. *Reduction and related phenomena in the New Red*
 701 *Sandstone of south-west England*, British Geological Survey, Technical report WP/92/1.
- 702 Benton, M. J., Cook, E., & Turner, P. 2002. *Permian and Triassic red beds and the Penarth*
 703 *Group of Great Britain*. Geological Conservation Review Series. Joint Nature
 704 Conservation Committee, Peterborough.
- 705 Benton, M. J. 1997. The Triassic reptiles from Devon. *Proceedings of the Ussher Society*, **9**, 141-
 706 152.
- 707 Burov, B. V., Zharkov, I. Y., Nurgaliev, D. K., Balabanov, Yu. P., Borisov, A. S. & Yasonov, P.
 708 G. 1998. Magnetostratigraphic characteristics of Upper Permian sections in the Volga

- 709 and the Kama areas. *In: Esaulova, N. K., Lozonsky, V. R., Rozanov, A. Yu. (eds).*
 710 *Stratotypes and reference sections of the Upper Permian in the regions of the Volga and*
 711 *Kama Rivers.* GEOS, Moscow, 236-270.
- 712 Butler, M. 1998. The geological history and the southern Wessex Basin- a review of new
 713 information from oil exploration. *In: Underhill, J. R. (ed.), Development, evolution and*
 714 *petroleum geology of the Wessex Basin.* Geological Society London Special Publication
 715 **133**, 67-86.
- 716 Carter, A. Yelland, A. Bristow, C. & Hurford, A. J. 1995. Thermal histories of Permian and
 717 Triassic basins in Britain derived from fission track analysis. *In: Boldy, S.A. R. (ed.),*
 718 *Permian and Triassic Rifting in Northwest Europe,* Geological Society Special
 719 Publication, **91**, 41-56.
- 720 Chapman, T. J. 1989. The Permian to Cretaceous structural evolution of the Western Approaches
 721 Basin (Melville sub-basin), UK. *In: M.A. Cooper (ed.), Inversion Tectonics,* Geological
 722 Society, London, Special Publications; **44**, 177-200.
- 723 Chen, B., Joachimski, M. M., Sun, Y., Shen, S. & Lai, X. 2011. Carbon and conodont apatite
 724 oxygen isotope records of Guadalupian–Lopingian boundary sections: Climatic or sea-
 725 level signal? *Palaeogeography, Palaeoclimatology, Palaeoecology*, **311**, 145-153.
- 726 Cocks, L. R. M. 1993. Triassic pebbles, derived fossils and the Ordovician to Devonian
 727 palaeogeography of Europe. *Journal Geological Society London*, **150**, 219-226.
- 728 Cornwall, J. D. 1967. Palaeomagnetism of the Exeter Lavas, Devonshire. *Geophys. Journal*
 729 *Royal Astro. Soc.*, **12**, 181-196.
- 730 Creer, K. M. 1957. The Natural Remanent Magnetization of Certain Stable Rocks from Great
 731 Britain. *Philosophical Transactions of the Royal Society of London. Series A, Mathematical*
 732 *and Physical Sciences*, **250**, 111-129.
- 733 Dangerfield, J. & Hawkes, J. R. 1969. Unroofing of the Dartmoor Granite and possible
 734 consequences with regard to mineralization. *Proc. Ussher Soc.*, **2**, 122-131.
- 735 Denison, R. E. & Peryt, T. M. 2009. Strontium isotopes in the Zechstein (Upper Permian)
 736 anhydrites of Poland: evidence of varied meteoric contributions to marine brines. *Geological*
 737 *Quarterly*, **53**, 15
- 738 Durand, M. 2006. The problem of the transition from the Permian to the Triassic Series in
 739 southeastern France: comparison with other Peritethyan regions. *In: Lucas, S. G., Cassinis,*
 740 *G. & Schneider J.W. (eds) Non-Marine Permian Biostratigraphy and Biochronology,*
 741 Geological Society, London, Special Publications, **265**, 281-296.

- 742 Durrance, E. M., Meads, R. E., Ballard, R. R. B. & Walsh, J. N. 1978. Oxidation state of iron in
 743 the Littleham Mudstone Formation of the new red sandstone series (Permian-Triassic) of
 744 southeast Devon, England. *Geological Society of America Bulletin*, **89**, 1231-1240.
- 745 Edwards, R. A. & Scrivener, R. C., 1999. *Geology of the country around Exeter. Memoir of the*
 746 *British Geological Survey, Sheet 325 (England and Wales)*, HMSO, London.
- 747 Edwards, R. A., Warrington, G., Scrivener, R. C., Jones, N. S., Haslam, H. W. & Ault, L. 1997.
 748 The Exeter Group, south Devon, England: a contribution to the early post-Variscan
 749 stratigraphy of northwest Europe. *Geological Magazine*, **134**, 177-197.
- 750 Ellwood, B. B. & Howard, J. H. 1981. Magnetic fabric development in an experimentally
 751 produced barchan dune. *Journal of Sedimentary Research*, **51**, 97-100.
- 752 Embleton, B. J. J., McElhinny, M. W., Zhang Z. & Li Z. X. 1996. Permo-Triassic
 753 magnetostratigraphy in China: the type section near Taiyuan, Shanxi Province, North
 754 China. *Geophys. J. Int.* **126**: 382–388
- 755 Enkin, R. J. 2003. The direction- correction tilt test: an all purpose tilt/fold test for
 756 palaeomagnetic studies. *Earth Planet. Sci. Lett.*, **212**, 151-166.
- 757 Evans, C. D. R. 1990. *The geology of the western English Channel and its western Approaches.*
 758 *UK Offshore regional report.* British Geological Survey, HMSO, London.
- 759 Frank, U. and Nowaczyk, N. R. 2008. Mineral magnetic properties of artificial samples
 760 systematically mixed from haematite and magnetite. *Geophys. J. Int.* **175**, 449–461.
- 761 Gallet, Y., Krystyn, L., Besse, J., Saidi, A. & Ricou, L-E. 2000. New constraints on the upper
 762 Permian and Lower Triassic geomagnetic polarity timescale from the Abadeh section
 763 (central Iran). *Journal of Geophysical Research*, **105**, 2805-2815.
- 764 Gallois, R.W. 2014. The position of the Permo-Triassic boundary in Devon, UK. *Geoscience in*
 765 *South-West England*, **13**, 328-338.
- 766 Haag, M. & Heller, F. 1991. Late Permian to Early Triassic magnetostratigraphy. *Earth Planet.*
 767 *Sci. Letter*, **107**, 42-54.
- 768 Hamblin, R. J. O., Crosby, A., Alson, R. S., Jones, S. M., Chadwick, R. A., Penn, I. E. & Arthur,
 769 M. J. 1992. *United Kingdom off-shore report: the geology of the English Channel.*
 770 British Geological Survey, HMSO, London.
- 771 Harvey, M. J. Stewart, S. A., Wilkinson, J.J., Ruffell, A. H. & Shall, R. K. 1994. Tectonic
 772 evolution of the Plymouth Bay Basin. *Proceedings of the Ussher Society*, **8**, 271-278.

- 773 Henderson, C. M., Davydov, V. I. & Wardlaw, B. R. 2012. The Permian Period. *In*: Gradstein,
 774 F.M., Ogg, J.G, Schmitz, M.D. & Ogg, G.M (eds), *The geologic time scale 2012*, vol. 2,
 775 Elsevier, Amsterdam, 653-679.
- 776 Henson, M. R. 1972. The form of the Permo-Triassic basin in south-east Devon. *Proc. Ussher*
 777 *Soc.* **3**, 447-457.
- 778 Hounslow, M.W. & McIntosh, G. 2003. Magnetostratigraphy of the Sherwood Sandstone Group
 779 (Lower and Middle Triassic): South Devon, U.K.: Detailed correlation of the marine and
 780 non-marine Anisian. *Palaeogeogr. Palaeoclimat. Palaeoecol.*, **193**, 325-348.
- 781 Hounslow M.W. & Muttoni G. 2010. The geomagnetic polarity timescale for the Triassic:
 782 Linkage to stage boundary definitions. *In*: Lucas, S. G. (ed.) *The Triassic timescale*.
 783 Special Publication of the Geological Society, **334**, 61-102.
- 784 Hounslow, M. W. (submitted). Palaeozoic geomagnetic reversal rates following superchrons
 785 have a fast re-start mechanism. *Nature Communications*.
- 786 Irving, A. 1888. The red-rock series of the Devon Coast section. *Quart. J. geol. Soc.*, **44**, 149-
 787 163.
- 788 Isozaki, Y., Aljinovic, D. & Kawahata, H. 2011. The Guadalupian (Permian) Kamura event in
 789 European Tethys. *Palaeogeography, Palaeoclimatology, Palaeoecology* **308**, 12–21.
- 790 Jin, Y. Shang, Q. & Cao, C. 2000. Late Permian magnetostratigraphy and its global correlation.
 791 *Chinese Science Bulletin*, **45**, 698-705.
- 792 Johnson, S. A., Glover B. W. & Turner, P. 1997. Multiphase reddening and weathering events in
 793 Upper Carboniferous red beds from the English West Midlands. *Journal of the*
 794 *Geological Society*, **154**, 735-745.
- 795 Kent, J. T., Briden, J. C. & Mardia, K. V. 1983. Linear and planar structure in ordered
 796 multivariate data as applied to progressive demagnetisation of palaeomagnetic remanence.
 797 *Geophysical Journal Royal Astronomical Society*, **81**, 75-87.
- 798 Kirschvink, J. L., Isozaki, Y., Shibuya, H., Otofujii, Y. I., Raub, T. D., Hilburn, I. A., Kasuya, T.,
 799 Yokoyama, M. & Bonifacie, M. 2015. Challenging the sensitivity limits of
 800 Paleomagnetism: Magnetostratigraphy of weakly magnetized Guadalupian–Lopingian
 801 (Permian) Limestone from Kyushu, Japan. *Palaeogeography, Palaeoclimatology,*
 802 *Palaeoecology*, **418**, 75-89.
- 803 Korte, C., Kozur, H. W. & Veizer, J. 2005. $\delta^{13}\text{C}$ and $\delta^{18}\text{O}$ values of Triassic brachiopods and
 804 carbonate rocks as proxies for coeval seawater and palaeotemperature. *Palaeogeography,*
 805 *Palaeoclimatology, Palaeoecology*, **226**, 287-306.

- 806 Kostadinova M., Jordanova N., Jordanova D. & Kovacheva M. 2004. Preliminary study on the
807 effect of water glass impregnation on the rock-magnetic properties of baked clay. *Studia*
808 *Geophysica et Geodaetica*, **48**, 637-646.
- 809 Laming, D. J. C. 1966. Imbrications, palaeocurrents and other sedimentary features in the Lower
810 New Red Sandstone, Devonshire, England. *Journal of Sedimentary Petrology*, **36**, 940-
811 959.
- 812 Laming, D. J. C. 1969. A guide to the New Red Sandstone of Tor Bay, Petitor and Shaldon.
813 Report *Transaction of Devonshire Association of Science, Literature and Art*, **101**, 207-
814 218.
- 815 Laming, D. J. C. 1982. The New Red Sandstone. In: Durrance, E. M. & Laming, D. J. C. (eds)
816 *The geology of Devon*. University of Exeter Press, Exeter, 148-178,
- 817 Laming, D. J. C. & Roche, D. P. 2013. Faulting in Permo-Triassic strata and buried channels
818 revealed by excavation of the Lymptstone-Powderham tunnel, Exe Estuary, Devon.
819 *Geoscience in South-West England*, **13**, 244.
- 820 Langereis, C. G., Krijgsman, W., Muttoni, G. & Menning, M. 2010. Magnetostratigraphy -
821 concepts, definitions, and applications. *Newsletters on Stratigraphy*, **43**, 3, 207-233
- 822 Lawton, D. E. & Roberson, P. P. 2003. The Johnston Gas Field, Blocks 43/26a, 43/27a, UK
823 Southern North Sea. In: Gluyas, J. & Hitchens, H. M. (eds), *United Kingdom Oil and Gas*
824 *Fields, Commemorative Millennium Volume*. Geological Society London Memoir, **20**,
825 749-759.
- 826 Legler, B., Gebhardt, U. & Schneider, J. W. 2005. Late Permian non marine to marine
827 transitional profiles in central southern Permian Basin, northern Germany. *Int. Journal of*
828 *Earth Sciences*, **94**, 851-862.
- 829 Leveridge, B. E. Scrivener, R. C. Goode, A. J. J. & Merriman, R. J. 2003. *Geology of the*
830 *Torquay district, a brief explanation of the geological map sheet 350 Torquay*.
831 Keyword: British Geological Survey, HMSO, London.
- 832 Løvlie, R. & Torsvik, T. 1984: Magnetic remanence and fabric properties of laboratory-deposited
833 hematite-bearing red sandstone. *Geophysical Research Letters*, **11**, 229-232.
- 834 Lowrie, W. 1990. Identification of ferromagnetic minerals in a rock by coercivity and unblocking
835 temperature properties. *Geophysical Research Letters*, **17**, 159-162.
- 836 Lucas, S. G. & Hunt, A. P. 2006. Permian tetrapod footprints: biostratigraphy and biochronology.
837 In: Lucas, S.G. Cassinis, G. & Schneider, J.W. (eds), *Non-marine Permian*

- 838 *biostratigraphy and biochronology*, Geological Society, London Special Publications,
839 **265**, 179-200.
- 840 Mangerud, G. 1994. Palynostratigraphy of the Permian and lowermost Triassic succession,
841 Finnmark Platform, Barents sea. *Review of Palaeobotany & Palynology*, **82**, 317-349.
- 842 McCann, T., Pascal, C., Timmerman, M. J., Krzywiec, P., López-Gómez, J., Wetzel, L. &
843 Lamarche, J. 2006. Post-Variscan (end Carboniferous-Early Permian) basin evolution in
844 western and central Europe. *In: Gee, D. G. & Stephenson, R. A. (eds) European*
845 *Lithosphere Dynamics*. Geological Society London Memoirs, **32**, 355–388.
- 846 McCann, T. 1998. Sandstone composition and provenance of the Rotliegendes of the NE German
847 Basin. *Sedimentary Geology*, **116**, 177-198.
- 848 McFadden, P. L. 1990. A new fold test for palaeomagnetic studies. *Geophysical Journal*
849 *International*, **103**, 163-169.
- 850 McFadden, P. L. & McElhinney, M. W. 1988. The combined analysis of remagnetisation circles
851 and direct observations in palaeomagnetism. *Earth Planetary Science Letters*, **87**, 161-
852 172.
- 853 McFadden, P. L. & McElhinny, M. W. 1990. Classification of the reversal test in
854 palaeomagnetism. *Geophysical Journal International*, **103**, 725-729.
- 855 McKeever, P. M. & Haubold, H. 1996. Reclassification of vertebrate trackways from the Permian
856 of Scotland and related forms from Arizona and Germany. *Journal of Paleontology*, **70**,
857 1011-1022.
- 858 McKie, T. & Williams, B. P. J. 2009. Triassic palaeogeography and fluvial dispersal across the
859 northwest European Basins. *Geological Journal*, **44**, 711-741.
- 860 Menning, M., Katzung, G. & Lützner, H. 1988. Magnetostratigraphic investigations in the
861 Rotliegendes (300-252 Ma) of Central Europe. *Z. geol. Wiss., Berlin*, **16**, 1045-1063.
- 862 Merefield, J. R., Brice, C. J. & Palmer, A. J. 1981. Caesium from former Dartmoor volcanism:
863 its incorporation in NewRed sediments of SW England. *Journal of the Geological Society*,
864 **138**, 145-152.
- 865 Molostovsky, E. A. 1983. *Paleomagnetic stratigraphy of the eastern European part of the*
866 *USSR*. University of Saratov, Saratov [In Russian].
- 867 Morton, A. C., Hounslow, M. W. & Frei, D. 2013. Heavy-mineral, mineral-chemical and zircon-
868 age constraints on the provenance of Triassic sandstones from the Devon coast, southern
869 Britain. *Geologos* **19**, 67–85.

- 870 Nawrocki, J. 1997. Permian to early Triassic magnetostratigraphy from the central European
871 basin in Poland: Implications on regional and worldwide correlations. *Earth. Planet. Sci*
872 *Lett.*, **152**, 37-58.
- 873 Newell, A. J. 2001. Bounding surfaces in a mixed aeolian-Fluvial system (Rotliegend, Wessex
874 Basin, SW UK). *Marine & Petroleum Geology*, **18**, 339-347.
- 875 Nishikane, Y., Kaiho, K., Henderson, C. M., Takahashi, S. & Suzuki, N. 2014. Guadalupian–
876 Lopingian conodont and carbon isotope stratigraphies of a deep chert sequence in Japan.
877 *Palaeogeography, Palaeoclimatology, Palaeoecology*, **403**, 16-29.
- 878 Ogg, J. G. & Steiner, M. B. 1991. Early Triassic polarity time-scale: integration of
879 magnetostratigraphy, ammonite zonation and sequence stratigraphy from stratotype
880 sections (Canadian Arctic Archipelago). *Earth and Planetary Science Letters*, **107**, 69–
881 89.
- 882 Ormerod- Wareing, G. 1875. On the Murchisonite beds of the Estuary of the Exe and an attempt
883 to classify the beds of the Trias thereby. *Quart. J. Geol. Soc. Lond.*, **31**, 346-354.
- 884 Park, M. E., Cho, H., Son, M. & Sohn, Y. K. 2013. Depositional processes, paleoflow patterns,
885 and evolution of a Miocene gravelly fan-delta system in SE Korea constrained by
886 anisotropy of magnetic susceptibility analysis of interbedded mudrocks. *Marine and*
887 *Petroleum Geology*, **48**, 206-223.
- 888 Pašava, J., Oszczepalski, S. & Du, A. 2010. Re–Os age of non-mineralized black shale from the
889 Kupferschiefer, Poland, and implications for metal enrichment. *Mineralium Deposita*,
890 **45**, 189-199.
- 891 Rieke, H., McCann, T., Krawczyk, C. M. & Negendank, J. F.W. 2003. Evaluation of controlling
892 factors on facies distribution and evolution in an arid continental environment: an
893 example from the Rotliegend of the NE German Basin. In: McCann, T. & Saintot, A.
894 (eds) *Tracing Tectonic Deformation Using the Sedimentary Record*. Geological Society,
895 London, Special Publications, **208**, 71- 94.
- 896 Roscher, M. & Schneider, J. W. 2006. Permo-Carboniferous climate: Early Pennsylvanian to late
897 Permian climate development of central Europe in a regional and global context. In:
898 Lucas, S. G. Cassinis, G. & Schneider, J. W. (eds) *Non-marine Permian biostratigraphy*
899 *and biochronology*, Geological Society, London Special Publication, **265**, 15-38.
- 900 Schwarzscher, W. 1951. Grain orientation in sands and sandstones. *Journal of Sedimentary*
901 *Research*, **21**, 162-172.

- 902 Scrivener, R. C. 2006. Cornubian granites and mineralization in SW England. *In*: Brenchley, P. J.
 903 & Rawson, P. F. *Geology of England and Wales*. Geological Society of London
 904 Publication, Bath, 257-267.
- 905 Selwood, E. B. Edwards, R. A., Simpson, S., Chesher, J. A. & Hamblin, R. A. 1984. *Geology of*
 906 *the country around Newton Abbot. Memoir for 1:50,000 geological sheet 339*, British
 907 Geological Survey, HMSO, London.
- 908 Shen, S-Z., Henderson, C. H., Bowring, S. A., Cao, C-Q. Wang, Y., Wang, W., Zhang, H.,
 909 Zhang, Y-C. & Mu, L. 2010. High-resolution Lopingian (Late Permian) timescale of
 910 South China. *Geological Journal*, **45**, 122–134.
- 911 Shu, O. 1999. A brief discussion on the occurrences of *Scutasporites unicus* and *Lueckisporites*
 912 *virkkiae* complexes in the northern hemisphere. *Permophiles*, **33**, 21-23.
- 913 Słowakiewicz, M., Kiersnowski, H. & Wagner, R. 2009. Correlation of the Middle and Upper
 914 Permian marine and terrestrial sedimentary sequences in Polish, German and USA
 915 Western Interior Basins with reference to global time markers. *Palaeoworld*, **18**, 193-
 916 211.
- 917 Steiner, M. 2006. The magnetic polarity timescale across the Permian-Triassic boundary. *In*:
 918 Lucas, S. G. Cassinis, G. and Schneider, J. W. (eds), *Non-marine Permian biostratigraphy*
 919 *and biochronology*, Geological Society, London Special Publication, **265**, 15-38.
- 920 Steiner, M. B., Ogg, J., Zhang, Z. & Sun, S. 1989. The Late Permian/early Triassic magnetic
 921 polarity time scale and plate motions of south China. *Journal Geophysical Research*, **94**,
 922 7343-7363.
- 923 Strachan, R. A., Linnemann, U., Jeffries, T., Drost, K. & Ulrich, J. 2014. Armorican provenance
 924 for the mélange deposits below the Lizard ophiolite (Cornwall, UK): evidence for Devonian
 925 obduction of Cadomian and Lower Palaeozoic crust onto the southern margin of Avalonia.
 926 *International Journal of Earth Sciences*, **103**, 1359-1383.
- 927 Szurlies, M., Bachmann, G. H., Menning, M., Nowaczyk, N. R. & Käding, K-C. 2003.
 928 Magnetostratigraphy and high resolution lithostratigraphy of the Permian- Triassic boundary
 929 interval in Central Germany. *Earth and Planetary Science Letters*, **212**, 263-278.
- 930 Szurlies, M. 2013. Late Permian (Zechstein) magnetostratigraphy in western and central Europe.
 931 *In*: Gasiewicz, A. & Słowakiewicz, M. (eds), *Palaeozoic climate cycles: their evolutionary*
 932 *and sedimentological impact*. Geological Society, London, Special Publications, **376**, 73-85.
- 933 Tarling, D. H. & Hrouda, F. 1993. *The magnetic anisotropy of rocks*. Chapman and Hall,
 934 London.

- 935 Thomas, H. H. 1909. A contribution to the petrography of the New Red Sandstone in the West
936 of England. *Quarterly Journal of the Geological Society, London*, **65**, 229-245.
- 937 Timmerman, M. J. 2004. Timing, geodynamic setting and character of Permo-Carboniferous
938 magmatism in the foreland of the Variscan Orogen, NW Europe. *In: Wilson, M.,*
939 *Neumann, E. -R., Davies, G. R., Timmerman, M. J., Heeremans, M. & Larsen, B. T.*
940 *(eds) Permo-Carboniferous Rifting and Magmatism in Europe*, Special Publication
941 Geological Society, London, **223**, 41-74.
- 942 Torsvik T. H. & Cocks L. R. M. 2005. Norway in space and time: A Centennial cavalcade.
943 *Norwegian Journal of Geology*, **85**, 73-86.
- 944 Turner, P. 1979. The palaeomagnetic evolution of continental red beds. *Geological Magazine*,
945 **116**, 289-301.
- 946 Turner, P., Burley, S. D. Rey, D. & Prosser, J. 1995. Burial history of the Penrith Sandstone
947 (Lower Permian) deduced from the combined study of fluid inclusion and palaeomagnetic
948 data. *In: Turner, P. & Turner, A. (eds) Paleomagnetic applications in hydrocarbon*
949 *exploration*. Geological Society London Special Publications, **98**, 43-78.
- 950 Turner, P., Chandler, P., Ellis, D., Leveille, G. P. & Heywood, M. L. 1999. Remanance
951 acquisition and magnetostratigraphy of the Leman Sandstone Formation: Jupiter Fields,
952 southern North Sea. *In: Tarling, D. H. & Turner, P. (eds) Palaeomagnetism and diagenesis*
953 *in sediments*, Geological Society of London special publications, **151**, 109-124.
- 954 Ussher, W. A. E 1876. On the Triassic rocks of Somerset and Devon. *Quart Jour. Geol. Soc.*,
955 **32**, 367-394.
- 956 Ussher, W. A. E 1913. *The geology of the country around Newton Abbott: explanation of sheet*
957 *339*. Geological Survey of Great Britain. HMSO, London.
- 958 Visscher, H. 1973. The Upper Permian of western Europe—a palynological approach to
959 chronostratigraphy. *In: Logan A. & Hills L.V. (eds) The Permian and Triassic systems and*
960 *their mutual boundary*. Can. Soc. Pet. Geol. Mem., **2**, 200-219.
- 961 Warrington, G. & Scrivener, R. C. 1990. The Permian of Devon, England. *Review Palaeobotany*
962 *Palynology*, **66**, 263-272.
- 963 Watson, G. S & Enkin, R. J. 1993. The fold test in palaeomagnetism as a parameter estimation
964 problem. *Geophysical Research Letters*, **20**, 2135-3137.
- 965 Wills, L. J. 1970. The Triassic succession in the central Midlands in its regional setting. *Jour.*
966 *Geol. Soc. Lond.*, **126**, 225-283.

- 967 Zheng, L., Yang, Z., Tong, Y., & Yuan, W. 2010. Magnetostratigraphic constraints on two-stage
968 eruptions of the Emeishan continental flood basalts. *Geochemistry, Geophysics,*
969 *Geosystems*, **11**, doi:10.1029/2010GC003267.
- 970 Zijderveld, J. D. A. 1967. The natural remanent magnetisation of the Exeter Volcanic Traps
971 (Permian, Europe). *Tectonophysics*, **4**, 121-153.
- 972 Underhill, J. R. & Stoneley, R. 1998. Introduction to the development, evolution and petroleum
973 geology of the Wessex Basin. *In*: Underhill, J. R. (ed.) *Development, Evolution and*
974 *Petroleum Geology of the Wessex Basin*, Geological Society, London, Special
975 Publications, **133**, 1-18.
- 976 Utting, J., 1996. Palynology of the Ufimian and Kazanian Stages of Russian stratotypes, and their
977 comparison to the Word and Road of Canadian Arctic. *In*: Esaulova, N. K. & Lozovsky,
978 V. R. (eds) *Stratotypes and reference sections of the Upper Permian of regions of the*
979 *Volga and Kama Rivers*. Izd. "Ecocentr", Kazan, 486-506.
- 980

981 **Figure Captions**

982 Fig. 1. Sketch map of the Permian-Triassic in SE Devon. Inset a) shows the study location within
 983 the UK, where grey=Lower Palaeozoic basement highs, dotted=Permian basins. CAB=Channel
 984 Approaches Basin, LRS=Lizard-Rhenish Suture, RHZ=Rheno-Hercynian Zone, STZ= Saxo-
 985 Thuringian Zone . In main map, numbers correspond to the sampling locations indicated in the
 986 Supplementary Data. Adapted from Selwood *et al.* (1984), Edwards *et al.* (1997). Sampling
 987 locations on coast indicated by } and in-land as ■.

988

989 Fig. 2. The stratigraphy of the Permian- Triassic around Exeter and the SE Devon coasts. Based
 990 on this work and Laming (1982), Selwood *et al.* (1984), Edwards & Scrivener (1999), Leveridge
 991 *et al.* (2003). Thicknesses of the coastal units is based on Selwood *et al.* (1984), Laming (1982)
 992 and this work. The chronology is based on Edwards *et al.* (1997), Edwards & Scrivener (1999)
 993 and this work. The Torbay Breccia Formation occurs west of the Stickepath fault zone (SFZ,
 994 dashed in grey), and is divisible into an upper unit (the Paignton breccias, PB) probably
 995 equivalent to the Oddicombe Breccia Fm , and a lower unit composed of several separate
 996 breccias units. PTM=Petit Tor Member. Arrows indicate overstepping units.

997

998 Fig. 3. A) The erosional boundary between the Littleham Mudstone Fm (below) and the Budleigh
 999 Salterton Pebble Beds Fm (photo courtesy of Richard Porter), B) Immature calcrete and
 1000 calcretised rootlets, top part of Straight Point Sandstone Member. C) Erosional boundary of
 1001 breccia (base of arrow) at base of the Littleham Mudstone Fm, Littleham Cove (photo courtesy
 1002 of Ian West). Scale arrow height=1.5 m. D) Unconformable boundary (marked in white) between
 1003 the Watcombe Fm and the Oddicombe Breccia Fm, Whitsands Bay, hammer for scale. E) Detrital
 1004 opaques (black) and pigmentary haematite grain coating (in red), fluvial sandstone, Dawlish
 1005 Sandstone Fm, Dawlish Station section. The right hand side opaque (a haematised rock fragment)
 1006 shows compactional deformation from surrounding framework grains. F) Detrital opaque
 1007 showing indentation due to compaction into the surrounding quartz grains. Pigmentary haematite
 1008 rims not present at opaque-quartz boundary. Fluvial sandstone in Dawlish Sandstone Fm. Pore
 1009 spaces in blue. E) and F) scale bar is 100 μm .

1010

1011 Fig. 4. Section logs and summary palaeomagnetic data (horizon polarity, demagnetisation
 1012 behaviour and specimen polarity) from sections in the Exeter Group. See Fig. 1 for location

1013 details. Symbols for specimen polarity and behaviour are larger for better quality behaviour.
 1014 Ticks adjacent to logs are sampling levels. Sample numbers indicated, for data shown on other
 1015 figures or in the supplementary data.

1016

1017 Fig. 5. Section logs and summary horizon magnetic polarity data for the stratigraphic section
 1018 between Lymptone (site 3 on Fig. 1) to the top of the Littleham Mudstone Fm at Budleigh
 1019 Salterton (Fig. 1). Bed numbers on the log for the Exmouth Mudstones and Sandstones Fm are
 1020 those of Selwood *et al.* (1984). The divisions in the Littleham Mudstone Fm are from this work
 1021 (detailed in the supplementary data). Ticks adjacent to logs are sampling levels. Sample numbers
 1022 indicated, for data shown on other figures or in the supplementary data.

1023

1024 Fig. 6. Isothermal remanent magnetisation curves (A, C, E) and thermal demagnetisation of
 1025 orthogonal isothermal remanent magnetisation (IRM) in B, D, F, for representative specimens.
 1026 The Two numbers after lithology type are the magnetic susceptibility in $\times 10^{-5}$ SI and NRM
 1027 intensity in mA/m, respectively. Specimen numbers are those shown on Figs. 4 and 5.
 1028 sst=sandstone; TBF= Teignmouth Breccia Fm, EBF= Exe Breccia Fm.

1029

1030 Fig. 7. Anisotropy of magnetic susceptibility data for the Littleham Mudstone Fm (A, E, I), The
 1031 Exmouth Mudstone and Sandstone Fm (B, F, J), aeolian sandstones in the Dawlish Sandstone
 1032 and Teignmouth Breccia formations (C, G, K), and the various breccia units (D, H, I). A), B), C),
 1033 D) are stereographic projections of the specimen K_{\max} and K_{\min} directions. E), F), G), H) are the
 1034 AMS ellipsoid shape ($T = [2(L_{\text{int}} - L_{\text{min}})/(L_{\text{max}} - L_{\text{min}})] - 1$; where $L = \ln(K_i)$) and strength ($P =$
 1035 K_{\max}/K_{\min} ; Tarling & Hrouda, 1993), I), J), K), L), rose diagrams showing the directions of the
 1036 K_{\max} axes (mirrored about 0-180 axis), indicating the preferred grain long-axis directions in the
 1037 bedding plane. Ns=number of specimens.

1038

1039 Fig. 8. Representative demagnetisation data from: (A, B) the Littleham Mudstone Fm, (C, D)
 1040 Exmouth Mudstone and Sandstone Fm, (E) Exe Breccia Fm, (F) Dawlish Sandstone Fm, (G)
 1041 Teignmouth Breccia and (H) Watcombe Fm. A) Specimen L35, normal polarity (behaviour S1,
 1042 ChRM 500-660°C), B) EM30-4, reverse polarity (behaviour T1, component A, 0-500°C), C) E20,
 1043 normal polarity (behaviour S2, ChRM 600°C to origin), D) EL63, reverse polarity (behaviour T1,
 1044 Component A, 0-300°C), E) EB8-1A, normal polarity (behaviour S2, ChRM 300-500°C & 540°C
 1045 to origin), F) DS21-1, reverse polarity (behaviour T1, steps 500°C and above noisy due to

1046 thermal alteration), G) DS4-2, reverse polarity (behaviour S2, ChRM 500-650°C), H) WB1-4,
 1047 reverse polarity (behaviour S1, ChRM 100-620°C, 680°C step shows thermal alteration). See
 1048 Figs. 4, 5 for specimen locations.

1049

1050 Fig. 9. a) Stereographic projection of all ChRM directions, with mean of these directions
 1051 indicated for the units from the Aylesbeare Mudstone Group. B) The progressive unfolding fold
 1052 test of Watson & Enkin (1993), using the data from the Exeter Group; showing the change in
 1053 Fisher k with unfolding (left) and a pseudo-sampling bootstrap (right) to estimate the 95%
 1054 confidence interval on the percentage unfolding.

1055

1056 Fig. 10. A) Detailed magnetostratigraphic data for the stratigraphic section between the
 1057 Lypstone sections (3 on Fig. 1) and Littleham Cove. i) Demagnetisation behaviour showing
 1058 categorisation into good (S1) and poor (S3) ChRM line-fits; great circle fit quality range from
 1059 good (T1) to poor (T3), and specimens with no Triassic magnetisation are indicated in the P/X
 1060 column. ii) Interpreted specimen polarity quality, with those in the greyed column not assigned a
 1061 polarity. Poorest quality in column headed '??'. iii) VGP latitude, with filled symbols for those
 1062 specimens possessing an S-class ChRM, and unfilled symbols for specimens with T-class, great-
 1063 circle behaviour. Polarity column: white= reversed polarity, black =normal polarity, grey=
 1064 uncertain, gap=X; half bar-width indicates a single useful specimen from this horizon. B)
 1065 Detailed magnetostratigraphic data for the stratigraphic section between Littleham Cove and
 1066 Budleigh Salterton (1 on Fig. 1). Column details as in A).

1067

1068 Fig. 11. Summary magnetostratigraphic data for European Permian sections, compared to the
 1069 composite geomagnetic magnetic polarity timescale (GPTS) of Hounslow (submitted). Southern
 1070 North Sea data for the Leman Sandstone Fm from Turner *et al.* (1999) and Lawton & Robertson
 1071 (2003). Czaplínek, Piła and Jaworzna IG-1 well data based on Nawrocki (1997) and
 1072 Słowakiewicz *et al.* (2009). Mirow well data from Menning *et al.* (1988) and Langereis *et al.*
 1073 (2010), Schlierbachswald-4 and Everdingen 1 wells from Szurlies *et al.* (2003) and Szurlies
 1074 (2013). Related Russian stages tied to the magnetostratigraphy from Hounslow (submitted).
 1075 Conodont zones labelled with Guadalupian (G) and Lopingian (L) zonal codes from Jin *et al.*
 1076 (2000) and Shen *et al.* (2010). Early Wuchiapingian carbon isotope excursions (CIE) and
 1077 Kamura event duration from Chen *et al.* (2011), Isozaki *et al.* (2011).

1078

1079

Type/ Location/ Unit	Dec (°)	Inc (°)	K	α_{95} (°)	NI/Np	Reversal Test	G_O/G_C (°)	Plat (°)	Plong (°)	Dp/Dm (°)
Littleham Mudstone Fm										
Line fits ^s	12.4	29.2	26.0	5.4	28/0	R-	11.9/10.4*	53.6	156.3	3.3/6.0
GC means ⁺	10.3	29.2	24.1	4.1	28/25	Rc	11.2/11.2	54.0	159.6	2.5/4.5
Exmouth Mudstone and Sandstone Fm										
Line fits ^s	14.0	27.1	22.2	4.3	52/0	Rc	11.3/13.3*	52.0	154.2	2.6/4.7
GC means ⁺	14.2	29.0	18.2	3.8	52/27	Rb	2.4/10.0*	53.1	153.5	2.3/4.2
Dawlish Sandstone and Exe Breccia fms										
Line fits ^s	5.0	26.6	40.4	7.3	11/0	Rc	7.5/20.0	53.2	168.5	4.3/7.9
GC means ⁺	359.4	32.7	8.1	11.3	11/12	Rc	9.6/11.9*	56.9	185.7	7.2/12.8
Teignmouth Breccia Fm										
GC mean ⁺	174.8	-25.1	25.1	8.5	10/3	-	-	52.4	184.8	4.9/9.1
Oddicombe Breccia Fm										
Shaldon and Maidencombe ^s	191.4	-24.4	116	3.4	16/0	-	-	51.1	158.6	2.0/3.6
Watcombe Fm, basal Oddicombe Breccia										
Watcombe ^s	173.4	-20.0	28.0	10.7	8/0	-	-	49.5	186.5	5.9/11.2
Other units and data										
Knowle Sandstone ^s	195	-17	6842	3	2/0	-	-	-	-	-
Exeter Volc. Fm ¹	198	-25	23	6.5	23/0	-	-	49.5	148.5	-3.8/7.0
Exeter Volc. Fm ²	189	-19	29	10	9/0	-	-	48	163	-5.4/10.4
Exeter Gp sediments ²	188	-14	24	26	3/0	-	-	-	-	-
Group means										
Aylesbeare Mudstone Gp	13.5	27.8	23.6	3.3	80/0	Rb	6.7/7.4*	52.5	154.9	2.0/3.6
Exeter Gp sediments	3.3	24.8	35.4	3.6	45/0	Rb	5.5/10.0*	52.4	171.2	2.1/3.9

Table 1. Directional means (with tectonic correction), reversal tests and VGP poles. ⁺=great circle combined mean using method of McFadden & McElhinney (1988). ^s=conventional Fisher mean. NI=number of specimens using with fitted lines, and Np =number of specimens with great circle planes used in the determining the mean direction. α_{95} , Fisher 95% cone of confidence. k, Fisher precision parameter. G_O is the angular separation between the inverted reverse and normal directions, and G_C is the critical value for the reversal test. In the reversal test the G_O/G_C values flagged with * indicate common K values, others not flagged have statistically different K-values for reverse and normal populations, in which case a simulation reversal test was performed. Plat and Plong are the latitude and longitude of the mean virtual geomagnetic pole. ¹From Zijderveld (1967); ² from Cornwall (1967)

Fig.1

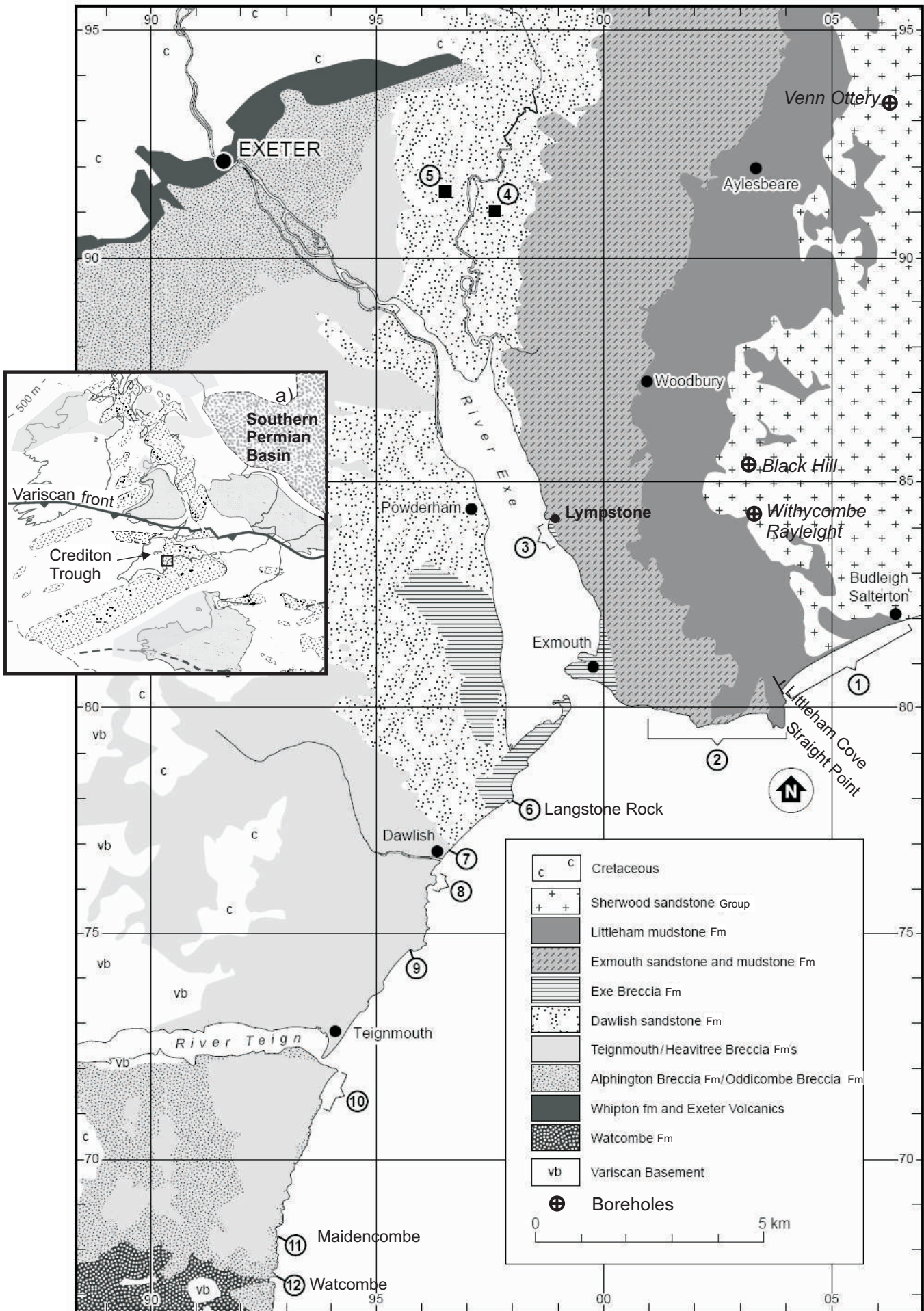


Fig.2

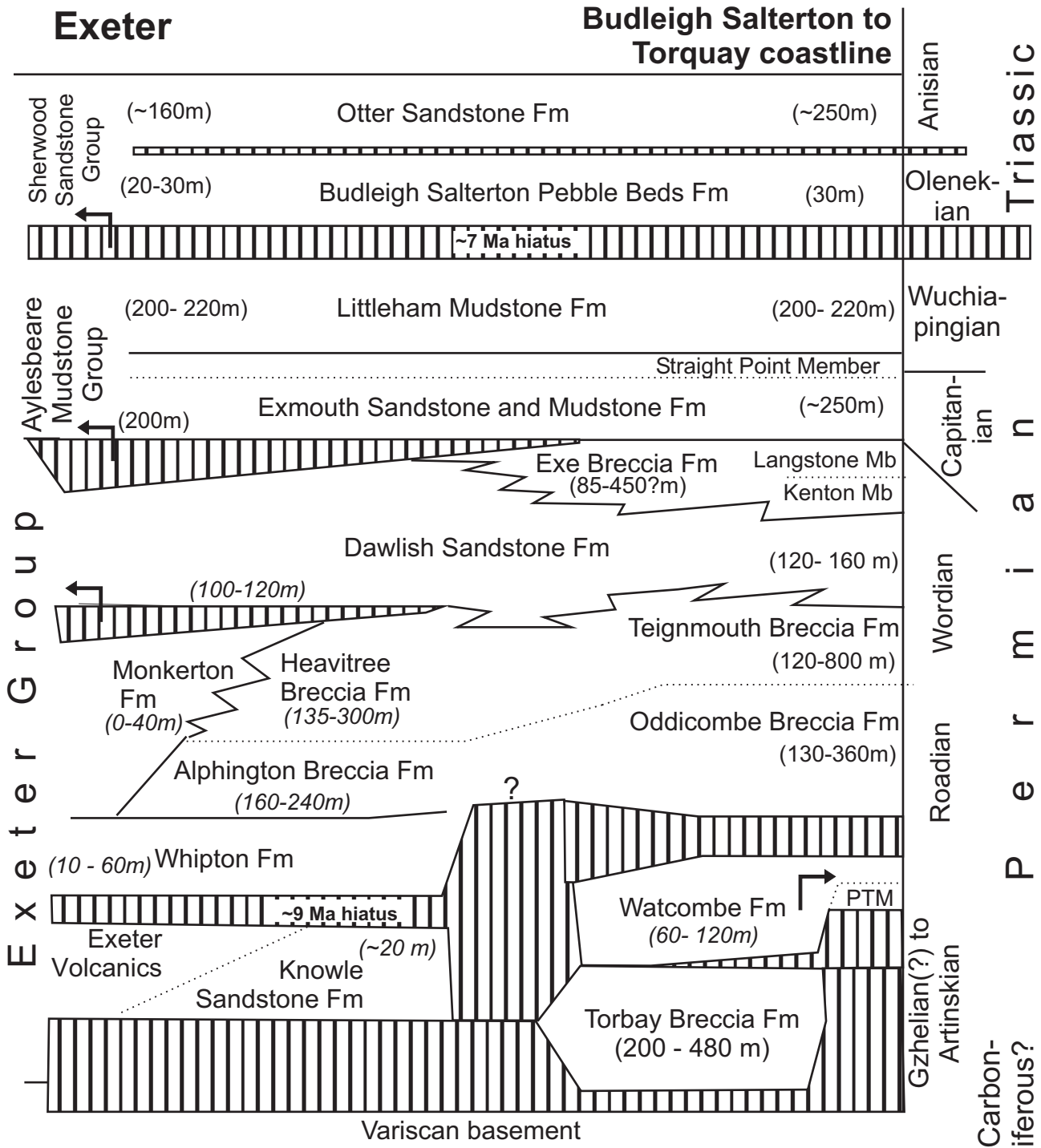
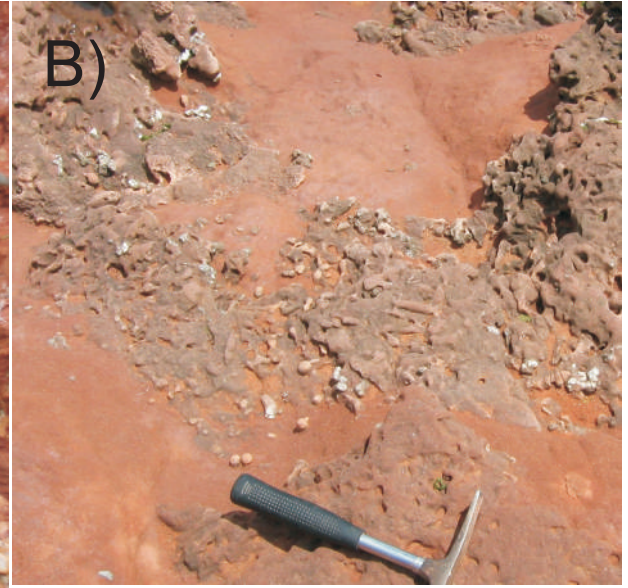


Fig.3

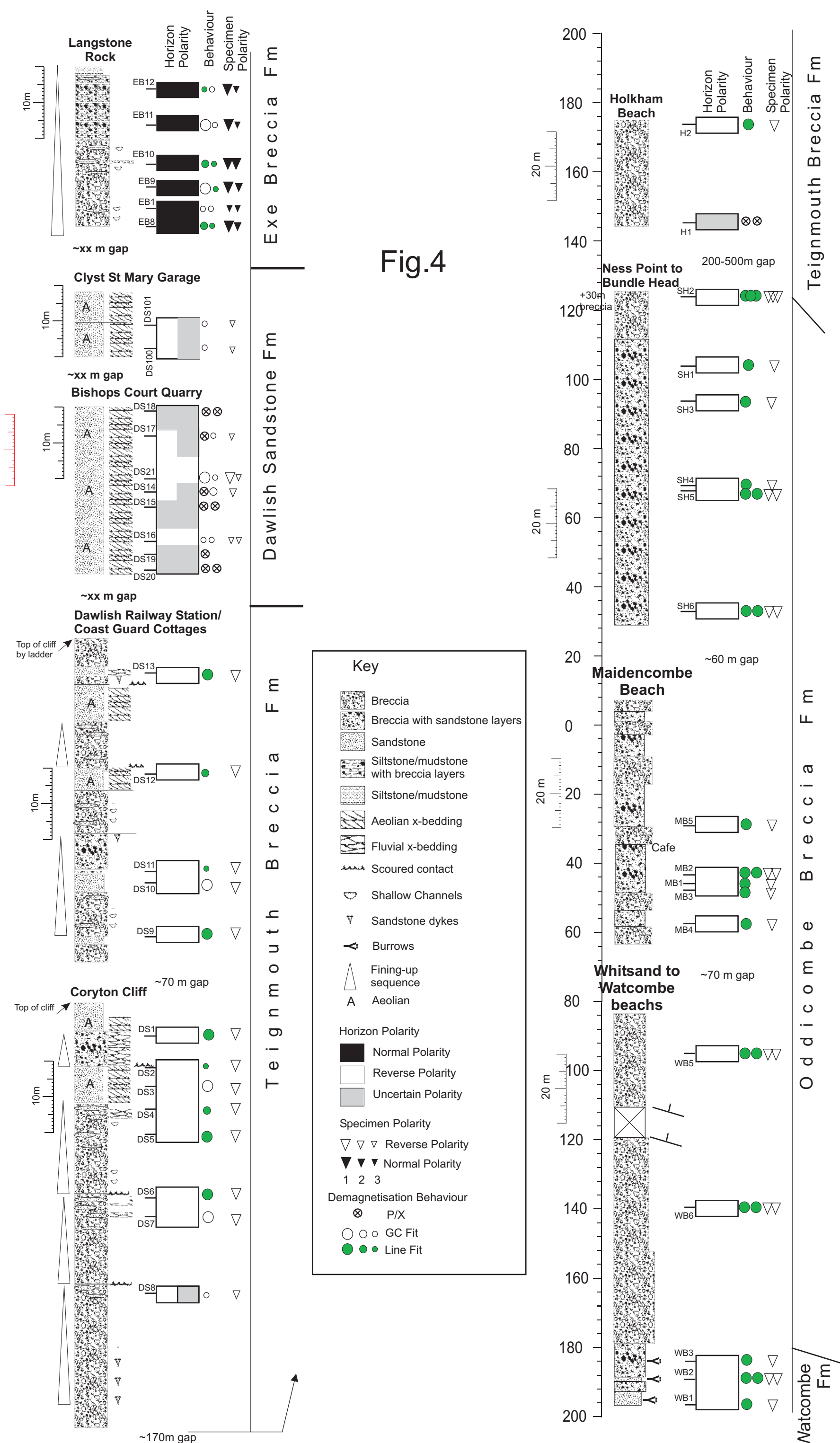


+Base Littleham Fm
Breccia (Sylvie?)

+Watcombe/Oddicombe
boundary (Deryck)

+Micrograph 1
(mwh)

+Micrograph 2
(mwh)



Watcombe Fm

Odcombe Breccia Fm

Maidencombe Breccia Fm

Teignmouth Breccia Fm

Dawlish Sandstone Fm

Exe Breccia Fm

Teignmouth Breccia Fm

Teignmouth Breccia Fm

Teignmouth Breccia Fm

Langstone Rock

Clyst St Mary Garage

Bishops Court Quarry

Dawlish Railway Station/
Coast Guard Cottages

Coryton Cliff

Holkham Beach

Ness Point to Bundle Head

Maidencombe Beach

Whitsand to Watcombe beaches

Watcombe Fm

Watcombe Fm

Watcombe Fm

Watcombe Fm

Watcombe Fm

Watcombe Fm

Watcombe Fm

Watcombe Fm

10m

Top of cliff by ladder

Top of cliff

+30m breccia

~60 m gap

~70 m gap

200-500m gap

~xx m gap

~xx m gap

~xx m gap

EB12
EB11
EB10
EB9
EB1
EB8

DS101
DS100

DS18
DS17
DS21
DS14
DS15
DS16
DS19
DS20

DS13
DS12
DS11
DS10
DS9

DS1
DS2
DS3
DS4
DS5
DS6
DS7
DS8

H2
H1

SH2
SH1
SH3
SH4
SH5
SH6

MB5
Cafe
MB2
MB1
MB3
MB4

WB5
WB6
WB3
WB2
WB1

Exe Breccia Fm

Dawlish Sandstone Fm

Teignmouth Breccia Fm

Teignmouth Breccia Fm

Teignmouth Breccia Fm

Maidencombe Breccia Fm

Odcombe Breccia Fm

Watcombe Fm

Fig.5

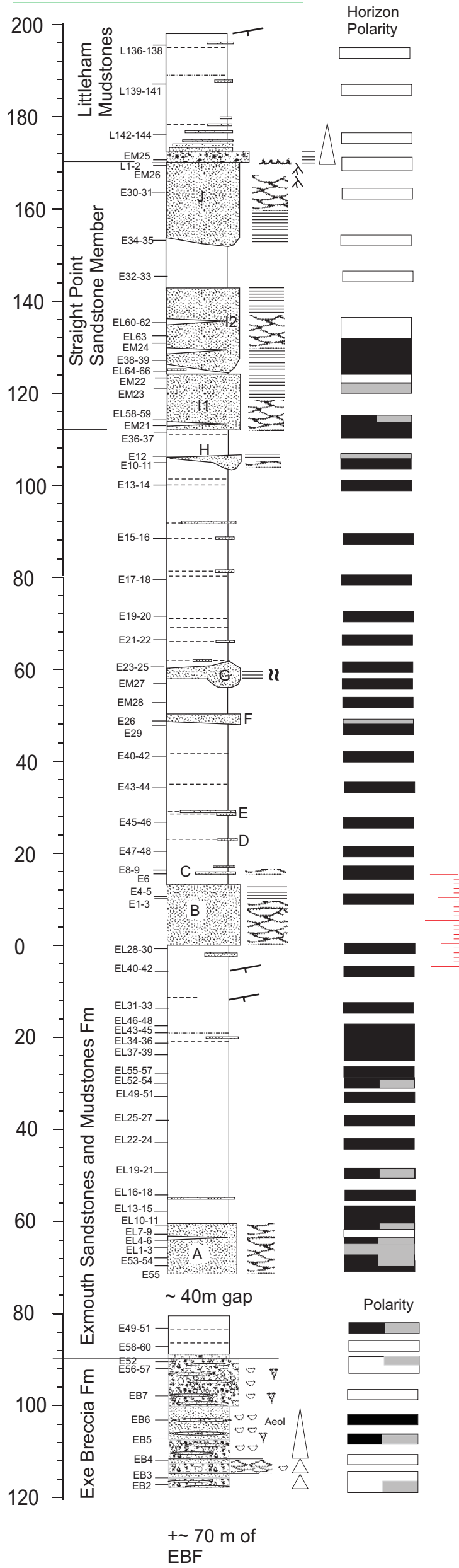
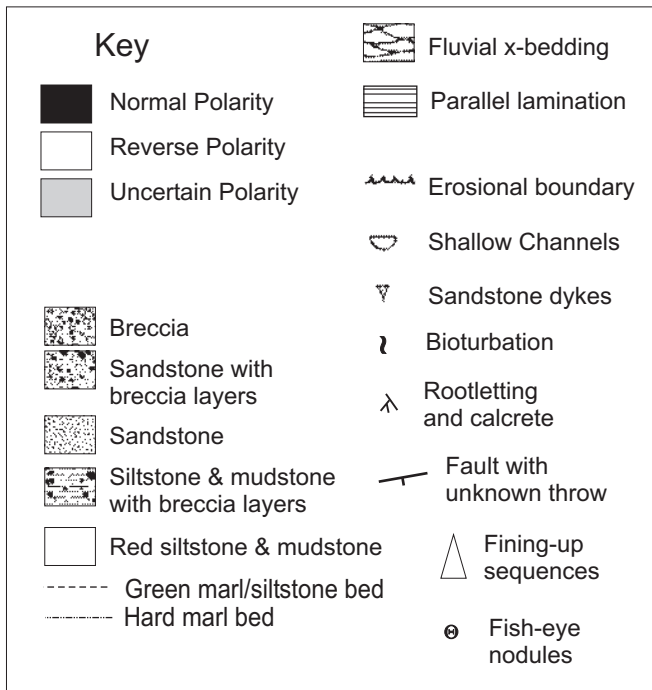
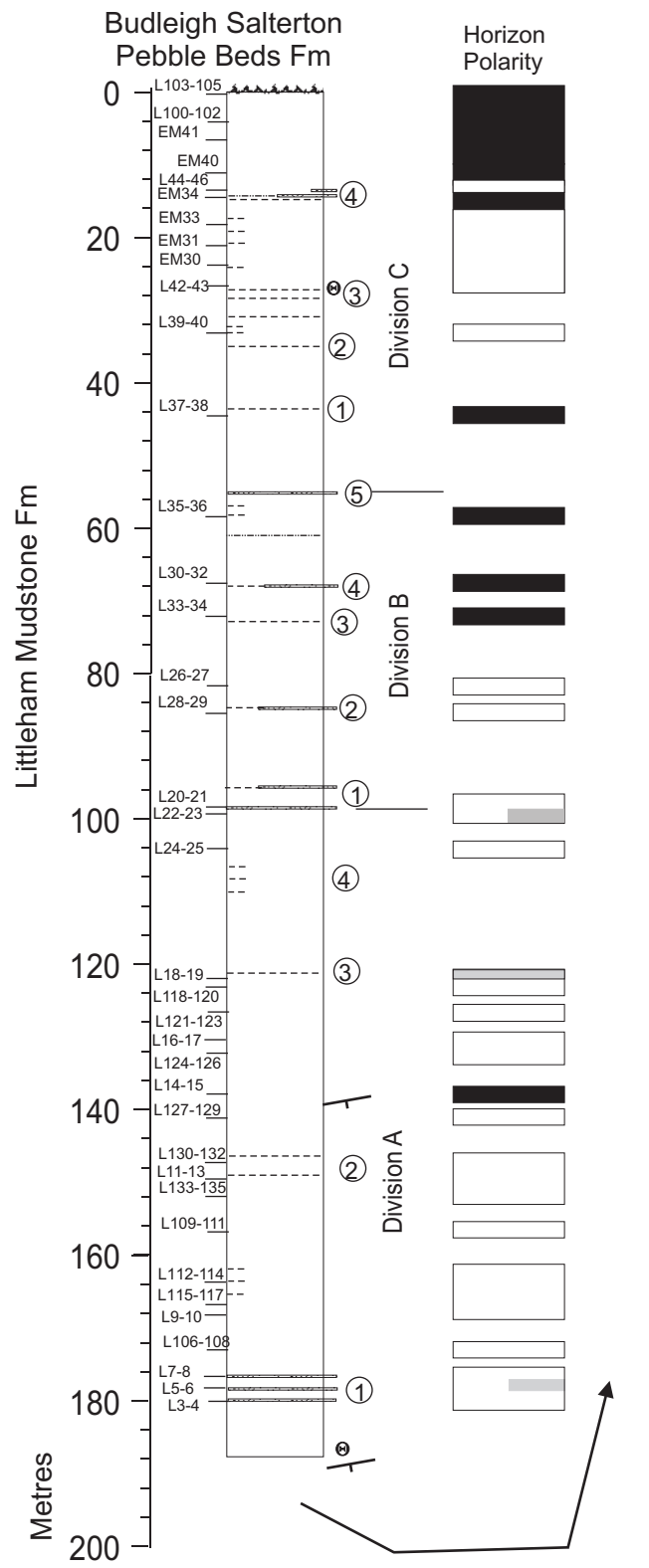


Fig.6

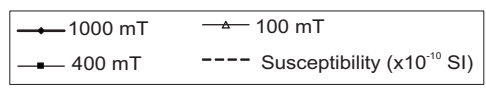
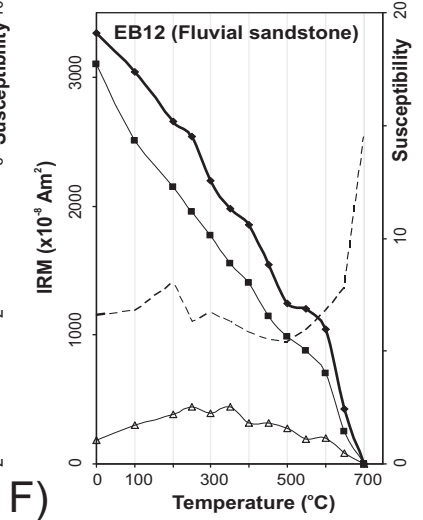
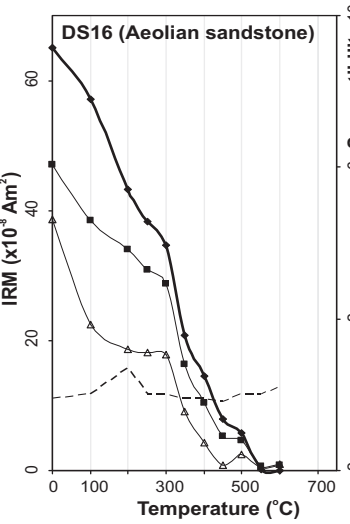
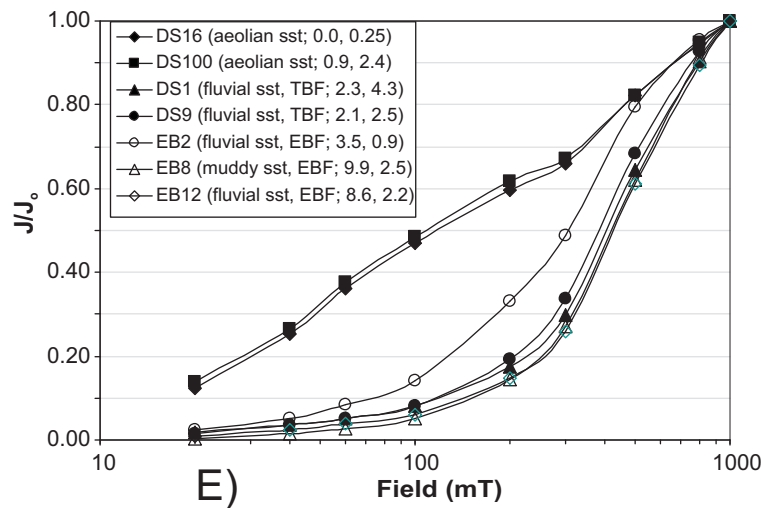
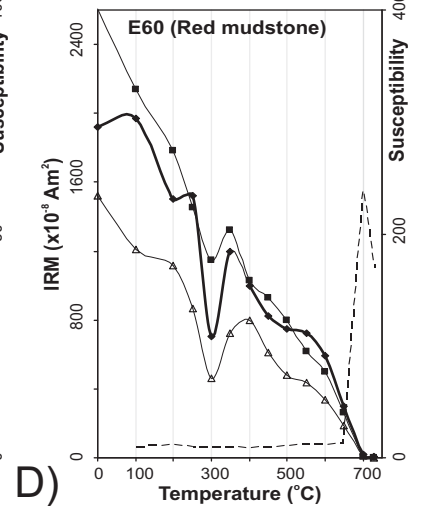
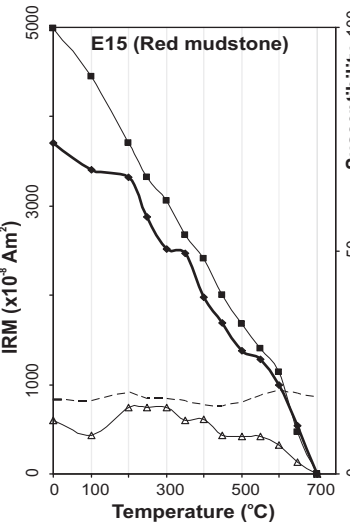
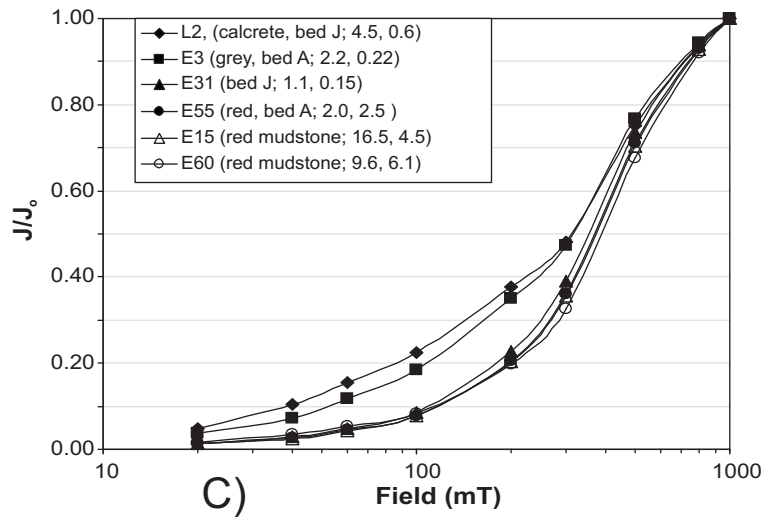
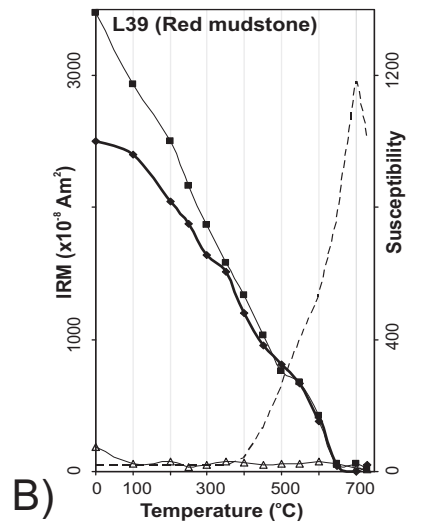
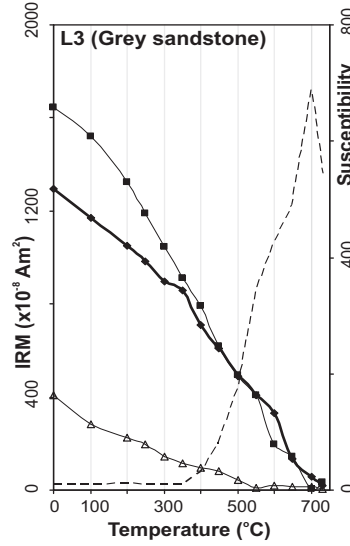
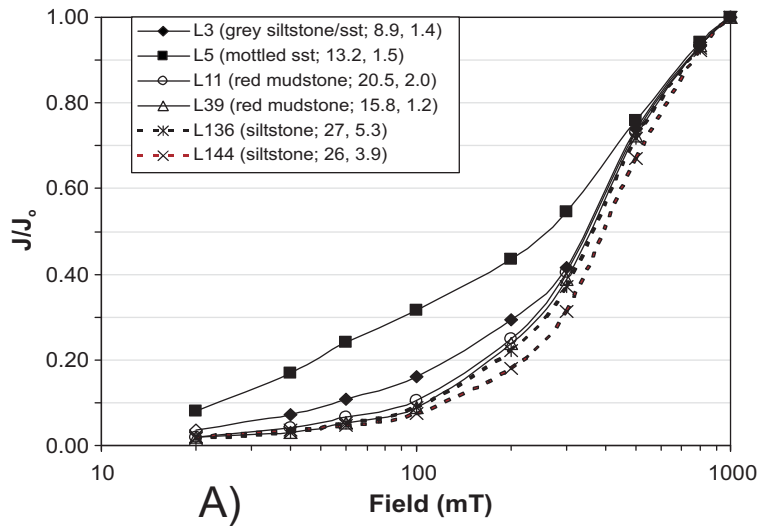
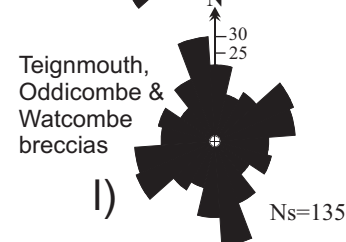
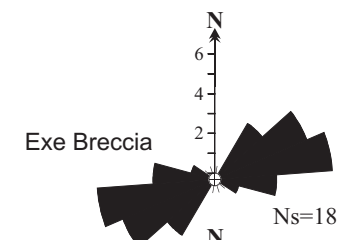
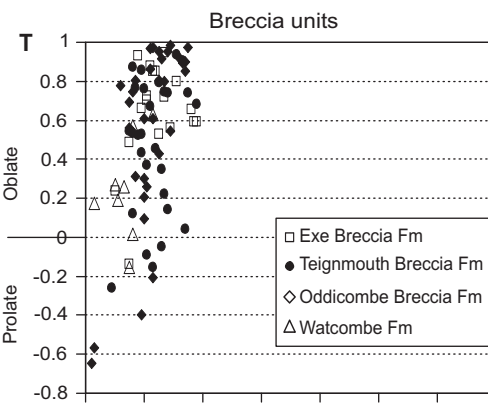
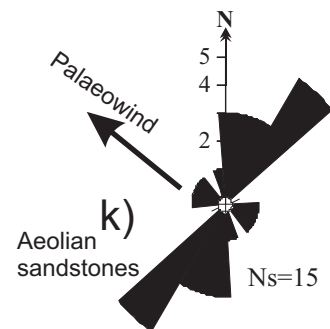
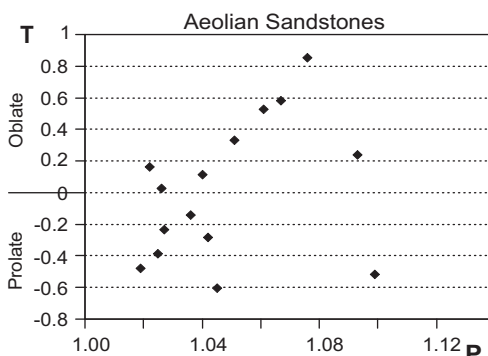
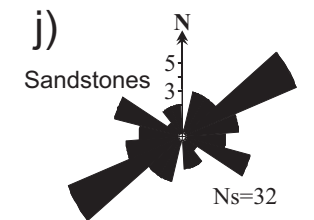
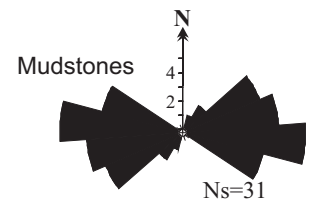
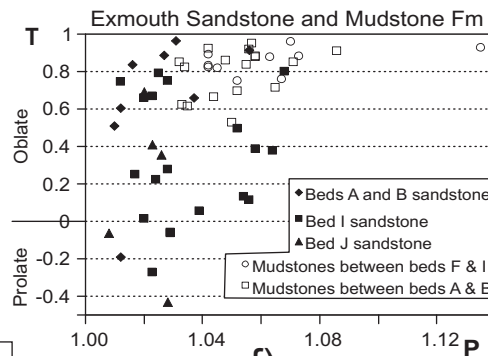
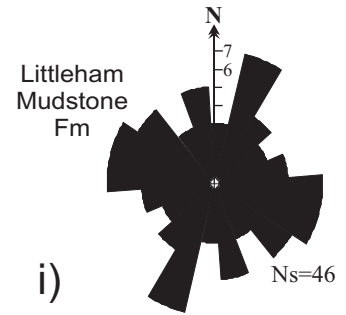
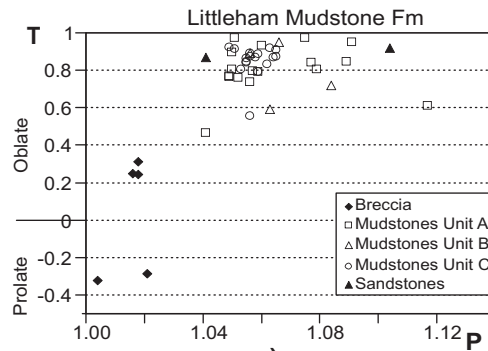
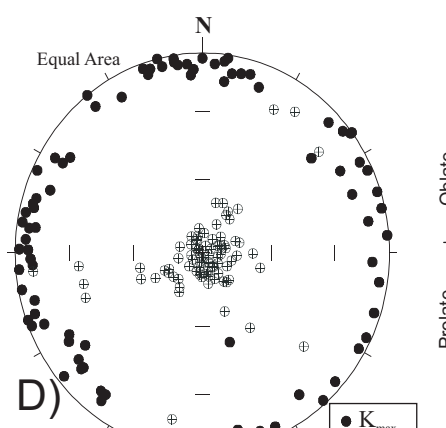
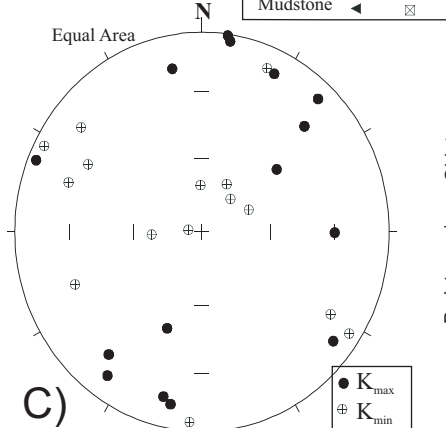
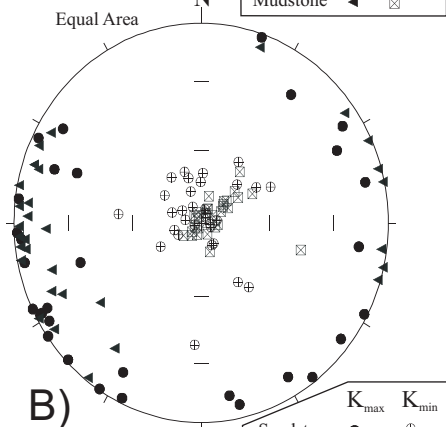
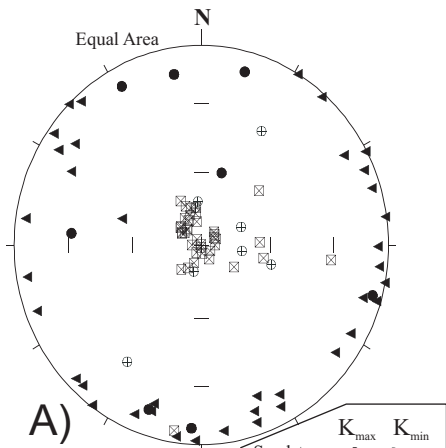
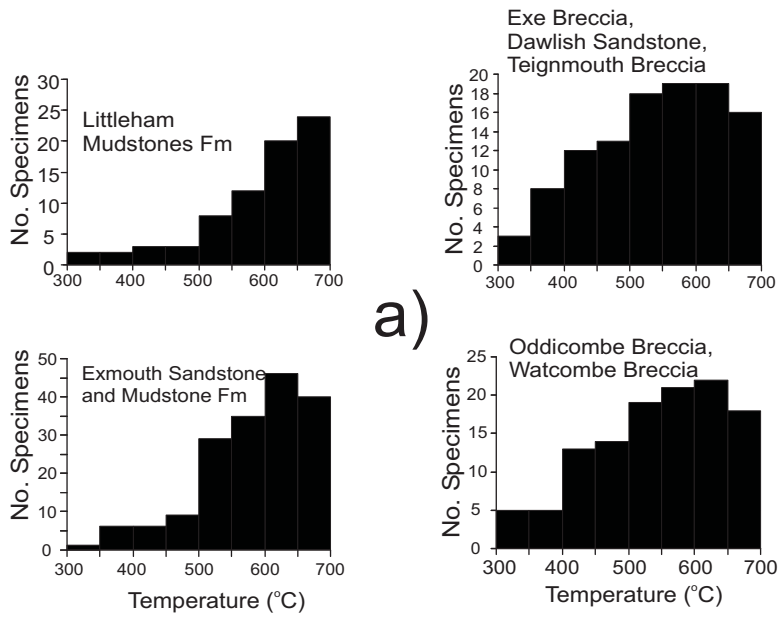


Fig.7





b)

		Class Ns	95	
Aylesbeare Mudstone Group	S1	23	5.7	2.1
	S2	28	10.6	2.4
	S3	29	13.9	3.2
	T1	21	18.1	2.9
	T2	21	20.7	2.2
	T3	24	19.8	2.9
Exeter Group	S1	31	3.2	2.9
	S2	5	5	2.9
	S3	8	9.6	3.8
	T1	7	17.3	3.2
	T2	2	8.5	2.5
	T3	13	16.5	4.0

Fig.9

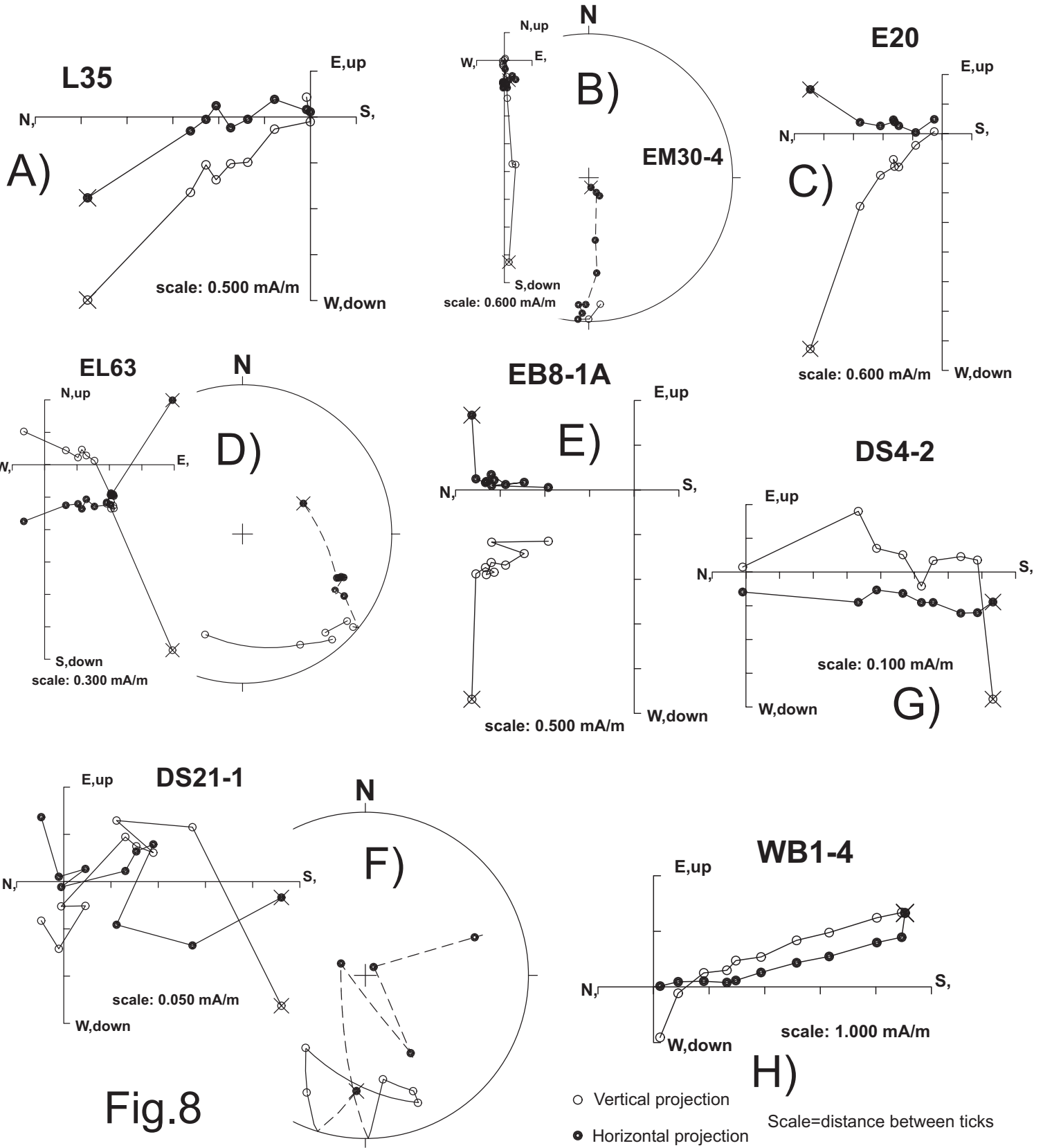
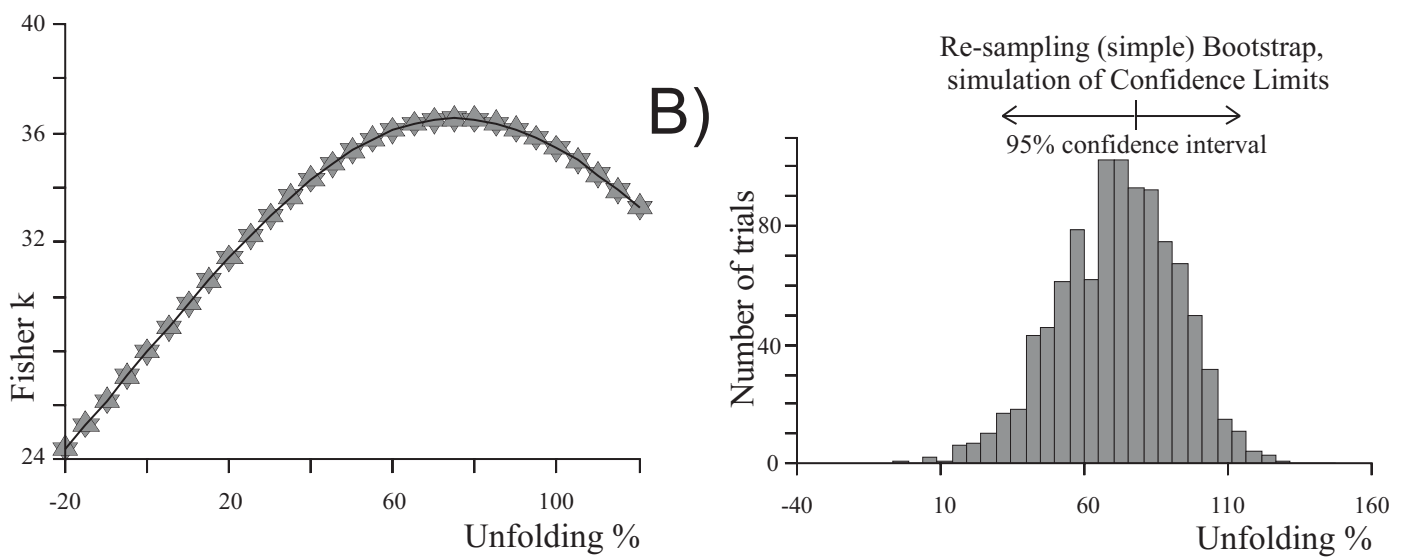
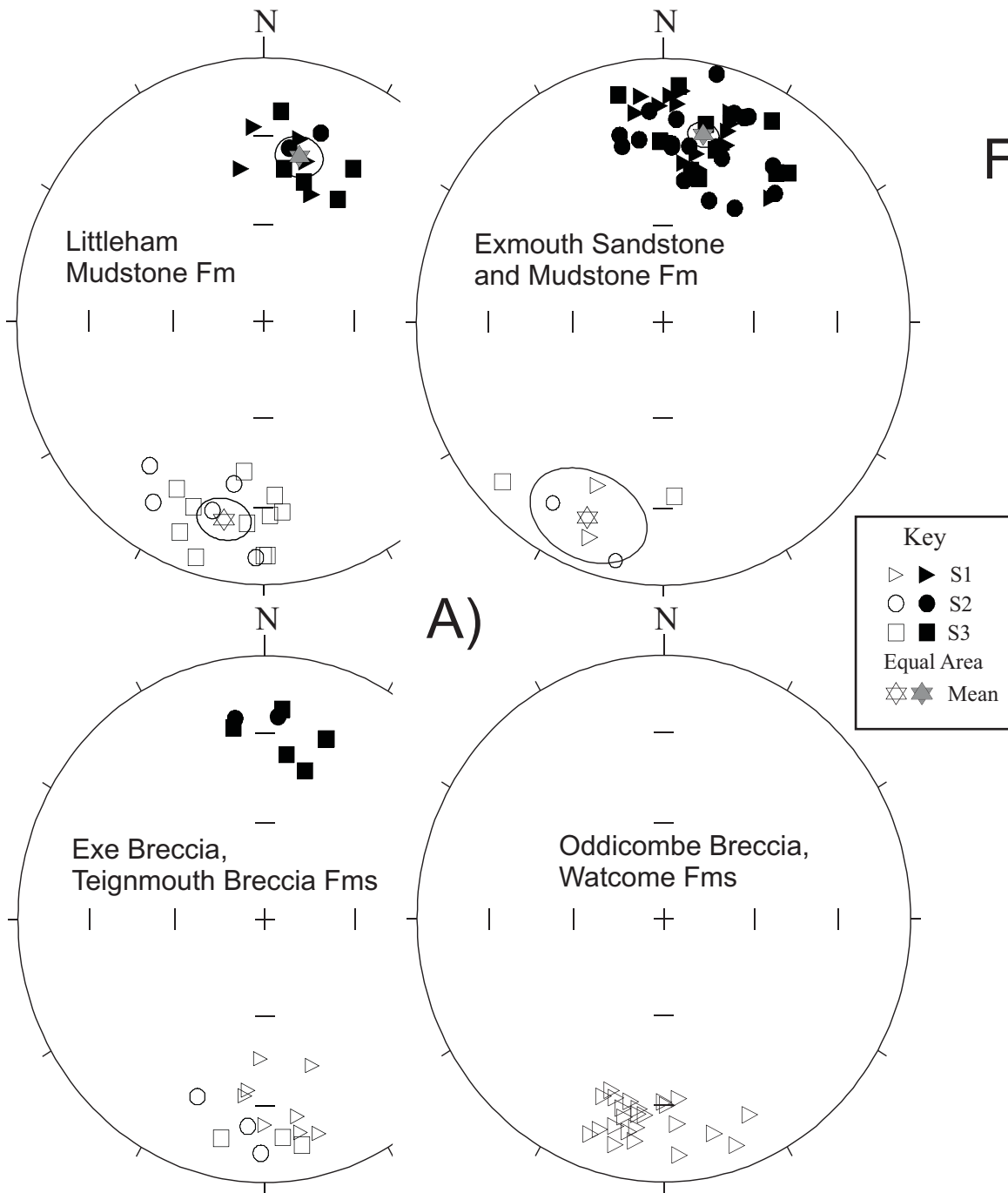


Fig.8

Fig.10



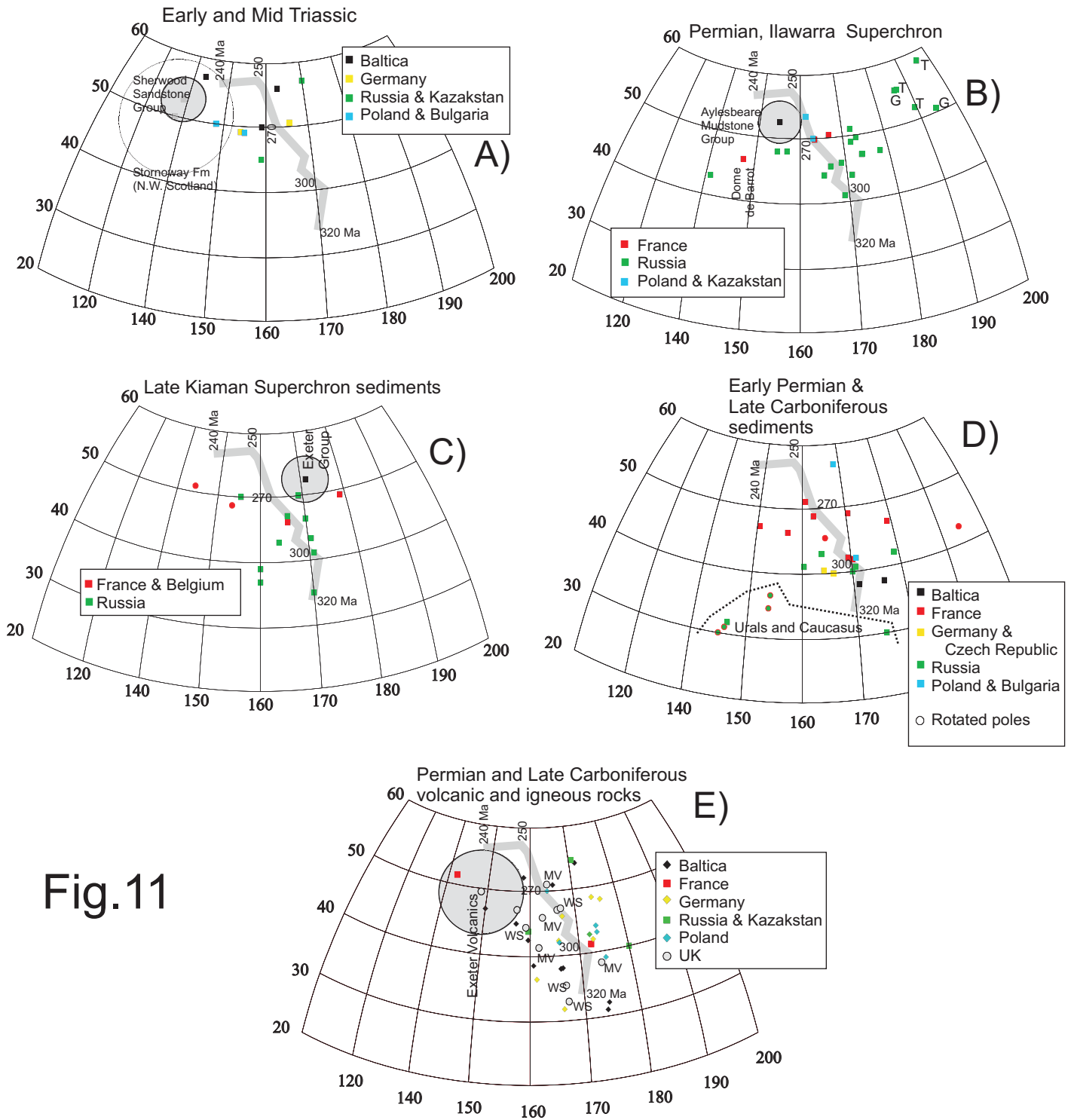


Fig.11

Fig.12

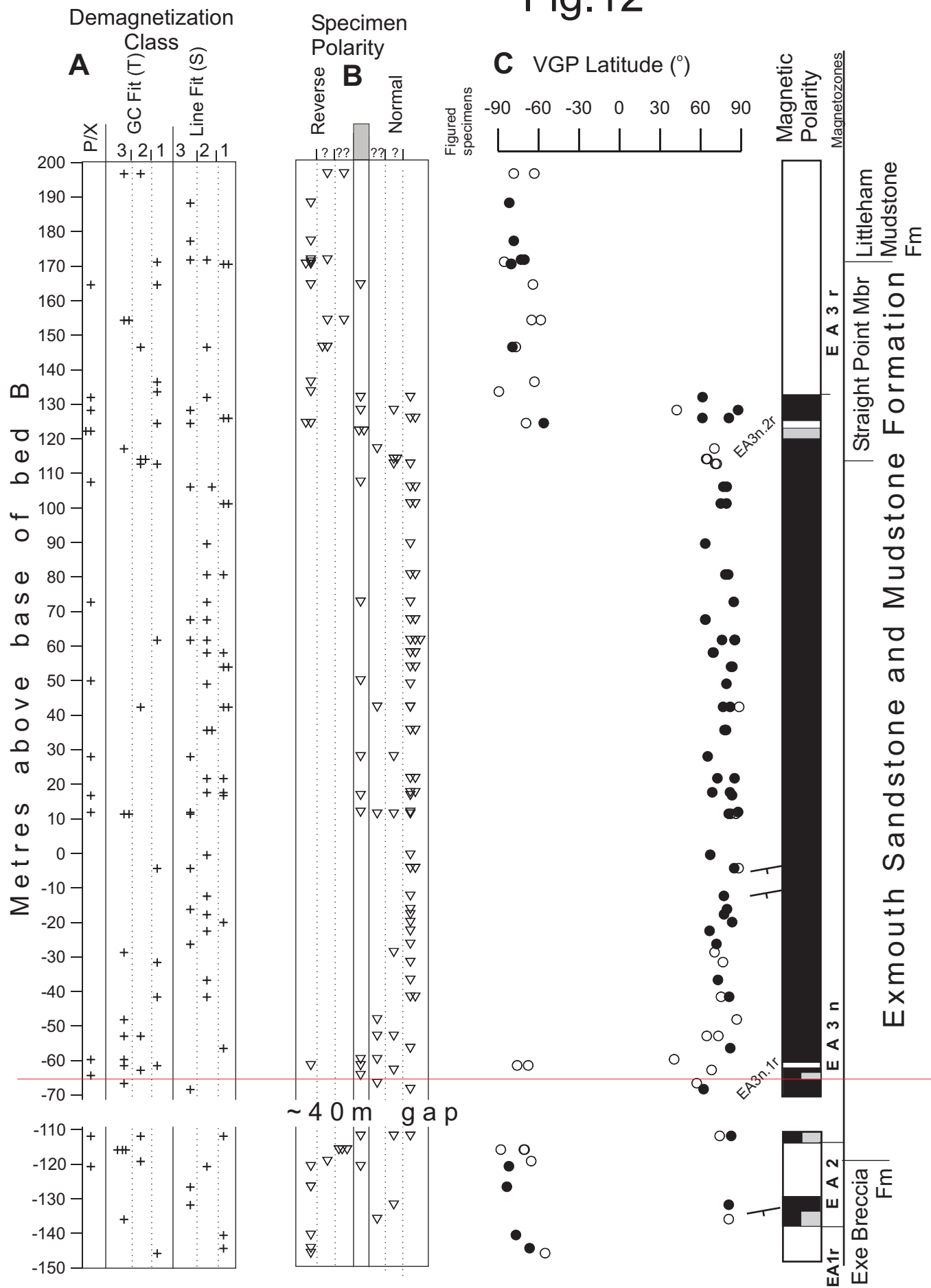
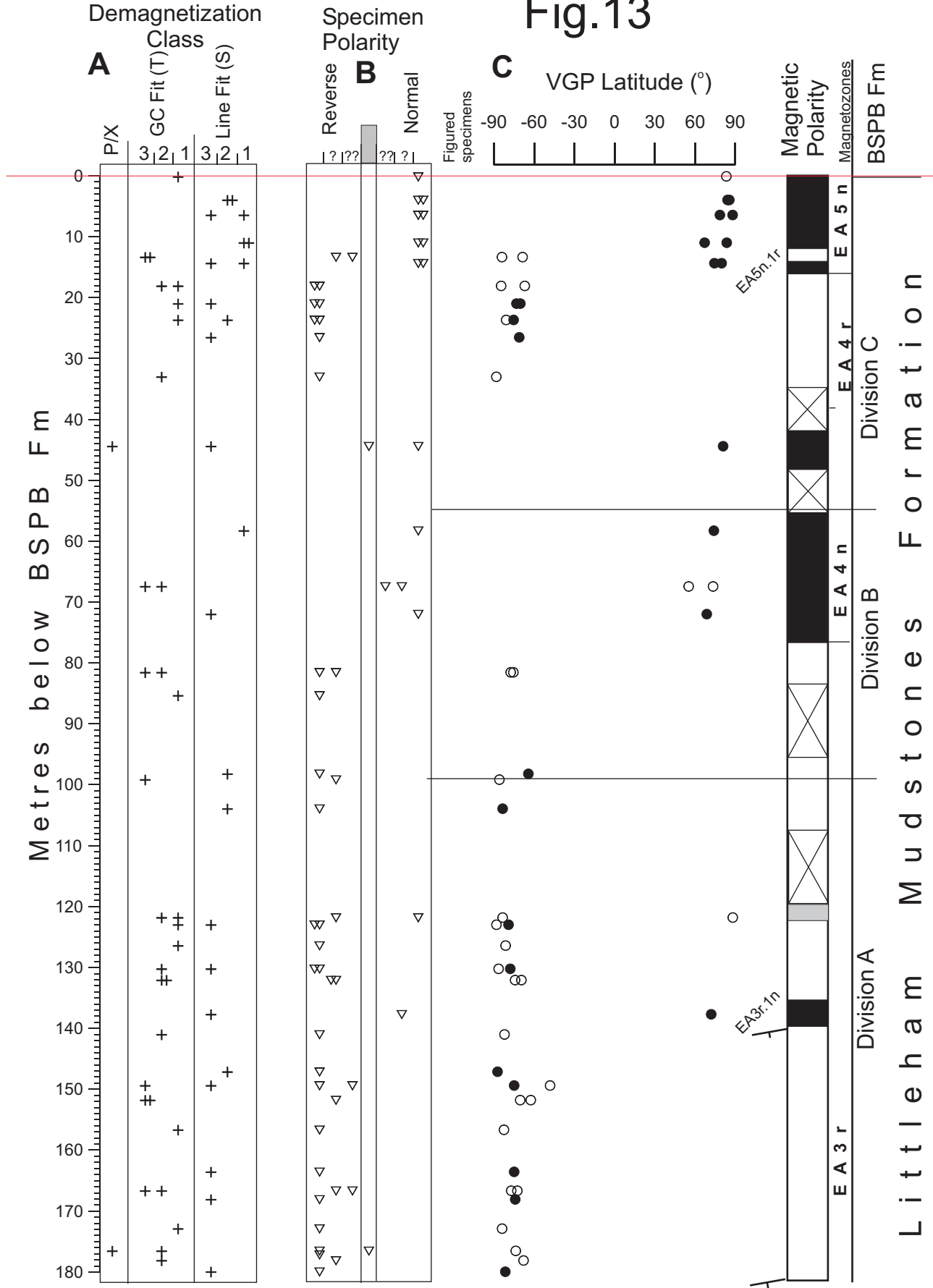
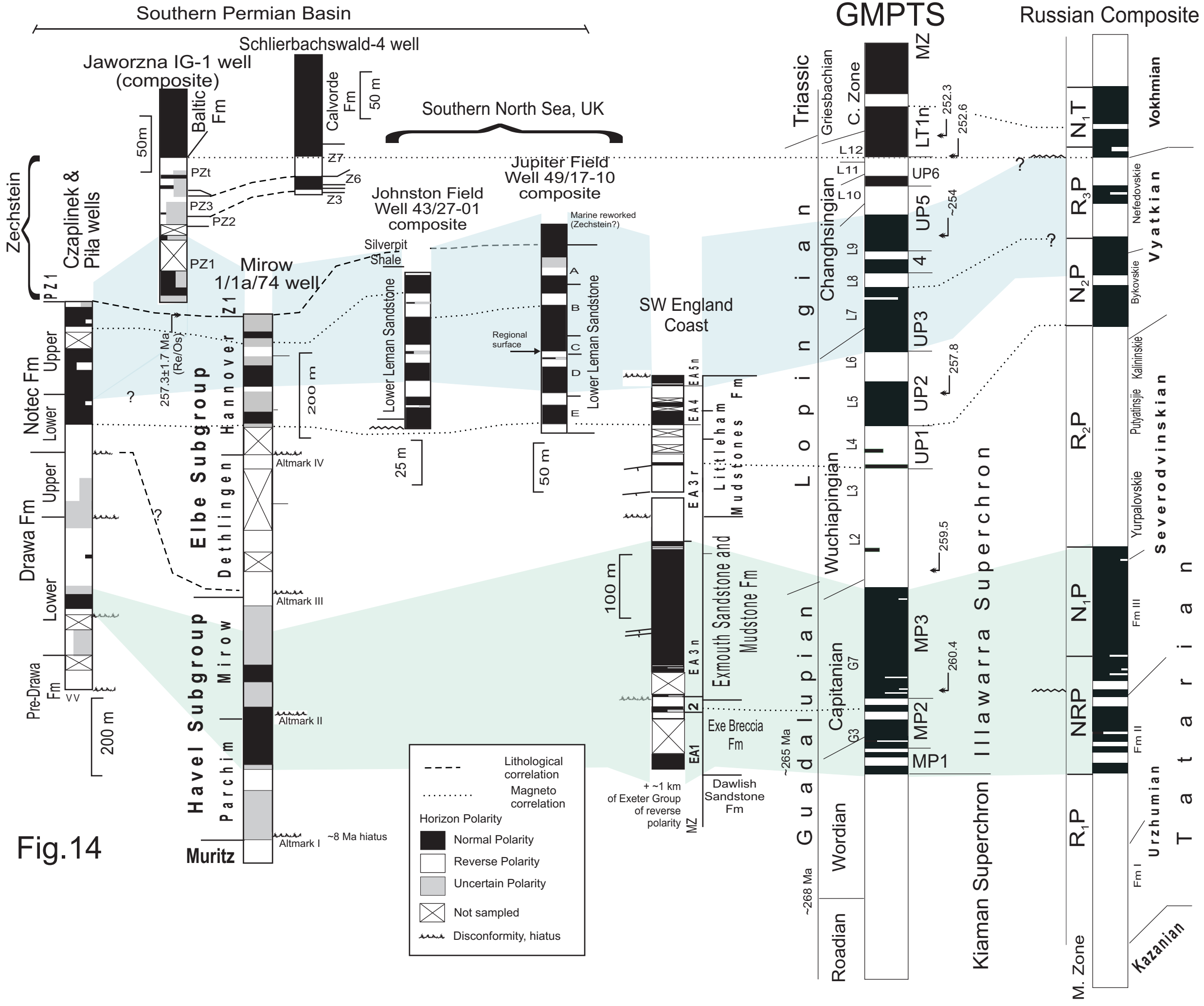


Fig.13





End of the Kiaman Superchron in the Permian of SW England: Magnetostratigraphy of the Aylesbeare Mudstone and Exeter groups.

Mark W. Hounslow, Gregg McIntosh, Richard A. Edwards, Deryck Laming, Vassil Karloukovski

Supplementary Data

The data here is composed of:

Table s1: Sampling site details, and mean magnetic properties.

Figure s1. The new bed-division of the Littleham Mudstone Fm, placed onto the photographs of the cliff outcrops.

Figure s2. Rose diagrams of the AMS Kmax axes, in the Aylesbeare Mudstone Group, against the sediment logs of the section.

Figure s3. The spatial variation in the AMS Kmax axes, of all Permian-Triassic west of Sidmouth, placed onto their sampling sites, and the palaeocurrent directions inferred from the sedimentology.

Figure s4. Component A data, and details of demagnetisation characteristics.

Figure s5. Additional rock magnetic data, pertaining to magnetic mineralogy

Figure s6. Petromagnetic data for all palaeomagnetic specimens.

Figure s7. Virtual geomagnetic pole data for Permian Europe, and a discussion of how the new data here fits with this data.

References.

Section	No. on Fig 1	Grid ref	Lat/long	Bedding strike/dip	N _H	J ₀ (x10 ⁻³ A/m)	κ _{lf} (x10 ⁻⁵ SI)	Formation/unit
Budleigh Salterton to Littleham Cove	1	SY040802 to SY063817	50.622N: - 3.342W	302/5	38	3.2	2.1	Littleham Mudstone Fm (LMF)
Straight Point to Maer	2	SY040802 to SY011799	50.608N: - 3.376W	340/5 to 013/8	60	4.0	1.35	Exmouth Mudstone and Sandstone Fm (EMSF), base of LMF
Sowden Lane to Lypstone Harbour	3	SX990836 to SX988842	50.638N: - 3.441W	321/9 to 315/8	10	2.1	3.3	Base of EMSF, top of Exe Breccia Fm
Clyst St Mary Garage	4	SX976910	50.710N: - 3.454W	045/5	2	2.4	0.68	Dawlish Sandstone Fm
Bishops Court Quarry	5	SX965915	50.711N: - 3.465W	045/5	6	0.74	0.57	Dawlish Sandstone Fm
Langstone Rock	6	SX980779	50.598N: - 3.445W	293/8	6	2.8	7.6	Exe Breccia Fm
Dawlish Station	7	SX964767	50.580N: - 3.465W	293/10	5	1.4	2.7	Teignmouth Breccia Fm
Coryton Cliff and Cove	8	SX962762	50.577N: - 3.468W	319/10	8	1.5	1.9	Teignmouth Breccia Fm
Holcombe Beach	9	SX957746	50.562N:- 3.475W	342/12	2	2.4	5.1	Teignmouth Breccia Fm
Ness Point to Bundle Head	10	SX941720 to SX937712	50.533N: - 3.500W	355/0 to 295/5	6	7.2	9.8	Oddicombe Breccia Fm
Maidencombe Beach	11	SX928684	50.505: - 3.514	275/10 to 346/6	5	9.3	7.0	Oddicombe Breccia Fm
Whitsand to Watcombe Beachs	12	SX927674	50.496: - 3.515	315/41 to 288/25	5	5.8	6.4	Watcombe Fm and Oddicombe Breccia Fm
West Sandford	Not on Fig. 1	SS811027	50.812N: - 3.689W	105/14	1	10.8	12.1	Knowle Sandstone Fm

Table. s1. Section and site details sampled, and average magnetic properties of the samples. N_H number of sampled horizons, J₀= Initial natural remanent magnetisation intensity, κ_{lf}= low frequency magnetic susceptibility. Most samples were collected from the sea cliffs, with those from Bishops Court Quarry from a working quarry (Table s1). Those from Dawlish Station and West Sandford were from small cuttings. Samples from below bed B to the base of bed A (Fig. 5), in the Exmouth Mudstone and Sandstone Fm, were from foreshore exposures and sea-cliffs, east of Exmouth. In the breccia units, suitable units for palaeomagnetic sampling were thin, discontinuous sandstone and mudstone beds.

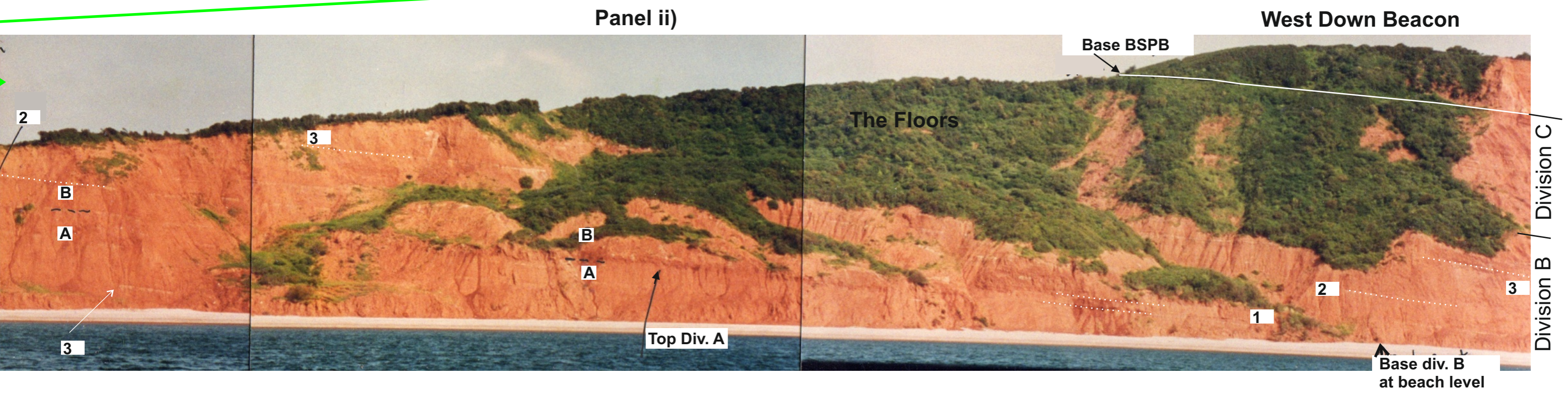
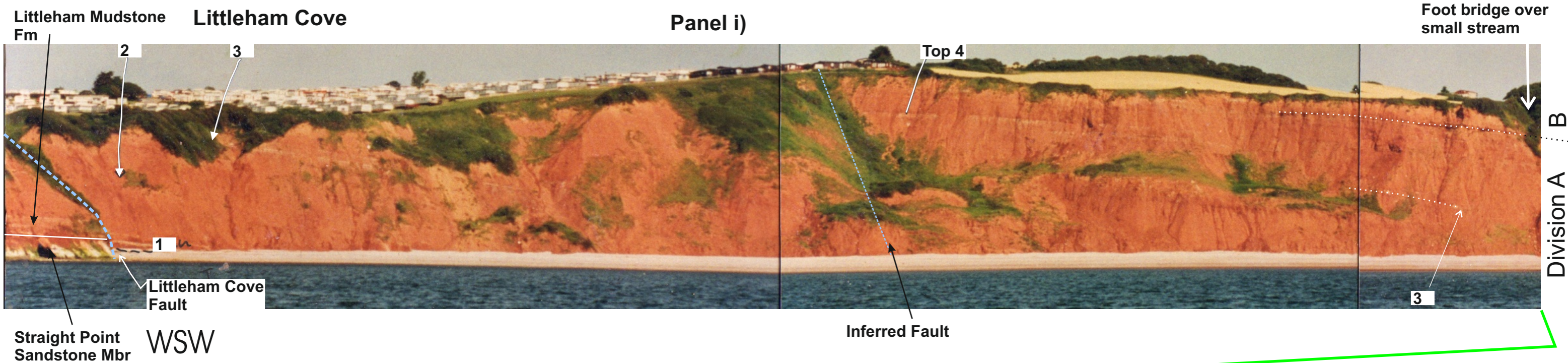
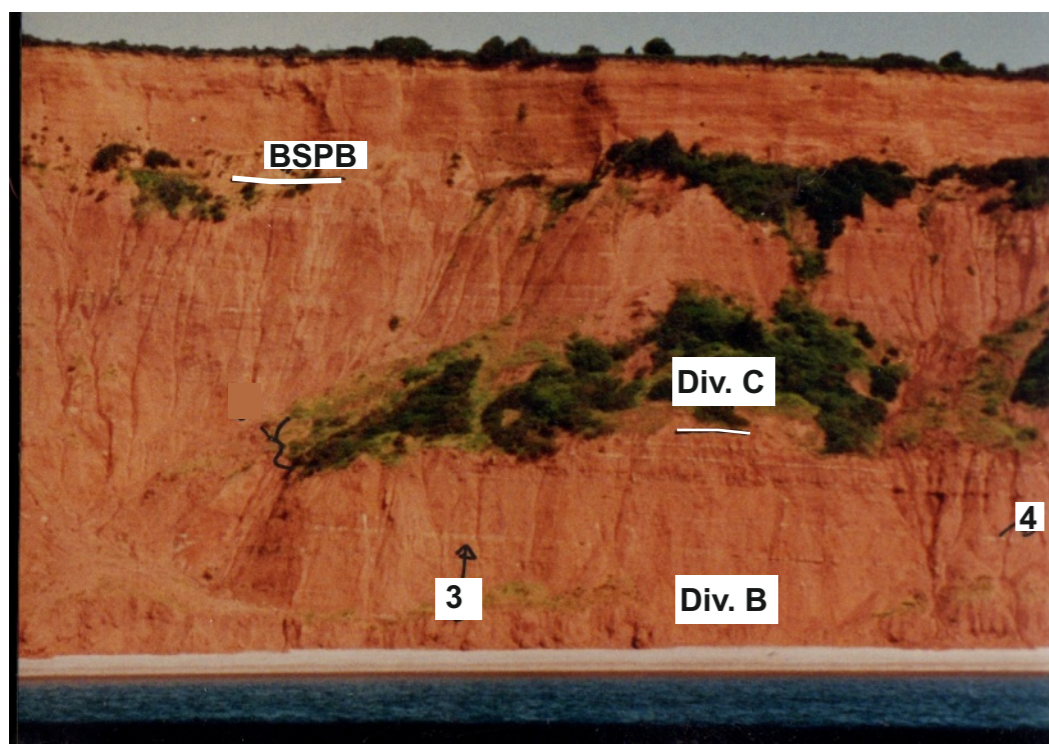


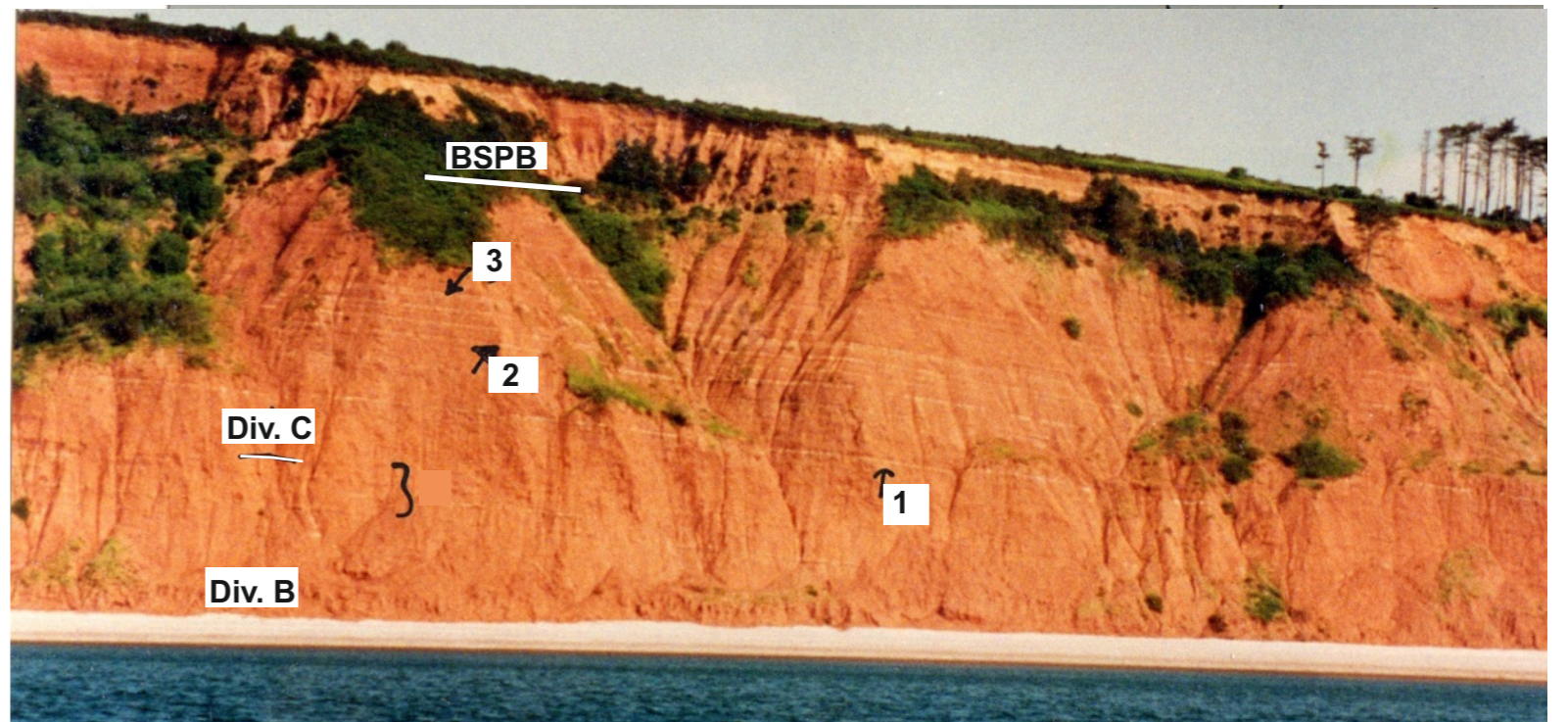
Fig.s1. Annotated photos of the cliff between Littleham Cove (panel i) and Budleigh Salterton (panel iv), indicating the bed and division sub-division of the Littleham Mudstones Formation. The three sub-divisions are a lower division A, mid division B, and an upper division C. The oldest part of the division A is exposed on the west side of the Littleham Cove fault. The W-E correlation across the Littleham Cove fault is not entirely clear, but the three sandstone beds (bed -1 in division A) may correlate to the upper-most units exposed west of the fault in the cliff adjacent to the path down the cliff. The succession is interrupted by a number of small landslips, which make the stratigraphy difficult to follow at beach level, without the photographs. The full succession can be examined by using the headwall scars behind the landslips.



Panel iii)

Gap between photos

Interval with many paler beds



Panel iv)

ENE

Gap between photos

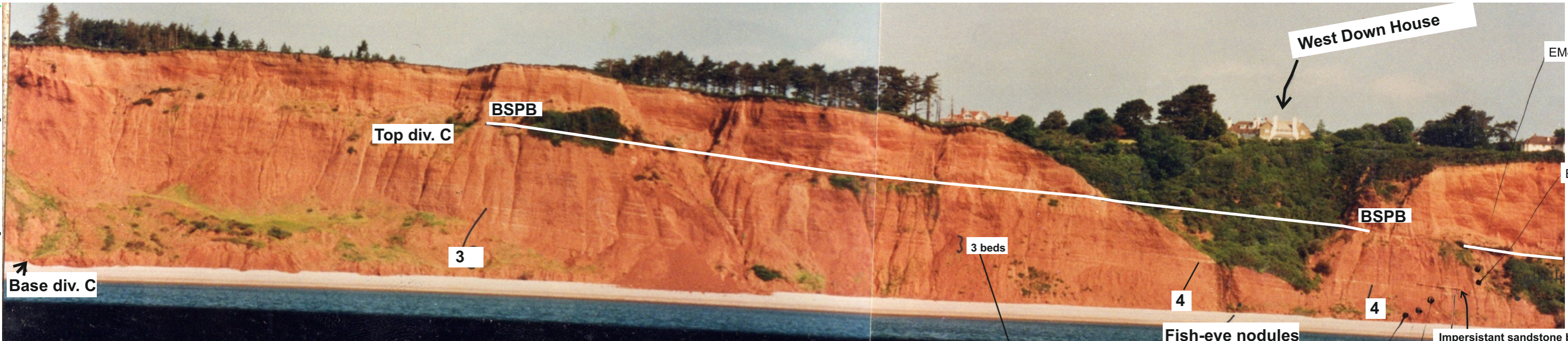


Fig.s1. Panels iii) and iv)

**Budleigh Salterton
Pebble Beds Fm**

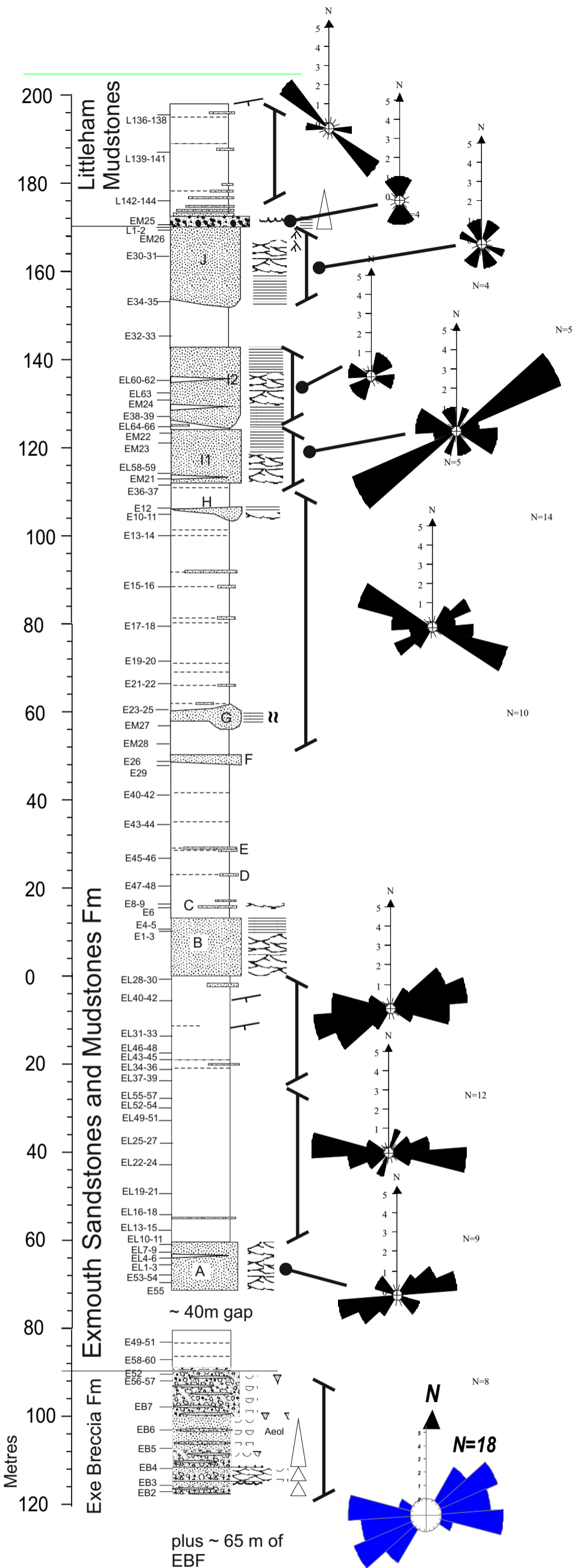
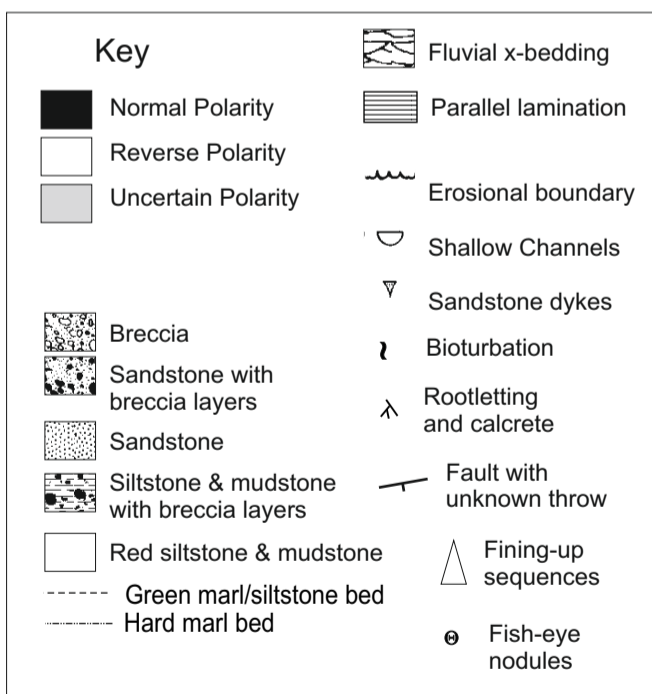
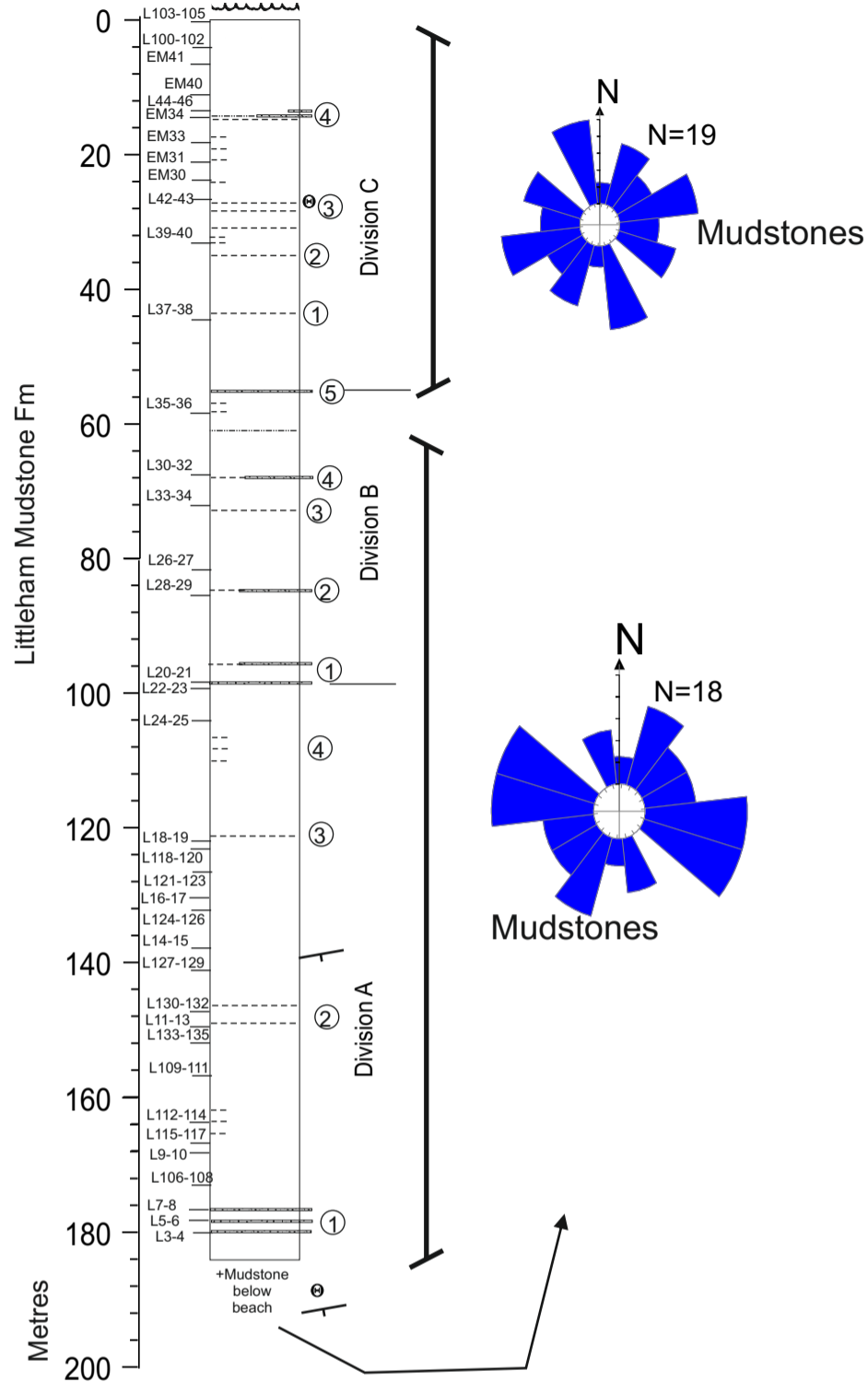


Fig.s2. K_{max} axis directions for samples from the Aylesbeare Mudstone Group. The directions have been mirrored about the 0-180 axis. The K_{max} axes directions illustrate the similarity in ENE or easterly flow directions between the Exe Breccia and the lower part of the Exmouth Mudstone and Sandstone Fm. The directions in the upper part of the Group are more variable, but likely indicate a more NE direction of sediment transport. The SE-NW K_{max} axes trends seen in the mudstones above bed G, and particularly in the Littleham Mudstones Fm may represent NW directed wind transport of the clay and silt in these units.

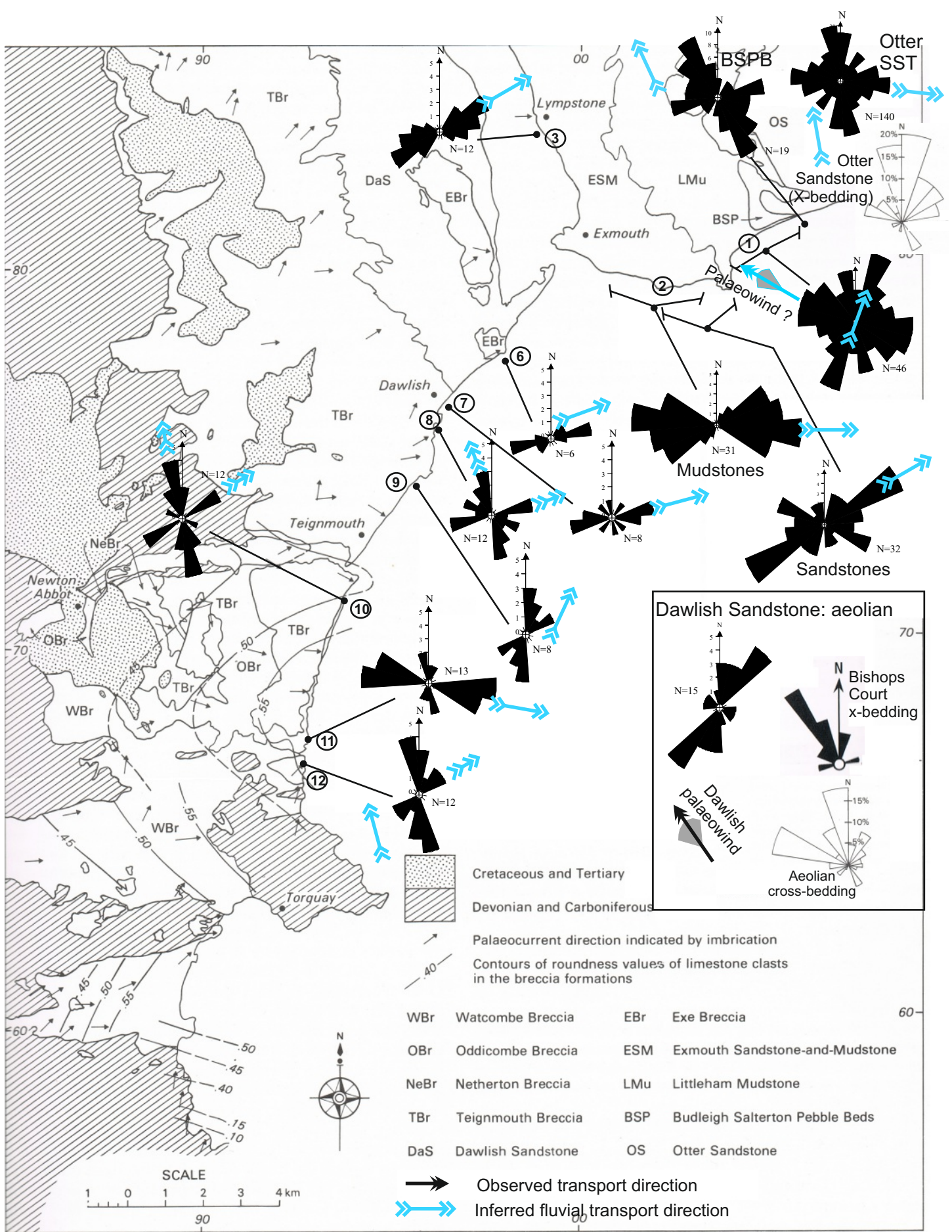


Fig.s3. Summary of transport directions and K_{max} axis directions for samples from the entire Permian, and Triassic successions west of Budleigh Salterton. Inset shows data for aeolian units, from the Dawlish Sandstone Fm (from Jones 1992, Selwood *et al.* 1984). The K_{max} directions have been mirrored about the 0-180° axis (fluvial transport data from Laming 1966; Henson 1971; Selwood *et al.* 1984; Smith & Edwards 1991). The Triassic AMS data (Otter Sandstone, Budleigh Salterton Pebble Beds, BSPB) is from the samples described by Hounslow & McIntosh (2003). The Exeter Group below the Dawlish Sandstone Fm typically has bi-modal groups inferred to display ENE to easterly fluvial transport and northerly transport. Its possible in some of the sandstone and mudstones, the northerly trend may be a wind-transport direction, like seen in the aeolian units in the Dawlish Sandstone. Fluvial units in and above the Dawlish Sandstone Fm into the lower Aylesbeare Mudstone Group, show strong ENE to easterly fluvial transport. In the Littleham Mudstone Fm directions may be transitional to the northerly transport clearly seen in the overlying BSPB and Otter Sandstone.

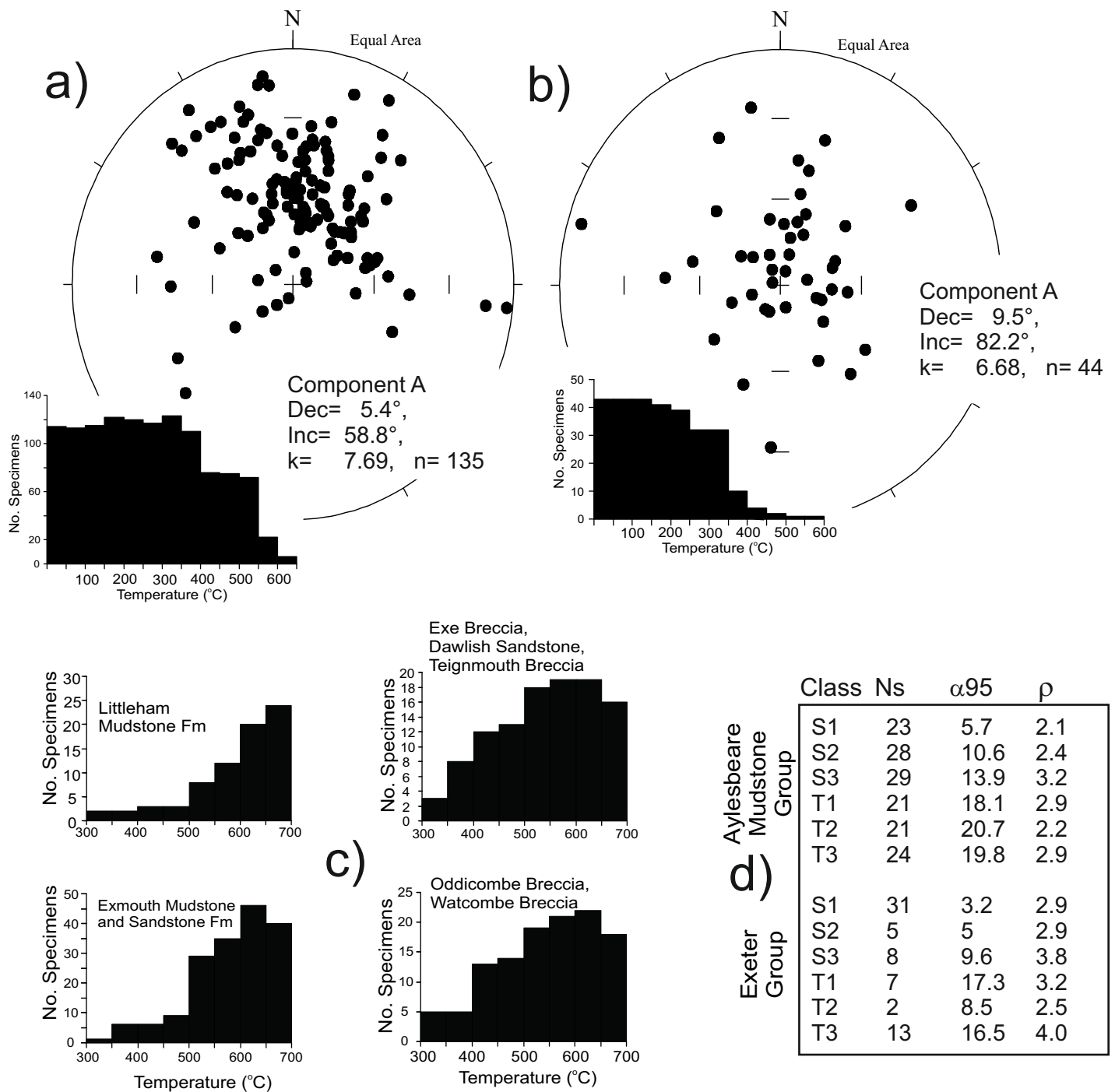


Fig.s4. Cumulative unblocking spectra for, a), b) the component A directions, from a) the Aylesbeare Mudstone Group, b) Exeter Group. C) The characteristic remanence ranges divided into stratigraphic groups. D) Statistics relating to the demagnetisation class, the number of specimens (Ns), the average α_{95} of the line (S-class) or plane (T-class) principle component fits, and the average excess standard deviation (ρ).

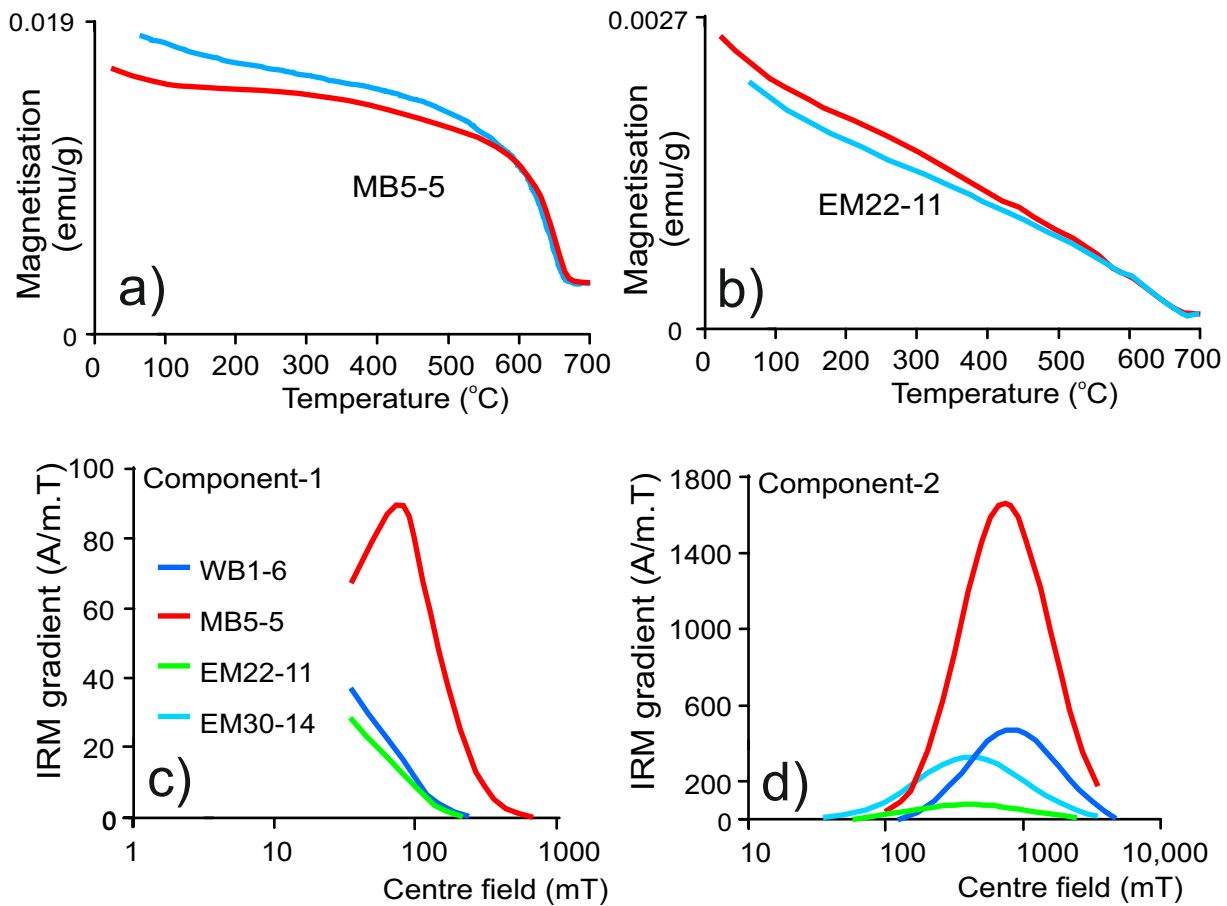
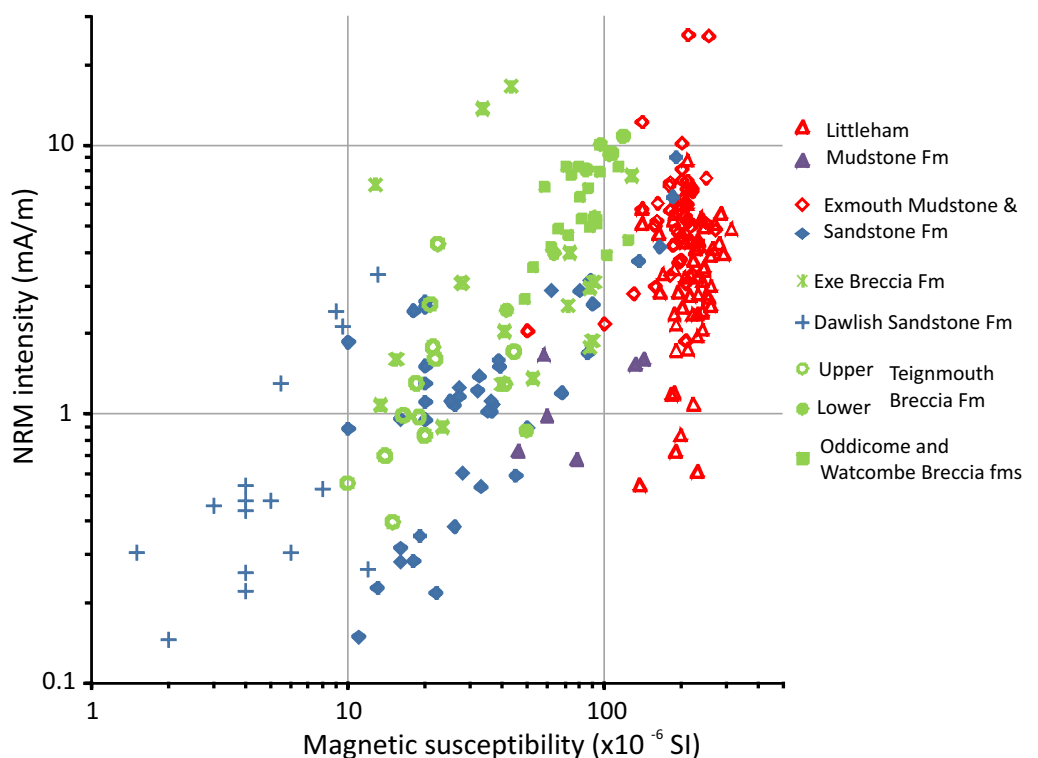


Fig.s5. A,b) Representative thermomagnetic data, measured using the vertical field translation balance (red=heating, blue= cooling). A subtle change in slope is seen at temperatures less than 200°C, which disappears when the estimated paramagnetic contribution is subtracted from the curves. C), d) log-Gaussian isothermal remanent magnetisation coercivity distributions (Kruiver *et al.* 2001) for selected samples, showing the fitted low field (component-1, c)) and high field components (component 2, d)). IRM data obtained with backfield data. Specimen WB1-6 and MB5-5 have higher coercivities (B_{cr}^* of 741-851 and 63 mT for the 2 components) than EM22-11 and EM30-14 (B_{cr}^* of 407-417 and 32 mT). Furthermore, these former 2 specimens had wider high coercivity distributions (dispersion parameter of 0.40-0.45 as compared to 0.32 for EM22-11 and EM30-14).

Fig.s6. Petro-magnetic data for the Exeter and Aylesbeare Mudstone groups. Sandstone samples in blue, mudstone samples in red, and sandstone & sandy-mudstone units from breccia units in green.



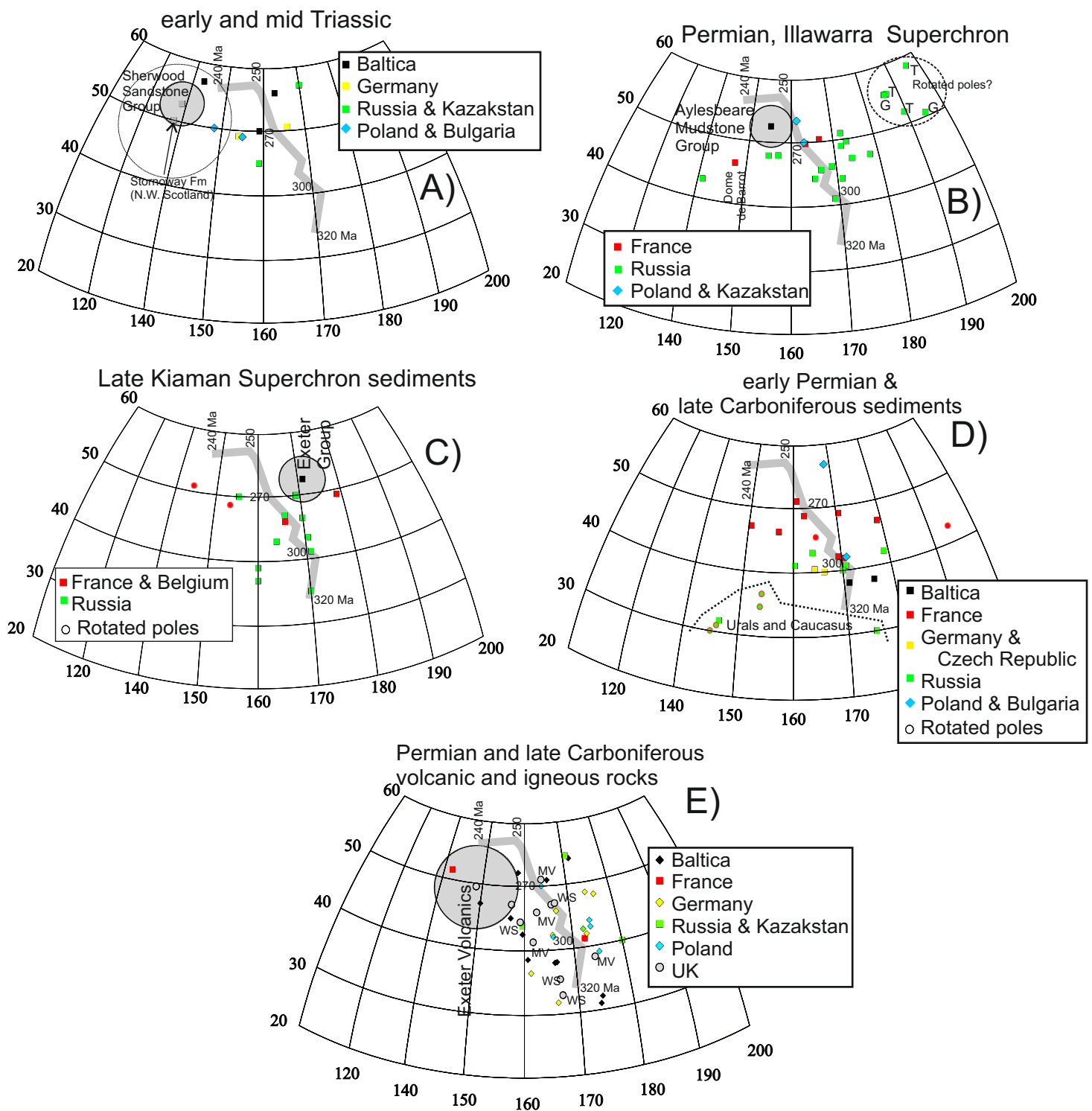


Fig. s7. Stable-Europe virtual geomagnetic poles (VGP) and their comparison to the VGP data from the latest Carboniferous, Permian and early-mid Triassic of the UK. Confidence cones for the units in SW England shown in grey, no confidence cones shown for other data. Each of the plots (A to E) shows the average European VGP path from Torsvik & Cocks (2005) labelled in Ma increments. (A) Lower and Middle Triassic sedimentary units, with Sherwood Sandstone Fm pole from Hounslow & McIntosh (2003), (B) Permian sedimentary VGP data younger than the end of the KRPS (i.e. mid-late Wordian and younger). T=data from Taylor *et al.* (2009), G=from Gialanella *et al.* (1997). (C) Sedimentary VGP data near the end of the KRPS. (D) Lower Permian and latest Carboniferous sedimentary poles. (E) Permian and latest Carboniferous volcanic and igneous-based VGP poles. MV=igneous units from the Scottish Midland Valley, WS= Whin sill data (from Liss *et al.* 2004). Data mostly from the Global Palaeomagnetic Database (<http://www.ngu.no/dragon/>), with newer data from Burov *et al.* (1998), Chen *et al.* (2006), Diego-Orozco *et al.* (2002), Nawrocki *et al.* (2008) and Bazhenov *et al.* (2008). In C) and D) rotated poles are filled circles.

Discussion of VGP data in Figure s7

Creer (1957), Zijdeveld (1967) and Cornwall (1967) presented palaeomagnetic data for the Exeter Volcanic Rocks, around Exeter and further north in the Crediton Trough. Cornwall (1967) also performed reconnaissance sampling of the successions in this study, and from the underlying Torbay Breccia Fm. Whilst Zijdeveld and Cornwall did use AF demagnetisation, and Cornwall in addition used thermal demagnetisation, relatively few of the sites measured by Cornwall (1967) had structural corrections, whereas the mean direction determined by Zijdeveld utilised tilt corrections (Table 1). Cornwall's (1967) mean direction for the Exeter Volcanic Rocks has overly shallow inclination due to inclusion of some southerly-directed magnetisations with positive inclinations, probably due to incomplete demagnetisation of the specimens. The mean VGP pole of Zijdeveld (1967) falls towards the end of the late Carboniferous to Permian European APWP path (Fig. s7e), which corresponds well to the range of VGPs from other late Carboniferous to Lower Permian volcanic and igneous units (Fig. S7e).

The sites from the Teignmouth Breccia and from Watcombe Cove have a significant number of specimens having declinations east of south (Table 1; Fig. 9a). The result of this is a more southerly mean, which does however, reflect new data acquired from the Russian Platform by Taylor *et al.* (2009) and Gialanella *et al.* (1997), which are clearly separated (Fig. s7b) from the bulk of previous Russian data obtained from successions younger than the Kiaman Superchron (i.e. Molostovsky 1983; Burov *et al.* 1998). Bazhenov *et al.* (2008) have discussed the problems of this new data as either due to mis-orientation, or vertical axis rotations, hitherto undetected in the eastern part of the Russian platform. Vertical axis rotations of up to 30° have also been inferred for Lower Permian sediments (Fig. s7c) in basins in France and Germany (Diego-Orozco *et al.* 2002; Chen *et al.* 2006), where there are clearer, strike-slip-related tectonic mechanisms to produce this. There are insufficient data in this study to attempt an answer to this for the UK successions, but the similarity in age and tectonic setting of these European basins, south of the Variscan Front infers a common geological or geomagnetic origin for these outlier VGP directions, warranting further investigation, beyond the scope of this study.

Supplementary Information References

- Bazhenov, M.L., Grishanov, A.N., Van der Voo, R. & Levashova, N.M. 2008. Late Permian palaeomagnetic data east and west of the Urals. *Geophys. J. Int.* **173**, 395-408.
- Burov, B. V., Zharkov, I. Y., Nurgaliev, D. K., Balabanov, Yu. P., Borisov, A. S. & Yasonov, P. G. 1998. Magnetostratigraphic characteristics of Upper Permian sections in the Volga and the Kama areas. In: Esaulova, N. K., Lozonsky, V. R., Rozanov, A. Yu. (eds). *Stratotypes and reference sections of the Upper Permian in the regions of the Volga and Kama Rivers*. GEOS, Moscow, 236-270.
- Cornwall, J. D. 1967. Palaeomagnetism of the Exeter Lavas, Devonshire. *Geophys. Journal Royal Astro. Soc.*, **12**, 181-196.
- Chen Y., Henry, B. Faure, M. , Becq-Giraudon , J-F, Talbot, J-Y, Daly, L. & Le Goff, M. 2006. New Early Permian paleomagnetic results from the Brive basin (French Massif Central) and their implications for Late Variscan tectonics. *Int. J Earth Sci.*, DOI 10.1007/s00531-005-0010-5.
- Creer, K. M. 1957. The Natural Remanent Magnetization of Certain Stable Rocks from Great Britain. *Philosophical Transactions of the Royal Society of London. Series A, Mathematical and Physical Sciences*, **250**, 111-129.
- Diego-Orozco, A., Chen, Y., Henry, B. & Becq-Giraudon, J-F. 2002. Paleomagnetic results from the Permian Rodez basin implications: the Late Variscan tectonics in the southern French Massif Central. *Geodynamica Acta*, **15**, 249-260.
- Gialanella, P.R, Heller, F., Haag, M., Nurgaliev, D., Borisov, A., Burov, B., Jasonov, P., Khasanov, D., Ibraginov, S. & Zharkov, I. 1997. Late Permian magnetostratigraphy on the eastern Russian Platform. *Geologie en Mijnbouw* **76**, 145-154.
- Henson, M.R. 1971. *The Permo-Triassic Rocks of South Devon*. Unpublished Ph.D. Thesis, University of Exeter.
- Hounslow, M.W. & McIntosh, G. 2003. Magnetostratigraphy of the Sherwood Sandstone Group (Lower and Middle Triassic): South Devon, U.K.: Detailed correlation of the marine and non-marine Anisian. *Palaeogeogr. Palaeoclimat. Palaeoecol.*, **193**, 325-348.
- Jones, N.S. 1992. *Sedimentology of the Permo-Triassic of the Exeter area, S.W. England*. British Geological Survey Technical Report, WH/92/122R.
- Kruiver, P. P., Dekkers, M. J. & Heslop, D. 2001. Quantification of magnetic coercivity components by the analysis of acquisition curves of isothermal remanent magnetisation. *Earth and Planetary Science Letters*, **189**, 269-276.
- Laming, D. J. C. 1966. Imbrications, palaeocurrents and other sedimentary features in the Lower New Red Sandstone, Devonshire, England. *Journal of Sedimentary Petrology*, **36**, 940-959.
- Liss, D., Owens, W. H. & Hutton, D. H. W. 2004. New palaeomagnetic results from the Whin Sill complex: evidence for a multiple intrusion event and revised virtual geomagnetic poles for the late Carboniferous for the British Isles. *Journal of the Geological Society, London*, **161**, 927-938.
- Molostovsky, E. A. 1983. *Paleomagnetic stratigraphy of the eastern European part of the USSR*. University of Saratov, Saratov [In Russian].
- Nawrocki, J., Fanning, M., Lewandowska, A., Polechońska, O. & Werner, T. 2008. Palaeomagnetism and the age of the Cracow volcanic rocks (S Poland). *Geophys. J. Int.*, **174**, 475-488.
- Selwood, E. B., Edwards, R. A., Simpson, S., Cheshier, J. A. & Hamblin, R. A. 1984. *Geology of the country around Newton Abbot*. Memoir for 1:50,000 geological sheet 339, British Geological Survey, HMSO, London.
- Smith, S.A. & Edwards, R.A. 1991. Regional sedimentological variations in Lower Triassic fluvial conglomerates (Budleigh Salterton Pebble Beds), southwest England: some implications for palaeogeography and basin evolution. *Geological Journal*, **26**, 65-83.
- Taylor, G. K., Tucker, C., Twitchett, R. J., Kearsley, T., Benton, M. J., Newell, A. J. & Tverdokhlebov, V. P. 2009. Magnetostratigraphy of Permian/Triassic boundary sequences in the Cis-Urals, Russia: No evidence for a major temporal hiatus. *Earth and Planetary Science Letters*, **281**, 36-47.
- Torsvik T. H. & Cocks L. R. M. 2005. Norway in space and time: A centennial cavalcade. *Norwegian Journal of Geology*, **85**, 73-86.
- Zijderveld, J. D. A. 1967. The natural remanent magnetisation of the Exeter Volcanic Traps (Permian, Europe). *Tectonophysics*, **4**, 121-153.